

DEPARTMENT OF COMMERCE
LUTHER H. HODGES, Secretary

WEATHER BUREAU
F. W. REICHELDERFER, Chief

MONTHLY WEATHER REVIEW

JAMES E. CASKEY, JR., Editor

Volume 91, Number 3

Washington, D.C.

MARCH 1963

GENERAL CIRCULATION EXPERIMENTS WITH THE PRIMITIVE EQUATIONS

I. THE BASIC EXPERIMENT*

J. SMAGORINSKY

General Circulation Research Laboratory, U.S. Weather Bureau, Washington, D.C.

[Manuscript received October 5, 1962; revised January 18, 1963]

ABSTRACT

An extended period numerical integration of a baroclinic primitive equation model has been made for the simulation and the study of the dynamics of the atmosphere's general circulation. The solution corresponding to external gravitational propagation is filtered by requiring the vertically integrated divergence to vanish identically. The vertical structure permits as dependent variables the horizontal wind at two internal levels and a single temperature, with the static stability entering as a parameter.

The incoming radiation is a function of latitude only corresponding to the annual mean, and the outgoing radiation is taken to be a function of the local temperature. With the requirement for thermal equilibrium, the domain mean temperature is specified as a parameter. The role of condensation is taken into account only as it effectively reduces the static stability. All other external sources and sinks of heat are assumed to balance each other locally, and are thus omitted. The kinematics are that of a fluid on a sphere bounded by smooth zonal walls at the equator and at approximately 64° latitude. The dissipative sinks are provided by: (a) surface stresses proportional through a drag coefficient to the square of the surface wind which is suitably extrapolated from above, (b) internal convective stresses proportional to the vertical wind shear, and (c) lateral diffusion of momentum and heat through an exchange coefficient which depends on the local horizontal rate of strain—a horizontal length scale entering as the governing parameter.

For a given specification of the parameters, an integration for 60 days has been made from initial conditions where random temperature disturbances have been superimposed on a zonally symmetric regime which is baroclinically unstable according to linear theory. This experiment not only displays the scale selective character of baroclinic instability, yielding zonal wave number 5 to 6, but also predicts an index or energy cycle. The period of this cycle is 11 to 12 days for the first 40 days of the experiment, then lengthening to 17 days while diminishing in amplitude during the latter part.

The resulting mean zonal velocity profile is in good qualitative agreement with observation, but too intense, presumably because the effective static stability parameter is taken too large. Furthermore this profile is found to be no more than 5 percent super-geostrophic poleward of the angular momentum maximum and no more than 2 percent sub-geostrophic equatorward. The total zonal angular momentum remains constant to within 2 percent irrespective of the phase of the index cycle. This balance is controlled by the surface wind distribution which agrees quite well with observation. The poleward transport is mainly accomplished by the large-scale eddies, whereas the internal vertical flux is predominantly a transfer of the earth's angular momentum by the meridional circulation.

The poleward heat transport is primarily accomplished by a Hadley circulation at low latitudes but by the large-scale horizontal eddies in mid-latitudes, where a Ferrel circulation tends to compensate through an equatorward flux. This compensation at mid-latitudes by an indirect meridional circulation is also quite evident in the potential-kinetic energy transformations. Comparison of the momentum and heat transfer with observed data when available shows reasonably good quantitative agreement.

The lateral transfer of momentum and heat by the non-linear diffusion, which parametrically is supposed to simulate the action of motions of sub-grid scale, accounts for a significant portion of the total eddy transfer. Although no direct comparison with the corresponding transfer in the real atmosphere is available, intuitively our small-scale diffusion appears to play too large a role.

A diagnosis is made of the transformations among the barotropic and baroclinic parts of the kinetic energy as well as the zonal mean and zonal perturbation parts of the available potential and kinetic energy. This reveals the dominant paths that the energy passes through from source to ultimate sinks and the processes responsible for these transformations. It is found that the partitioning of dissipation by the energy components may differ considerably from estimates made from observation.

*Preliminary results of this work were first presented before the American Association for the Advancement of Science, Washington, D.C., December 1958.

CONTENTS

	Page
1. Introductory Remarks	100
2. The Differential Equations	101
3. Energy Sources	102
4. Small-Scale Eddy Diffusion	103
5. The Computational Boundary Conditions	106
6. The Initial Conditions of the Experiment	107
7. Synoptic Manifestations	108
8. The Energy Balance and the Transformations by Which It Is Maintained	113
a. The Energy Components	113
b. Derivation of the Energy Transformations	113
c. Properties of the Transformations Involving Only the Zonally Symmetric Circulation	119
d. Properties of the Transformations Involving Only Zonal Perturbations	119
e. Properties of the Transformations Between the Zonal Perturbations and the Zonally Sym- metric Circulation	119
f. The Experimental Results	120
g. Effects of Truncation Error	121
9. The Heat Balance	121
10. The Zonal Angular Momentum Balance	131
11. The Mean Zonal Wind and Meridional Circulation	132
12. The Mean Meridional Mass Flux and the Zonal Geo- strophic Balance	138
13. Computational Aspects	143
14. Summary and Conclusions	146
Acknowledgments	148
References	148
Appendix A: The Parameterization of Non-Adiabatic Heat- ing for the Vertically Integrated Atmosphere	150
Appendix B: A Non-Dimensional Form of the Baroclinic In- stability Criterion	151
Appendix C: Notation Conventions	153
Parameters of the Numerical Model	159

This work is dedicated to the fond memory of Harry Wexler whose enthusiasm and confidence were a constant source of inspiration.

1. INTRODUCTORY REMARKS

In constructing a dynamical model of the atmosphere for the purpose of accounting for the features of the general circulation, two obvious courses present themselves:

(i) to treat transient dynamics of the large-scale motions explicitly and then to calculate the statistical-mechanics of the evolutions,

or

(ii) to treat the large-scale motions as turbulence which is somehow related to the mean properties of the flow.

The latter course has a natural appeal following the successful application of such techniques by Prandtl and von Kármán to small-scale motions through analogy to kinetic theory. The application to large-scale cyclones and anticyclones has been suggested by Defant [11] and from time to time attempts have been made, e.g., by Berson [4] and others. In fact, it is employed implicitly by Namias [34] in operational 5- and 30-day forecasts by techniques which thus far have evaded quantitative formulation. More recently some success has been

attained in theoretical studies, e.g., Thompson [57]. The still incomplete understanding of the statistical-dynamics of large-scale baroclinic transient motions in terms of the mean flow and particularly the maintenance of the westerlies by the non-linear transfer of perturbation energy leaves course (i) as the painful alternative. One would hope however that this explicit approach would ultimately contribute to the formulation of a "turbulence" theory. The advent of high speed computing machines and the parallel development of techniques of short range numerical prediction permit reducing the turbulence threshold from cyclone-scale to a characteristic length of a few hundred kilometers—a horizontal scale for which the eddy transport in the direction of the mean gradient is assumed to be valid, i.e., the grid scale lies within an inertial sub-range.

In a now classic experiment, Phillips [40] did precisely this within the framework of quasi-geostrophic hydrodynamics. Despite the restrictive kinematics of a rectangular β -plane and rather simple heating and viscous dissipation, he managed to demonstrate the scale-selective character of baroclinic instability and how this process balances the meridional radiation gradient, maintaining the westerlies.

The most obvious deficiency in Phillips' model was the geostrophic approximation. It was impossible for him to adequately account for essentially non-geostrophic dynamics of the equatorial Hadley circulation and also for interactions of the inertio-gravitational motions with the quasi-geostrophic motions in extratropical latitudes. Furthermore the quasi-geostrophic character of the general circulation is an important feature to explain, and it cannot be explained adequately by a purely geostrophic model. The present study is an attempt to employ the primitive equations for general circulation experiments. The embarkation on this study was predicated on devising stable techniques for numerically integrating the primitive equations—a problem which at the time had not yet been resolved for even short-period calculations. The methods since developed have been reported on elsewhere [53] and will form the basis for the discussion in the following sections.

The present work is an outgrowth of collaboration with J. G. Charney, N. A. Phillips, and J. von Neumann, who engaged in the initial planning stages of this investigation. Their suggestions at that time were responsible for the launching of this study.

The model employed departs from that of Phillips principally in that many of the hydrodynamic and kinematic constraints have been removed:

(1) The primitive equations of motion are employed in which only gravitational motions of the external type and vertical sound propagation are filtered a priori; vertical momentum transport is taken into account.

(2) The motion is confined to a zonal channel consisting of smooth walls at the equator and 64.4° latitude so that the longest waves are bounded by the local circumference of earth.

(3) The kinematics of motion on a sphere are taken into account by appropriate mapping of the equations. This is done conformally onto a Mercator projection. The grid interval is 5° longitude which corresponds approximately to 555 km. at the equator and 240 km. at the northern boundary.

Furthermore, the finite difference form of the equations possesses integrals which correspond exactly to their respective angular momentum and potential temperature counterparts in the continuum.

For the present purposes, certain sacrifices for simplicity have been made in the details of the thermodynamic processes. The vertical structure has been designed for a minimal accounting of baroclinic processes, i.e., a two-level model is employed. The static stability enters as a fixed parameter of the model, and hence its large-scale dynamical adjustments, which are small but may be important, are ignored.

Available observational and theoretical evidence suggests that the essential features of the general circulation such as the methods of angular momentum and heat transfer, the existence of an index cycle, and the characteristic time and space scale of extratropical disturbances are primarily independent of zonal asymmetries of the earth's surface. That is not to say that the distribution of oceans and continents and of large-scale orographic features does not affect the general circulation. There is ample evidence (e.g. [10], [5], [51], [48]) that they do excite quasi-stationary very long disturbances (wave numbers 2 and 3) which by non-linear interaction bias the phase of the shorter waves of maximum baroclinic instability (wave numbers 5 and 6). Since the primary mechanisms of the general circulation have yet to be fully understood, the present investigation will deal with an underlying boundary surface of uniform geopotential, roughness, and thermal conductivity.

The main body of this paper describes the construction of the model elements, the experimental conditions, the synoptic manifestations of the evolutions, and most important, a diagnosis of their dynamical characteristics. The Appendices A and B are subsidiary studies which lend an insight into what may be expected of some aspects of the numerical experiment. They are based on certain theoretical results as well as on observational material. Although these Appendices make reference to results of the main text, it is recommended that they be read first. Appendix C is a compilation of the notation and the model parameters.

2. THE DIFFERENTIAL EQUATIONS

It was shown in Smagorinsky [53] (with some changes in notation; cf. Appendix C) that the equations for a two-level model mapped conformally onto a Mercator projection are:

$$\frac{\partial \hat{\Phi}}{\partial t} = -\frac{\partial}{\partial x}\left(\frac{\hat{\Phi}\bar{u}}{2}\right) - m^2 \frac{\partial}{\partial y}\left(\frac{\hat{\Phi}\bar{v}}{2m^2}\right) - \gamma_s^2 \hat{\mathcal{D}} + \kappa Q + H \quad (2.1)$$

[53(74)]

$$\frac{\partial \hat{\mathbf{v}}}{\partial t} = m \hat{\mathbf{G}} - m \nabla \hat{\Phi} \quad (2.2)$$

[53(29)]

$$\nabla^2 \psi^* = \text{curl } \bar{\mathbf{G}} \quad (2.3)$$

[53(28)]

where

$$\mathbf{G}_k = -\mathbf{I}_k + \mathbf{F}_k \quad (2.4)$$

[53(19)]

$$\left. \begin{aligned} m \mathbf{I}_1 &= \mathbf{i} \left(\frac{\partial u_1^2}{\partial x} + m^4 \frac{\partial}{\partial y} \left(\frac{u_1 v_1}{m^4} \right) - \frac{\hat{\mathcal{D}} \bar{u}}{4} - f v_1 \right) \\ &\quad + \mathbf{i} \left(\frac{\partial u_1 v_1}{\partial x} + m^3 \frac{\partial}{\partial y} \left(\frac{v_1^2}{m^3} \right) - \frac{\hat{\mathcal{D}} \bar{v}}{4} + \left(f + \frac{\alpha u_1}{a} \right) u_1 \right) \\ m \mathbf{I}_3 &= \mathbf{i} \left(\frac{\partial u_3^2}{\partial x} + m^4 \frac{\partial}{\partial y} \left(\frac{u_3 v_3}{m^4} \right) + \frac{\hat{\mathcal{D}} \bar{u}}{4} - f v_3 \right) \\ &\quad + \mathbf{i} \left(\frac{\partial u_3 v_3}{\partial x} + m^3 \frac{\partial}{\partial y} \left(\frac{v_3^2}{m^3} \right) + \frac{\hat{\mathcal{D}} \bar{v}}{4} + \left(f + \frac{\alpha u_3}{a} \right) u_3 \right) \end{aligned} \right\} \quad (2.5)$$

[53(75)*]

$\Phi \equiv \phi'' = \phi - \{\phi\}$ is the deviation from the domain mean geopotential (see C10), and γ_s^2 is a measure of the static stability. The rate of non-adiabatic heating per unit mass Q will be discussed in Section 3, while the small scale eddy heat flux divergence H and the viscous force vector \mathbf{F} will be treated in Section 4.

The equations for the vertical mean wind

$$\left. \begin{aligned} \frac{\partial \bar{u}}{\partial t} &= -m^2 \frac{\partial \psi^*}{\partial y} = m \bar{G}_x - m^2 \frac{\partial \bar{\Phi}}{\partial x} \\ \frac{\partial \bar{v}}{\partial t} &= m^2 \frac{\partial \psi^*}{\partial x} = m \bar{G}_y - m^2 \frac{\partial \bar{\Phi}}{\partial y} \end{aligned} \right\} \quad (2.6)$$

[53(26), (27)]

are never used explicitly since they and the external gravity wave filtering constraint

$$\nabla \cdot \bar{\nabla} \equiv 0 \quad (2.7)$$

are inherent in the elliptic consistency condition (2.3).

It is of interest that the sum of the inertial and pressure gradient forces may be written in the form:

$$\begin{aligned} m \hat{\mathbf{I}} + m^2 \left(\mathbf{i} \frac{\partial \hat{\Phi}}{\partial x} + \mathbf{j} \frac{\partial \hat{\Phi}}{\partial y} \right) &= \mathbf{i} \left(-\hat{\mathcal{D}} \bar{u} + m^2 \frac{\partial \hat{\mathcal{B}}}{\partial x} \right) \\ &\quad + \mathbf{j} \left(\hat{\mathcal{B}} \bar{v} + m^2 \frac{\partial \hat{\mathcal{B}}}{\partial y} \right) \end{aligned} \quad (2.8)$$

$$\begin{aligned} m \hat{\mathbf{I}} + m^2 \left(\mathbf{i} \frac{\partial \bar{\Phi}}{\partial x} + \mathbf{j} \frac{\partial \bar{\Phi}}{\partial y} \right) &= \mathbf{i} \left(-\bar{v} \eta + \bar{D} \bar{u} + m^2 \frac{\partial \bar{\mathcal{B}}}{\partial x} \right) \\ &\quad + \mathbf{j} \left(\bar{u} \eta + \bar{D} \bar{v} + m^2 \frac{\partial \bar{\mathcal{B}}}{\partial y} \right) \end{aligned} \quad (2.9)$$

where the divergence \bar{D} , absolute vorticity η , and \mathcal{B} , are:

*The left sides of this equation in [53] should have been multiplied by m .

$$\left. \begin{aligned} D &= \frac{\partial u}{\partial x} + m^2 \frac{\partial v/m^2}{\partial y} \\ \eta &= f + \frac{\partial v}{\partial x} - m^2 \frac{\partial u/m^2}{\partial y}, \quad f \equiv 2\Omega\alpha \\ B &= \frac{u^2 + v^2}{2m^2} + \phi \end{aligned} \right\} \quad (2.10)$$

Although these forms were not used in the present forecast calculations they have some obvious computational advantages over the Eulerian form. For example, there are no truncation errors due to mapping such as in terms α/am^2 ; in fact, these equations are identically the same for any conformal projection if m is the map factor and if x, y and u, v are the map distances and velocity components.

It was pointed out in [53] that care must be taken in differencing differential equations of the form

$$\frac{\partial \xi}{\partial t} = v \xi \quad (2.11)$$

For central time differencing

$$\xi^{r+1} - \xi^{r-1} = 2\Delta t v \xi^r \quad (2.12)$$

is computationally unstable for $v < 0$ for all Δt , but for forward differencing

$$\xi^{r+1} - \xi^{r-1} = 2\Delta t v \xi^{r-1} \quad (2.13)$$

the solution is stable. To reduce the truncation error one may use an implicit method

$$\xi^{r+1} - \xi^{r-1} = \Delta t v (\xi^{r+1} + \xi^{r-1}) \quad (2.14)$$

or

$$\xi^{r+1} = \left(\frac{1 + v\Delta t}{1 - v\Delta t} \right) \xi^{r-1} \quad (2.15)$$

provided $v\Delta t \neq 1$. We shall have occasion to refer to these computational stability considerations when we introduce the heating and viscous terms in the following sections.

3. ENERGY SOURCES

The discussion in Appendix A shows that the net heating of an atmospheric column may be significantly different from that deduced from radiative transfer alone. Evaporation, condensation, and ocean transports, although balancing out hemispherically, give rise to a diminished meridional heating scale, instead of the characteristically monotonic latitudinal decrease of the net radiation itself. For the present calculations, we will simplify the heating function derived in Appendix A to a form which essentially corresponds to that used by Charney [9]. In (A30) and (A10) we take $\Gamma = \nu_{\downarrow} = \nu_{\uparrow} = 1$. Moreover we assume that $E_L + M$ is balanced by that part of the condensation heating which contributes to the domain mean, i.e.

$$E_L + M \approx \frac{p_4}{\kappa g} 0.2 \gamma_s^2 |\hat{D}| \quad (3.1)$$

Locally this assumed balance should not be taken too literally, since table A5.1 shows that $E_L + M < 0$ at very high latitudes. We then have with (A7) that

$$\left. \begin{aligned} \kappa Q &= \kappa Q_R + 0.2 \gamma_s^2 \hat{D} \\ \text{where } \frac{p_4 Q_R}{g} &= A - \sigma T_2^4 \end{aligned} \right\} \quad (3.2)$$

Upon linearizing T_2 as in (A15) and requiring a domain heat balance, i.e.:

$$\left\{ \left[\frac{p_4 Q}{g} \right] \right\} = 0 \quad (3.3)$$

then since $\{\hat{D}\} = 0$ we have that

$$\{[T_2]\}^4 = \frac{\{[A]\}}{\sigma} \quad (3.4)$$

and

$$\frac{p_4 Q_R}{g} = c_R - b T_2'' \quad (3.5)$$

where

$$c = A - \{[A]\} \quad (3.6)$$

$$b = 4\sigma \{[T_2]\}^3 \quad (3.7)$$

We shall use Houghton's [19] calculations for A which from table A3.7 give $\{[A]\} = 463 \text{ ly. day}^{-1}$, which with (3.4) yields $\{[T_2]\} = 251^\circ \text{ A}$. To insure a value of b which gives a dependence of the outgoing long-wave radiation upon temperature corresponding to Houghton's L_{\uparrow} , we do not use (3.7) directly, but rather the linearized form of (A4) with $\Gamma = \nu_{\uparrow} = 1$, (3.7), and then (3.4):

$$b = \frac{L_{\uparrow} - \{[A]\}}{T_2''} \quad (3.8)$$

With $T_2(\theta)$ interpolated from London's [24] data and calculating T_2'' (his $\{[T_2]\} = 259^\circ \text{ A}$) we get as the average over all latitudes $b = 4.7 \text{ ly. day}^{-1} \text{ deg.}^{-1}$. If calculated directly from (3.7), $b = 7.4 \text{ ly. day}^{-1} \text{ deg.}^{-1}$, giving a much larger meridional gradient of the long-wave cooling for the same T_2'' . Hence the adopted values of $b = 4.7 \text{ ly. day}^{-1} \text{ deg.}^{-1}$ and $\{[T_2]\} = 251^\circ \text{ A}$, although accommodating Houghton's and London's empirical determinations, are inconsistent with (3.7).

The above meridional means are from equator to pole. If we wish to retain radiative balance for our domain from equator to 64.4° latitude then c must be normalized such that its mean over the reduced latitudinal span vanishes. Therefore in (3.6) we replace $\{[A]\} = 463 \text{ ly. day}^{-1}$ by 493 ly. day^{-1} .

The temperature change due to Q is Q/c_p and the corresponding change in geopotential thickness is κQ . Hence in terms of the geopotential thickness departure $\hat{\Phi} \equiv R T_2''$:

$$\kappa Q_R = \frac{\kappa g}{p_4} \left(c_R - \frac{b}{R} \hat{\Phi} \right) \quad (3.9)$$

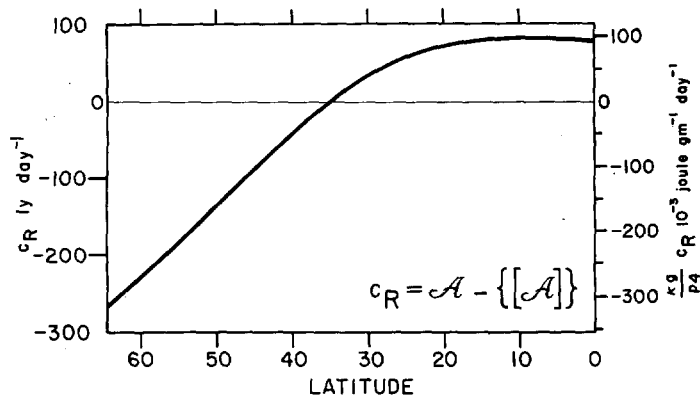


FIGURE 3.1.—The latitude dependent part of the radiative heating function used in the numerical integrations. c_R is the deviation from the mean of the assumed total absorption of solar radiation by the atmosphere and the ground.

where $\kappa g/p_4 = 1.19 \times 10^{-3}$ joule gm. $^{-1}$ ly. $^{-1}$ and we have taken $\kappa b/p_4 R = 0.0192$ day $^{-1}$. Summarizing, the radiative parameters adopted for our domain are $\{[T_2]\} = 251^\circ$ A., $b = 4.7$ ly. day $^{-1}$ deg. $^{-1}$ and c_R is plotted on figure 3.1 as a function of latitude.

To assess the effect of the linearization of T_2 and the normalization to our smaller latitudinal span, we plot in figure 3.2 Houghton's $A - L_\uparrow$, its linearized form (3.5) using London's climatological T_2 , and the normalized form of the latter (the $0-64.4^\circ$ latitude means of both c_R and T_2'' are zero). The associated fluxes (fig. 3.3) are however a more sensitive indication of the consequences. Although the linearization gives a 10 percent reduction in the maximum flux, which occurs at 37° latitude, the normalization gives a much larger reduction (almost 40 percent). This must be kept in mind in the interpretation of the dynamical results in Section 9.

We now rewrite the thermodynamic equation (2.1) using (3.2) as

$$\frac{\partial \hat{\Phi}}{\partial t} = -\frac{\partial}{\partial x}\left(\frac{\hat{\Phi}\bar{u}}{2}\right) - m^2 \frac{\partial}{\partial y}\left(\frac{\hat{\Phi}\bar{v}}{2m^2}\right) - \gamma^2 \hat{\mathcal{D}} + \kappa Q_R + H \quad (3.10)$$

where $\gamma^2 = 0.8\gamma_s^2 = 3300$ m. 2 sec. $^{-2}$ is a measure of the effective static stability. From this point on Q_R will be defined as the energy source, whereas that part due to condensation which effectively alters the static stability will ultimately be included in the definition of available potential energy (Section 8) and in the poleward heat transfer by the mean meridional circulation (Section 9).

In the finite difference form of (3.10), (3.9) was evaluated implicitly according to (2.15).

4. SMALL-SCALE EDDY DIFFUSION

The frictional force in general is due to horizontal and vertical stresses:

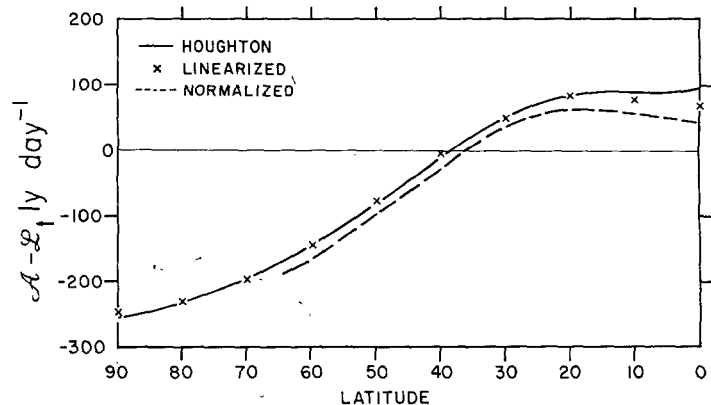


FIGURE 3.2.—The difference between the total absorption of solar radiation, A , and the total outgoing long wave radiation, L_\uparrow , as a function of latitude: according to Houghton [19]; when L_\uparrow is calculated from a linearized form of the Stephan-Boltzmann Law $L_\uparrow \approx \{[A]\} + b T_2''$, where $b = 4.7$ ly. day $^{-1}$ deg. $^{-1}$, T_2'' is from London's [24] 500-mb. climatological temperature distribution and A is from Houghton's calculations, $\{[A]\} = 463$ ly. day $^{-1}$; the linearized form normalized to $0-64.4^\circ$ latitude (the domain of the numerical experiment) by taking $\{[A]\} = 493$ ly. day $^{-1}$.

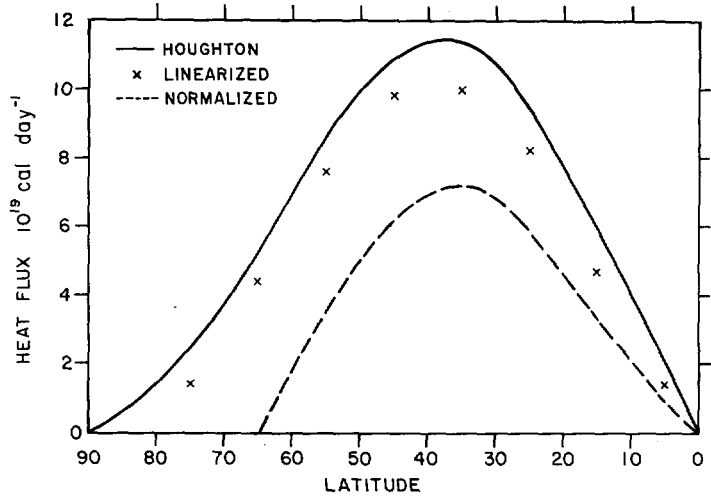


FIGURE 3.3.—The heat flux corresponding to the heating rates given in figure 3.2.

$$\mathbf{F} = H\mathbf{F} + v\mathbf{F} \quad (4.1)$$

With

$$v\mathbf{F} = -g \frac{\partial \boldsymbol{\tau}}{\partial p} \quad (4.2)$$

where $\boldsymbol{\tau}$ is the vertical stress vector, then

$$v\mathbf{F}_k = \frac{g}{\hat{p}} (\boldsymbol{\tau}_{k+1} - \boldsymbol{\tau}_{k-1}) \quad (4.3)$$

Assuming the stress at the top of the atmosphere, $\boldsymbol{\tau}_0$, to vanish we have that

$$\left. \begin{aligned} v\mathbf{F}_1 &= \frac{g}{\hat{p}} \tau_2, & v\mathbf{F}_3 &= \frac{g}{\hat{p}} (\tau_4 - \tau_2) \\ \text{or that} & & & \\ v\tilde{\mathbf{F}} &= \frac{g}{\hat{p}} \tau_4, & v\hat{\mathbf{F}} &= \frac{g}{\hat{p}} (2\tau_2 - \tau_4) \end{aligned} \right\} \quad (4.4)$$

τ_4 is the lower boundary stress due to surface roughness, while τ_2 is the internal stress identifiable with convective motions in the atmosphere.

We shall assume that the vertical stress is proportional to the vertical wind shear

$$\tau = -Kg\rho^2 \frac{\partial \mathbf{V}/m}{\partial p} \quad (4.5)$$

where K is the eddy viscosity.

Under conditions of neutral static stability, the stress is independent of height in the surface layer so that the wind increases logarithmically, having the same direction as the stress, giving

$$\tau_4 = \left(\frac{K\rho}{\epsilon} \frac{|\mathbf{V}|}{m} \right)_4 \quad (4.6)$$

where we have taken p_4 to lie somewhere in the surface layer. ϵ_4 is related to the roughness by

$$\epsilon_4 = (z_4 + z_*) \ln \frac{z_4 + z_*}{z_*} \quad (4.7)$$

where z_4 is the height of the p_4 level and z_* is the roughness length.

Furthermore K_4 is proportional to the magnitude of the wind

$$K_4 = k_0^2 \frac{z_4 + z_*}{\ln \frac{z_4 + z_*}{z_*}} \frac{|\mathbf{V}_4|}{m} \quad (4.8)$$

where k_0 is von Kármán's constant. Hence (4.6) may be written as

$$\tau_4 = \left(\rho \frac{c_d}{2} \frac{|\mathbf{V}_4| |\mathbf{V}|}{m^2} \right)_4 \quad (4.9)$$

where

$$\left(\frac{c_d}{2} \right)_4 = \left(\frac{k_0}{\ln \frac{z_* + z}{z_*}} \right)^2 = \left(\frac{K}{\epsilon |\mathbf{V}| / m} \right)_4 \quad (4.10)$$

depends on the roughness and the height z_4 . If δ is the acute angle between \mathbf{V}_4 and the geopotential lines, then we may write the identity

$$\mathbf{V}_4 = \left\{ \frac{|\mathbf{V}| \left(i \left(\frac{\partial \Phi}{\partial y} \cos \delta + \frac{\partial \Phi}{\partial x} \sin \delta \right) + j \left(\frac{\partial \Phi}{\partial y} \sin \delta - \frac{\partial \Phi}{\partial x} \cos \delta \right) \right)}{\sqrt{\left(\frac{\partial \Phi}{\partial x} \right)^2 + \left(\frac{\partial \Phi}{\partial y} \right)^2}} \right\}_4 \quad (4.11)$$

At the lateral boundaries $v_4 = 0$ so that (4.9) becomes

$$\tau_4 = i \left(\rho \frac{c_d}{2} \frac{|u| u}{m^2} \right)_4 \text{ on } y=0, Y \quad (4.12)$$

and δ is not specified.

Hence τ_4/ρ_4 may be calculated from (4.9) and (4.11) provided we know $\nabla \Phi_4$, $|\mathbf{V}_4|$, δ , and $(c_d/2)_4$. Since the pressure gradient as well as τ_4/ρ_4 may be regarded as quasi-constant in the surface layer, then δ is quasi-independent of height. On the other hand $(c_d/2)_4$ and $|\mathbf{V}_4|$ depend on where in the surface layer we take z_4 .

Let us denote by z_4' the height of the boundary between the surface layer (Prandtl layer) and the layer where the inertial and pressure gradient forces become of consequence (Ekman layer). Since p_4 is taken to be within the surface layer, then $z_4 < z_4'$. The Ekman theory may be developed for a lower boundary condition (in this case at z_4') such that the stress is in the direction of the wind (see [18]), requiring δ to be governed by

$$\operatorname{ctn} \delta = 1 + \epsilon_4' \sqrt{\frac{2f}{K_E}} \quad (4.13)$$

where K_E is the mean eddy viscosity in the Ekman layer. Of course K itself must be continuous at z_4' , and some theories are developed about this condition (e.g. [46]). However none of these theories of the planetary boundary layer has displayed sufficient fidelity to observation to warrant being employed too literally. We, in fact, shall use (4.13) only to give the variation of δ with latitude. We take $\delta = 22\frac{1}{2}^\circ$ at $f = 10^{-4} \text{ sec.}^{-1}$. This defines $\epsilon_4'^2/K_E = 10^4$ sec. and thus permits δ to be calculated at all other latitudes. Note that provided $\epsilon_4'^2/K_E$ is bounded, irrespective of its value, $\delta \rightarrow 45^\circ$ as $\alpha \rightarrow 0$. This is fairly well substantiated by observation, despite the fact that the Ekman theory becomes singular at the equator.

Because the pressure field varies relatively uniformly with height, an extrapolation of Φ or ϕ is fairly stable. With $p_4 = 1000 \text{ mb}$. and assuming a lapse rate of $6.50^\circ \text{ C. km.}^{-1}$ then integration of the hydrostatic equation gives that

$$\phi_4 = \frac{1}{2} (\bar{\phi} - 1.384 \hat{\phi}) \quad (4.14)$$

Note that linear extrapolation according to pressure gives $\phi_4 = (\bar{\phi} - 2\hat{\phi})/2$ which is equivalent to assuming an isothermal lapse rate. Equation (4.14) together with (2.6) yield

$$\left. \begin{aligned} \frac{\partial \Phi_4}{\partial x} &= \frac{1}{2} \left(\frac{\bar{G}_x}{m} + \frac{\partial \psi^*}{\partial y} - 1.384 \frac{\partial \hat{\phi}}{\partial x} \right) \\ \frac{\partial \Phi_4}{\partial y} &= \frac{1}{2} \left(\frac{\bar{G}_y}{m} - \frac{\partial \psi^*}{\partial x} - 1.384 \frac{\partial \hat{\phi}}{\partial y} \right) \end{aligned} \right\} \quad (4.15)$$

For the purpose of calculating $|\mathbf{V}_4|$ we assume that \mathbf{V} can be extrapolated geostrophically according to (4.14) but that $|\mathbf{V}_4|$ is some fraction, l , of the magnitude of the vectorially extrapolated wind:

$$|\mathbf{V}_4|^2 = \frac{l^2}{4} ((\bar{u} - 1.384\hat{u})^2 + (\bar{v} - 1.384\hat{v})^2) \quad (4.16)$$

We take $l=0.6$.

Finally we assume $(c_d/2)_4=0.012$ to be a constant. This value is 4 times the "usual" value, but since we have seen that $(c_d/2)_4$ depends on where in the surface layer we evaluate $|\mathbf{V}_4|$, the appropriateness of the value can best be examined from the resulting momentum interchange between atmosphere and earth [21 (fig. 7.5.5, p. 354)]. Hence in evaluating the surface wind we have assumed the velocity to be a non-linear function of pressure in the boundary layer. Elsewhere, however, we assume linearity in the velocity profile. This inconsistency, for example in the energy, should not give rise to serious error.

It is apparent that the pseudo-boundary layer employed here is subject to a considerable degree of arbitrariness. There certainly would be valid question in applying it to a condition of variable surface roughness. A more sophisticated general circulation model could no doubt benefit by introducing an explicit boundary layer which consistently accounts for the interactive flux of heat and moisture as well as momentum.

The internal vertical transport of zonal angular momentum can be accomplished by the interaction of the earth's rotation and the meridional circulation, by the correlation of the vertical and zonal wind components (which is neglected in a geostrophic formulation) and by the internal small-scale stress τ_2 . The latter is manifest in the form of dry and moist convection and from (4.5) may be written in the form

$$\tau_2 = -(\rho K)_2 \left(\frac{g \rho_2}{\hat{p}} \right) \frac{\hat{\mathbf{V}}}{m} \quad (4.17)$$

$-\hat{p}/g\rho_2=7.9$ km. is the depth of the 750-250-mb. layer and $(\rho K)_2$ is an exchange coefficient which probably depends on the local Richardson number. However in the absence of a rational means for deducing the functional form we must content ourselves with a reasonable mean value.

The two extreme estimates of $(\rho K)_2$ are that of Rossby and Montgomery [46] for stable conditions, $50 \text{ gm. cm.}^{-1} \text{ sec.}^{-1}$, and that of Riehl [45], $500 \text{ gm. cm.}^{-1} \text{ sec.}^{-1}$. An intermediate value has been given by Palmén [36]: $225 \text{ gm. cm.}^{-1} \text{ sec.}^{-1}$. The calculation of Charney [9] involved both Palmén's and Riehl's estimates. In the present calculations we have assumed Rossby and Montgomery's value.

To summarize, the frictional forces due to stresses in vertical planes at the lower boundary τ_4 and in mid-atmosphere τ_2 may be expressed in terms of

$$v\bar{\mathbf{F}} = -\left(\frac{g \rho c_d}{p}\right)_4 \frac{|\mathbf{V}_4| \mathbf{V}_4}{m^2} \quad (4.18)$$

and

$$v\mathbf{F}_1 = -\left(\frac{g \rho}{p}\right)_2 K_2 \frac{\hat{\mathbf{V}}}{m} \quad (4.19)$$

since by (4.4)

$$\begin{aligned} v\mathbf{F}_3 &= v\bar{\mathbf{F}} - v\mathbf{F}_1 \\ v\hat{\mathbf{F}} &= 2v\mathbf{F}_1 - v\bar{\mathbf{F}} \end{aligned} \quad (4.20)$$

Hence from (4.1)

$$\begin{aligned} \bar{\mathbf{F}} &= H\bar{\mathbf{F}} + v\bar{\mathbf{F}} \\ \hat{\mathbf{F}} &= H\hat{\mathbf{F}} - v\bar{\mathbf{F}} + 2v\mathbf{F}_1 \end{aligned} \quad (4.21)$$

It will be shown separately [55] that the non-linear lateral diffusion may be formulated on the basis of the Heisenberg similarity theory. Assuming the forms desired are applicable to lateral diffusion within constant pressure surfaces and that we may ignore density variations, we take the viscous forces due to lateral stresses in our model to be

$$\begin{aligned} H\mathbf{F}_x &= (k_H \Delta)^2 m^3 \left(\frac{\partial}{\partial x} \left(\frac{|D|}{m^2} D_T \right) + \frac{\partial}{\partial y} \left(\frac{|D|}{m^2} D_S \right) \right) \\ H\mathbf{F}_y &= (k_H \Delta)^2 m^3 \left(\frac{\partial}{\partial x} \left(\frac{|D|}{m^2} D_S \right) - \frac{\partial}{\partial y} \left(\frac{|D|}{m^2} D_T \right) \right) \end{aligned} \quad (4.22)$$

where the tension and shearing strains are

$$D_T \equiv \frac{\partial u}{\partial x} - \frac{\partial v}{\partial y}, \quad D_S \equiv \frac{\partial v}{\partial x} + \frac{\partial u}{\partial y} \quad (4.23)$$

and

$$|D| \equiv \sqrt{D_T^2 + D_S^2} \quad (4.24)$$

and $k_H \approx 0.28$.

With cyclic boundary conditions on x and with $v=0$ on the lateral boundaries $y=0, Y$, the change of the domain mean relative zonal angular momentum due to $H\mathbf{F}$ is proportional to $\{ |D| D_S / m^2 \}_{y=0}^Y$. Likewise dissipation of kinetic energy due to $H\mathbf{F}$ is proportional to $\{ |D|^3 \}_{y=0}^Y - \{ u |D| D_S / m^2 \}_{y=0}^Y$. The first term is due to internal lateral stresses and the second due to lateral stresses on the boundary. If we require that the lateral boundaries be smooth in the sense that due to $H\mathbf{F}$ there is no flux of zonal angular momentum through them and that they do not affect the kinetic energy, then the weakest possible condition is that

$$D_S \equiv 0 \text{ on } y=0, Y \quad (4.25)$$

This together with the streamline condition $v=0$ gives through (4.23) that $\partial u / \partial y = 0$.

If we assume the lateral heat diffusion to be forced then also according to [55] H in (3.10) becomes

$$H = (k_H \Delta)^2 m^2 \left(\frac{\partial}{\partial x} \left(\frac{|\bar{D}|}{2} \frac{\partial \hat{\Phi}}{\partial x} \right) + \frac{\partial}{\partial y} \left(\frac{|\bar{D}|}{2} \frac{\partial \hat{\Phi}}{\partial y} \right) \right) \quad (4.26)$$

The domain mean temperature change due to H is proportional to $\{ |\bar{D}| \partial \hat{\Phi} / \partial y \}_{y=0}^Y$. This is a measure of the net heat flux through the lateral boundaries due to H . Since we have required thermal equilibrium for the domain, the weakest condition we can apply is

$$\frac{\partial \hat{\Phi}}{\partial y} = 0 \text{ on } y=0, Y \quad (4.27)$$

In the finite difference form of the non-linear diffusion terms, (4.18), (4.22), and (4.26) were evaluated non-centrally according to (2.13), while the linear internal vertical diffusion (4.19) was evaluated implicitly according to (2.15).

5. THE COMPUTATIONAL BOUNDARY CONDITIONS

To recapitulate, the primary physical boundary conditions are that all dependent variables and their derivatives are cyclically continuous in x

$$\frac{\partial^n \xi}{\partial x^n}(x) = \frac{\partial^n \xi}{\partial x^n}(x+L) \quad (5.1)$$

and that

$$v_k = \frac{\partial u_k}{\partial y} = \frac{\partial \hat{\Phi}}{\partial y} = 0 \text{ on } y=0, Y \quad (5.2)$$

Furthermore, it was shown in [53] that since the vertically integrated flow is non-divergent we have the streamline condition

$$\psi(0)=0 \text{ and } \psi(Y) \text{ is a function of time only} \quad (5.3)$$

and that by [53(47) and (48)]

$$\begin{aligned} \psi^*(0) &= 0 \\ \psi^*(Y) &= -\frac{1}{L} \int_0^Y \oint \frac{\bar{G}_x}{m} dx dy \end{aligned} \quad (5.4)$$

As a further consequence we have the following corollary boundary conditions on $y=0, Y$: From (4.3) and (4.12)

$$vF_{vk}=0 \quad (5.5)$$

From (4.25)

$$D_{sk}=0 \quad (5.6)$$

Since $\partial \bar{v}/\partial t=0$ then from (2.6)

$$\frac{\bar{G}_y}{m} = \frac{\partial \bar{\Phi}}{\partial y} \quad (5.7)$$

and since $\partial \hat{v}/\partial t=0$ then from (2.2), (2.4), (5.2), (4.1), and (5.5)

$$\hat{G}_y=0, \quad \hat{I}_v=\hat{F}_v=F_v \quad (5.8)$$

As was pointed out in [53] the central difference analogs of (3.10), (2.2), and (2.3) yield redundant solutions at alternate grid points. These can be made consistent with each other by imposing computational boundary conditions which have the property that each of the solutions preserves integral properties in the transformation from differential to discrete difference form. Hence to insure that $\{\hat{D}\} \equiv 0$, \hat{D} on $y=0, Y$ must be calculated according to [53(76)].

For the solution of the Dirichlet problem constituted

by (2.3) and (5.4), we need \bar{G}_x on $y=0, Y$ and not \bar{G}_y as was erroneously stated in [53] by [53 (79) and (81)]. In order that

$$\frac{\partial \{\bar{u}\}}{\partial t} = \{[m \bar{G}_x]\} = -\psi^*(Y) \quad (5.9)$$

be preserved, $m^4 \partial(uv/m^4)/\partial y$ must be calculated according to [53(78)]. Similarly we need only F_x on $y=0, Y$, for which $\partial v/\partial y$ in D_T must be calculated according to [53 (82) and (83)], and $\partial(|D|D_s/m^2)/\partial y$ according to

$$\left. \begin{aligned} \left(\frac{\partial |D|D_s}{\partial y m^2} \right)_{i,0} &= \frac{1}{\Delta} \left(\frac{|D|D_s}{m^2} \right)_{i,1} \\ \left(\frac{\partial |D|D_s}{\partial y m^2} \right)_{i,J-1} &= -\frac{1}{\Delta} \left(\frac{|D|D_s}{m^2} \right)_{i,J-2} \end{aligned} \right\} \quad (5.10)$$

The above supply us with the quantities necessary to calculate $\partial \hat{u}/\partial t$ on the boundaries and $\partial \hat{v}/\partial t$ adjacent to the boundaries.

To preserve the condition

$$\int_0^Y \frac{\bar{u}}{m^2} dy = -\psi(Y) \quad (5.11)$$

\bar{u} on $y=0, Y$ must be determined from

$$\left. \begin{aligned} \left(\frac{\bar{u}}{m^2} \right)_{i,0} &= -\left(\frac{\partial \psi}{\partial y} \right)_{i,0} = -\frac{1}{\Delta} (\psi_{i,1} - \psi_{i,0}) \\ \left(\frac{\bar{u}}{m^2} \right)_{i,J-1} &= -\left(\frac{\partial \psi}{\partial y} \right)_{i,J-1} = -\frac{1}{\Delta} (\psi_{i,J-1} - \psi_{i,J-2}) \end{aligned} \right\} \quad (5.12)$$

In the thermodynamic equation, the integral condition to be satisfied is that

$$\frac{\partial}{\partial t} \{\hat{D}\} = 0 \quad (5.13)$$

which requires \hat{D} and $m^2 \partial(\hat{\Phi} \bar{v}/2m^2)/\partial y$ on the boundaries to be given by [53(76) and (77)], respectively. In addition the small-scale lateral heat flux divergence with (4.27) must satisfy

$$\left. \begin{aligned} \left(\frac{\partial}{\partial y} |\bar{D}| \frac{\partial \hat{\Phi}}{\partial y} \right)_{i,0} &= \frac{1}{\Delta} \left(|\bar{D}| \frac{\partial \hat{\Phi}}{\partial y} \right)_{i,1} \\ \left(\frac{\partial}{\partial y} |\bar{D}| \frac{\partial \hat{\Phi}}{\partial y} \right)_{i,J-1} &= -\frac{1}{\Delta} \left(|\bar{D}| \frac{\partial \hat{\Phi}}{\partial y} \right)_{i,J-2} \end{aligned} \right\} \quad (5.14)$$

Finally, although $\bar{\phi}$ is never used explicitly in the calculations, its reconstruction as given in [53] is erroneous on $y=0, Y$ since \bar{G}_y is not known on the boundary. Hence we cannot determine $\partial \bar{\phi}/\partial y$ on $y=0, Y$ and $\bar{\phi}$ can only be reconstructed for the interior half-points. Therefore Section 4c of [53] should be corrected to start the numerical quadrature by arbitrarily setting the datum $\bar{\phi}_{\frac{1}{2}, \frac{1}{2}}=0$ (rather than $\bar{\phi}_{\frac{1}{2}, -\frac{1}{2}}$) and summing to $J-1\frac{1}{2}$ (rather than to $J-\frac{1}{2}$). Hence $\bar{\phi}$ cannot be determined on the material boundaries.

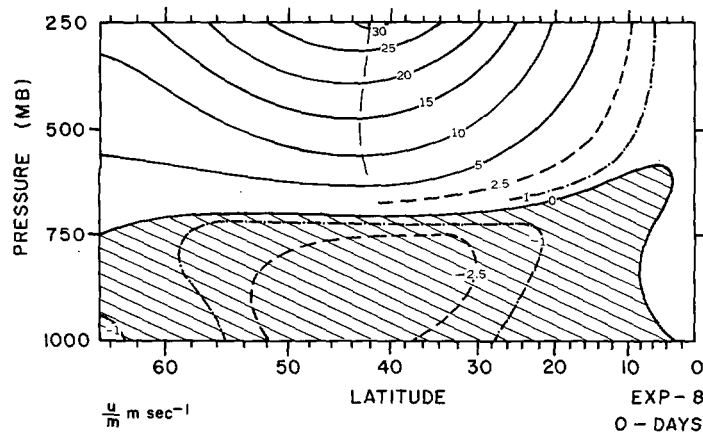


FIGURE 6.1.—The initial zonally symmetric zonal wind distribution. The negative values (hatched area) are easterly winds.

6. THE INITIAL CONDITIONS OF THE EXPERIMENT

The object was to begin the experiment in roughly the same way that Phillips did, i.e. to superimpose random disturbances on a zonally symmetric current which is baroclinically unstable according to linear theory. The virtue of this approach is that the creation of such a current computationally from rest by a radiative gradient can be accomplished relatively rapidly for the zonally symmetric equations, i.e. with $\partial/\partial x \equiv 0$. For such a system $\bar{v} = m^2 \partial \psi / \partial x \equiv 0$, thus insuring that $\bar{D} \equiv 0$. Hence the elliptic consistency condition on $\bar{\phi}$ to insure that $\partial \bar{D} / \partial t \equiv 0$ is not needed.

The creation of this zonally symmetric current was calculated by Phillips (personal communication) using half-hour time steps. Figure 6.1 gives the resulting zonal wind distribution u/m after five atmosphere weeks. This distribution has been interpolated from u_1 and u_3 . For the same time figure 6.2 gives the meridional wind component at 250 mb., $v_1/m (= -v_3/m)$, and the mean temperature, T_2 .

Without large-scale eddies a single direct meridional cell is mainly responsible for the northward heat flux. Since this is a relatively inefficient means for balancing the radiative gradient, the meridional temperature gradient continues to increase. As a result a west wind maximum is established at 250 mb. at about 42° latitude and weak easterlies appear at almost all latitudes at 750 and 1000 mb.

The quasi-geostrophic linear baroclinic stability criterion for a 2-level model in a rectangular domain has been worked out by Phillips [39] (also see our Appendix B). Figure 6.3 gives the conventional display of the critical stability curves for mid-latitudes as a function of the mean vertical shear of the zonal wind, the horizontal scale, and the static stability. For an effective static stability of 0.8 of the standard, instability occurs

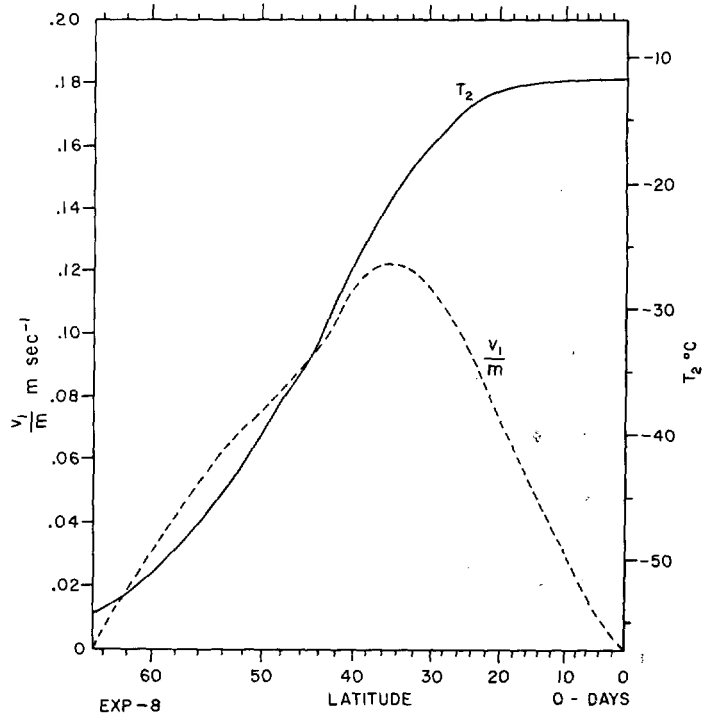


FIGURE 6.2.—The initial zonally symmetric 500-mb. temperature, T_2 (before the disturbance is introduced), and the meridional wind component at 250 mb., v_1/m .

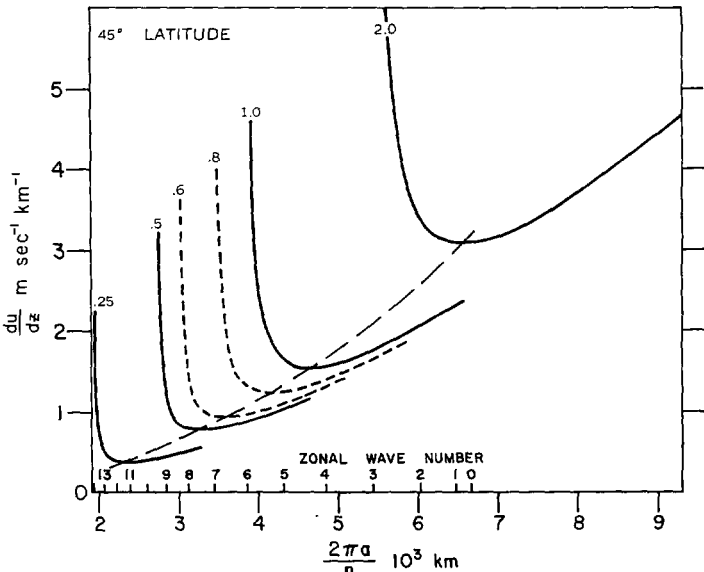


FIGURE 6.3.—Critical baroclinic stability curves [39] as a function of static stability for 45° latitude. Numbers on curves denote factor times standard stability ($2\gamma_s^2 = 8250 \text{ m}^2 \text{ sec}^{-2}$). The upper scale on the abscissa is the zonal wave number (the number of waves around the 45° latitude circle) for a meridional wave number of 6.

for $\partial U / \partial z > 1.2 \text{ m. sec.}^{-1} \text{ km.}^{-1}$ with a zonal wave number of maximum instability of 5 to 6. However, we see from figure 6.1 that the maximum shear at 40° latitude between 250 and 750 mb. is about $4 \text{ m. sec.}^{-1} \text{ km.}^{-1}$ with a mean

for all latitudes of about 3 m. sec.⁻¹ km.⁻¹. Hence the zonally symmetric current is supercritical according to linear theory.

In introducing a 2-dimensional disturbance it is expedient to disturb the temperature rather than the momentum since the latter would require balancing to satisfy $\bar{D} \equiv 0$. We therefore add a random distribution of temperature disturbances to the zonal mean such that its area mean value is zero with variance approximately 2.5° C. Since these disturbances were random only with respect to the entire domain, the latitudinal mean may have been changed by a fraction of a degree C. The available potential energy depends on the square of the perturbation temperature (see Section 8); consequently the two-dimensional disturbance adds a finite amount of available potential energy, most of which goes into that of the perturbation from the zonal mean. Of course the kinetic energy is unaltered.

At this point we set our time datum: $t=0$.

7. SYNOPTIC MANIFESTATIONS

As the baroclinic instability theory suggests, from the initial "white noise" disturbance, east-west wave numbers 5 and 6 are selected for growth at the expense of the available potential energy of the basic current (wave number zero). By approximately 10 days the initial transient motions are to a large extent damped and the flow undergoes a fairly orderly cyclic evolution of synoptic states with a period of 11 to 12 days. The details may be seen by mapping the synoptic properties at four stages spanning one such cycle at 14, 17, 20, and 23 days. This is shown in figures 7.1, 7.2, 7.3, and 7.4.

The evolution from 14 to 17 days is characterized by a transition from moderate amplitude disturbances with SW-NE tilt to practically zonal flow with disturbances of zero or slightly NW-SE tilt. We shall refer to the state of minimum perturbation amplitude as a "high index" state.* At this point we would expect a minimum in the northward transport of heat and momentum. By 20 days the meridional temperature gradient has increased radiatively and the disturbances are developing again. The 1000-mb. anticyclones are moving southward and the cyclones northward. The mid-latitude vertical motion field is becoming better organized in the large scale and is intensifying. Its relative phase to the temperature perturbations indicates transformations of potential to kinetic energy. The baroclinically unstable waves are now transporting momentum northward because of their SW-NE tilt. Heat is also transported northward because the isotherms lag to the west of the streamlines. In mid-latitudes the extremes of vertical velocity are about 3 cm. sec.⁻¹. At 23 days the disturbances have attained their maximum amplitude—that is "low index". The kinks

in the 1000-mb. contours suggest frontal structure—each of the waves is apparently in a slightly different stage of the occlusion process. One can also detect nascent secondary waves. The maps at 25 days (not included) are quite similar to those at 14 days.

The heating rate, which determines the rate of creation of zonal mean available potential energy, is considerably less than that occurring in winter. The calculated disturbances at 1000 mb. have a maximum difference between high and low geopotential equivalent to about 20 mb., which is close to what one observes in the annual mean. However none of these disturbances at low index is as intense as the most intense extratropical cyclones which one observes in the atmosphere. To understand this we first note that the calculated wave number 5 or 6 does correspond to the atmosphere. On the other hand, in the atmosphere, only 2 or 3 of the waves are very intense, the others being weak, which is unlike the present calculations where we have 5 or 6 waves of more-or-less uniform but moderate intensity. The distribution of continents and oceans through their kinematic and thermal influences excites waves of number 2 or 3. By linear argument, these forced quasi-stationary geographical waves may be superimposed on the shorter self-excited baroclinic waves, reinforcing the latter at some longitudes and counteracting at others. The net disturbance has a longitudinal bias with major trough activity at east coasts [51]. One would expect however that the geographically fixed long waves should contribute much less than the transient waves to the net meridional heat transfer. Hence in these calculations the purely self-excited disturbances of moderate amplitude, acting in concert, bring about the required total heat transfer which in the real atmosphere is mainly accomplished by the 2 or 3 most intense waves.

A word should be said of the small-scale vertical motion fields which appear at low latitudes. The extremes are rarely in excess of 10 cm. sec.⁻¹ and vary smoothly in time with a period of more than 12 hours. They vary in wavelength between 10° and 50° of longitude. Taking as an average 30° longitude at the equator, we find that internal gravitational waves with a phase velocity of $\gamma = 57.5$ m. sec.⁻¹ have a period of 16 hours. The maps show that the effect of these vertical motions on the horizontal flow and the temperature is small. It is speculated that these gravitational waves are excited at higher latitudes due to small departures from geostrophic balance, and are propagated in all directions, but amplify near the equator because of the proximity of the wall and the lack of the stabilizing influence of the earth's rotation. It may be that such divergent disturbances have a counterpart in the atmosphere even in the absence of a wall at the equator.

The discussion thus far has been qualitative, in order to relate the model evolutions to synoptic experience. We shall now attempt to determine the energy and transport properties of these evolutions and compare them with observations wherever possible.

*This definition of the index cycle departs from the traditional one which is based on variations of the intensity of the zonal wind. The present definition is chosen as a more sensitive and yet more clearly defined measure of essentially the same phenomenon.

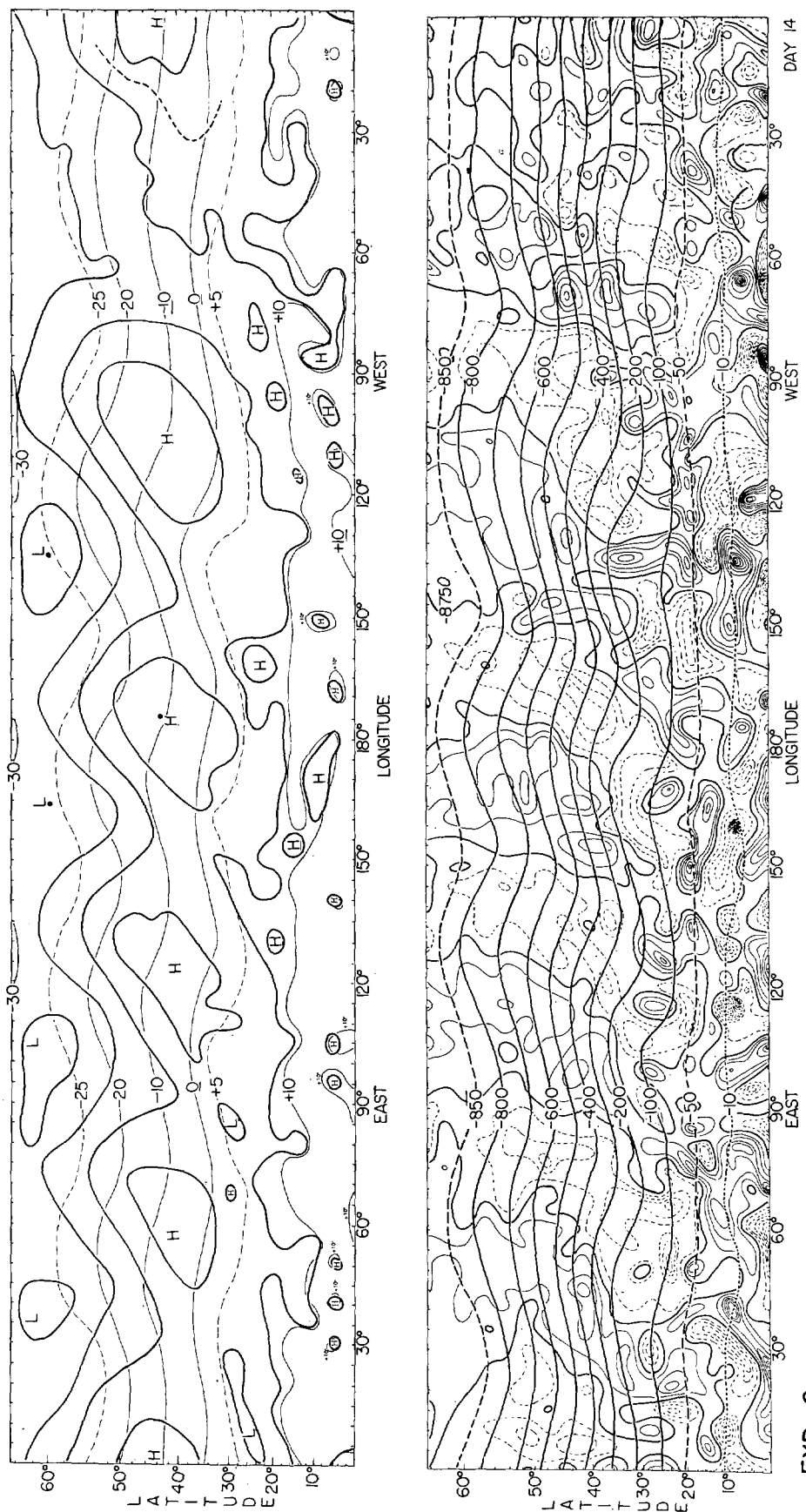


FIGURE 7.1.—Synoptic maps of forecast variables at 14 days. Upper map: ϕ_1 , 1000-mb. geopotential in intervals of $50 \text{ m.} \times 9.81 \text{ m. sec.}^{-2}$, origin arbitrary (heavy lines); T_2 , 500-mb. temperature, subtract 22 to obtain degrees Celsius (light lines). Lower map: ψ , the stream function corresponding to vertically integrated flow in intervals of $100 \text{ m.} \times 9.81 \times 10^4 \text{ m. sec.}^{-1}$, origin arbitrary (heavy lines); w_2 , the vertical velocity at 500 mb. for every cm. sec. -1 (heavy transverse lines are the nodes, light solid and dashed lines are $w_2 > 0$ and < 0 , respectively).

EXP - 8

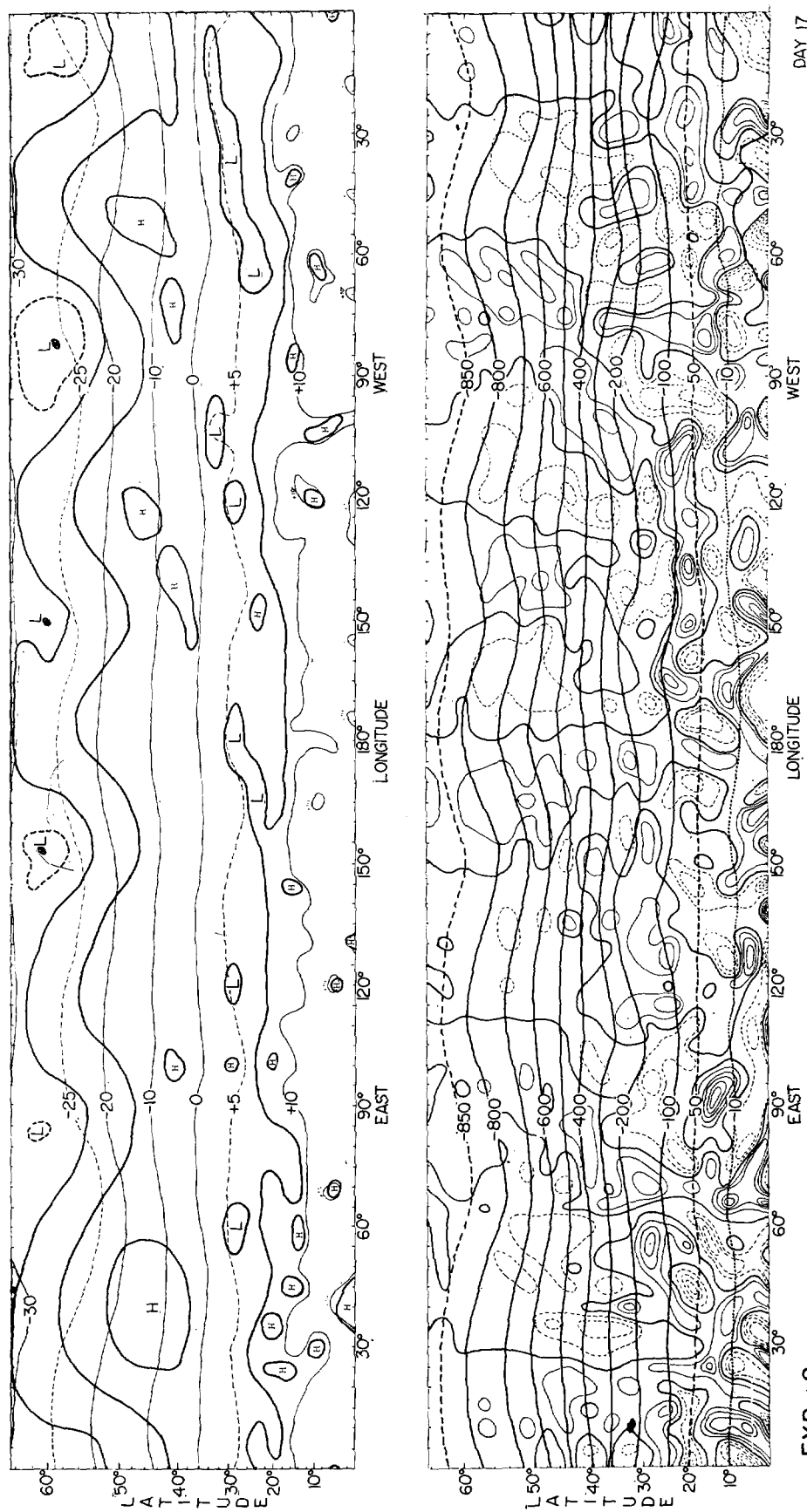


FIGURE 7.2.—Same as figure 7.1 but at 17 days.

EXP - 8

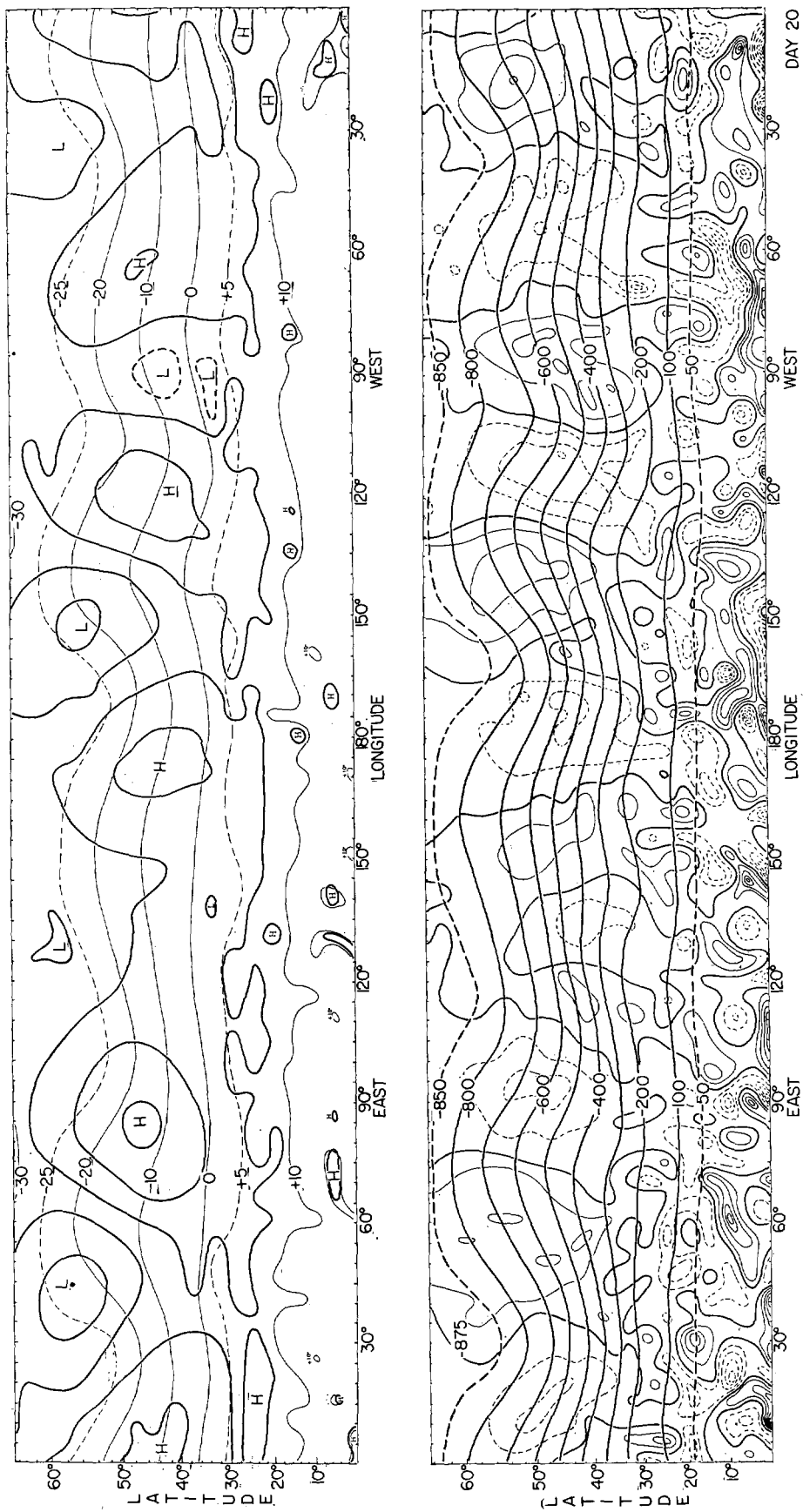


FIGURE 7.3.—Same as figure 7.1 but at 20 days.

EXP - 8

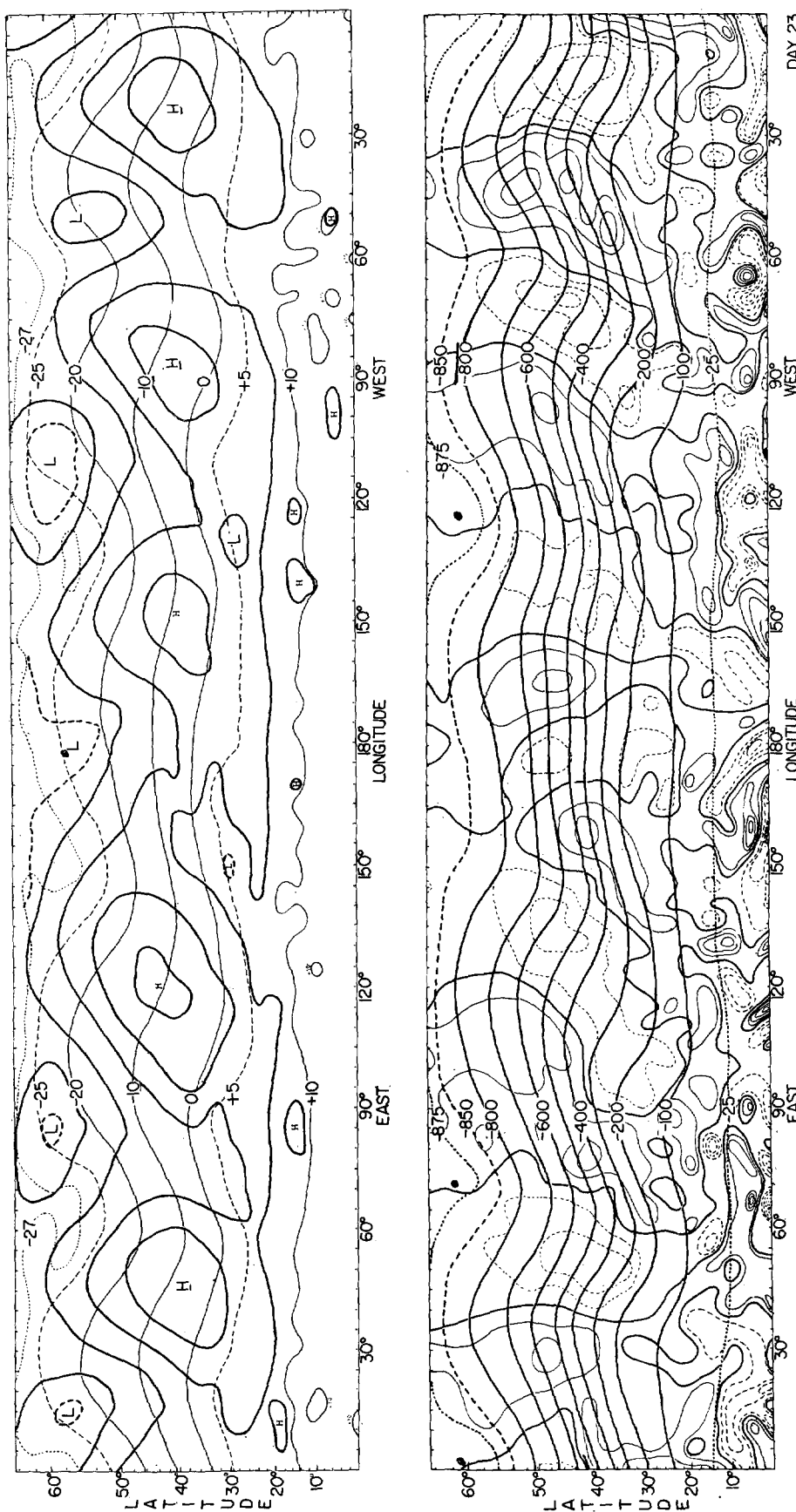


FIGURE 7.4.—Same as figure 7.1 but at 23 days.

EXP-8

8. THE ENERGY BALANCE AND THE TRANSFORMATIONS BY WHICH IT IS MAINTAINED

a. THE ENERGY COMPONENTS

From (C1), (C3), and (C7) we have that the area mean kinetic energy per unit mass may be written as

$$\frac{1}{2} \left\{ \left[\left(\frac{\mathbf{V}}{m} \right)^2 \right] \right\} = \frac{1}{2} \left\{ \left[\frac{u}{m} \right]^2 + \left[\frac{v}{m} \right]^2 \right\} + \frac{1}{2} \left\{ \left[\left(\frac{u'}{m} \right)^2 + \left(\frac{v'}{m} \right)^2 \right] \right\} \quad (8.1)$$

One may express the kinetic energy in a vertical column in terms of that of the vertical mean and vertical shear wind:

$$\frac{\mathbf{V}_1^2 + \mathbf{V}_3^2}{2m^2} = \frac{(\bar{\mathbf{V}})^2 + (\hat{\mathbf{V}})^2}{4m^2}$$

Hence the total kinetic energy is

$$K = \bar{K} + \hat{K} \quad (8.2)$$

where

$$\begin{aligned} \bar{K} &\equiv \left\{ \left[\left(\frac{\bar{\mathbf{V}}}{2m} \right)^2 \right] \right\} \equiv [\bar{K}] + \bar{K}' \\ \hat{K} &\equiv \left\{ \left[\left(\frac{\hat{\mathbf{V}}}{2m} \right)^2 \right] \right\} \equiv [\hat{K}] + \hat{K}' \end{aligned} \quad (8.3)$$

and

$$\begin{aligned} [\bar{K}] &\equiv [\bar{K}_x] \equiv \left\{ \left[\left(\frac{\bar{u}}{2m} \right)^2 \right] \right\}, \quad [\bar{K}_y] \equiv 0 \\ [\hat{K}] &\equiv [\hat{K}_x] + [\hat{K}_y], \quad [\hat{K}_x] \equiv \left\{ \left[\left(\frac{\hat{u}}{2m} \right)^2 \right] \right\}, \quad [\hat{K}_y] \equiv \left\{ \left[\left(\frac{\hat{v}}{2m} \right)^2 \right] \right\} \\ \bar{K}' &\equiv \left\{ \left[\left(\frac{\bar{u}'}{2m} \right)^2 + \left(\frac{\bar{v}'}{2m} \right)^2 \right] \right\} \\ \hat{K}' &\equiv \left\{ \left[\left(\frac{\hat{u}'}{2m} \right)^2 + \left(\frac{\hat{v}'}{2m} \right)^2 \right] \right\} \end{aligned} \quad (8.4)$$

where we have used $[\bar{v}] \equiv 0$. We note that \hat{K} contains the kinetic energy of the mean meridional circulation $[\hat{K}_y]$.

The available potential energy per unit mass [26] is

$$\mathcal{P}_d \equiv \frac{g}{2} \frac{\{ [T_2''] \}}{\{ [T_2(\Lambda_d - \Lambda)_2] \}} \quad (8.5)$$

where T_2'' is the deviation from the domain mean temperature as defined by (C10), $\Lambda = -\partial T/\partial z$ is the lapse rate, and $\Lambda_d = g/c_p$ is the adiabatic lapse rate. By [53(23)]

$$2\gamma_s^2 = \hat{p}^2 \left\{ \left[\frac{\partial \phi}{\partial p} \frac{\partial \ln \Theta}{\partial p} \right] \right\}_2 = \frac{R^2}{g} \{ [T_2(\Lambda_d - \Lambda)_2] \} \quad (8.6)$$

and

$$\hat{\phi} = RT_2 \quad (8.7)$$

then

$$\mathcal{P}_d = \left\{ \left[\left(\frac{\hat{\Phi}}{2\gamma_s} \right)^2 \right] \right\} \quad (8.8)$$

It will be more convenient for us to include the available latent energy, whence

$$\mathcal{P} \equiv \left\{ \left[\left(\frac{\hat{\Phi}}{2\gamma} \right)^2 \right] \right\} \quad (8.9)$$

where $\mathcal{P}_d/\mathcal{P} = \gamma^2/\gamma_s^2 = 0.8$. Hence with

$$\mathcal{P} \equiv [\mathcal{P}] + \mathcal{P}' \quad (8.10)$$

then

$$\begin{aligned} [\mathcal{P}] &\equiv \left\{ \left[\frac{\hat{\Phi}}{2\gamma} \right]^2 \right\} \\ \mathcal{P}' &\equiv \left\{ \left[\left(\frac{\hat{\Phi}'}{2\gamma} \right)^2 \right] \right\} \end{aligned} \quad (8.11)$$

Finally the total energy is

$$\mathcal{E} = K + \mathcal{P} = [\bar{K}_x] + [\hat{K}_x] + [\bar{K}_y] + [\mathcal{P}] + \bar{K}' + \hat{K}' + \mathcal{P}' \quad (8.12)$$

It is the seven energy components on the right side of (8.12) that we shall be concerned with.

b. DERIVATION OF THE ENERGY TRANSFORMATIONS

In order to calculate the energy transformation functions between components we define the transformation from a component A to a component B as $\langle A * B \rangle$. The transformation from B to A must be the negative

$$\langle A * B \rangle \equiv -\langle B * A \rangle \quad (8.13)$$

and since there may be no transformation between a component and itself then

$$\langle A * A \rangle \equiv 0 \quad (8.14)$$

Finally this convention is taken to follow the distributive law

$$\langle A * (B + C) \rangle \equiv \langle A * B \rangle + \langle A * C \rangle \quad (8.15)$$

If we denote the energy sources by S_k (S is not to be confused with the solar radiation notation of Appendix A) and energy sinks by F_j , then the rate of change of an energy component \mathcal{E}_i (i, j, k as used here are not to be confused with the space-difference indices) may be expressed as an interaction between it and all other components, the sources and the sinks

$$\frac{d\mathcal{E}_i}{dt} = \langle (\mathcal{E} + S + F) * \mathcal{E}_i \rangle \quad (8.16)$$

where summations are implied; i.e. $\mathcal{E} = \sum_i \mathcal{E}_i$, $S = \sum_k S_k$, $F = \sum_j F_j$.

In our formulation F_j will represent energy dissipations due to surface friction $v\bar{F}$, internal vertical momentum diffusion $v\mathbf{F}_1$, lateral momentum diffusion $h\mathbf{F}$, and lateral

heat diffusion H as defined by (4.18), (4.19), (4.22), and (4.26), respectively. S_e will represent energy sources due to Q_R as defined by (3.9), since the latent energy is included in our definition of \mathcal{P} .

The transformations between any two-way partition of total energy (say $\mathcal{E} = \mathcal{E}_1 + \mathcal{E}_2$) are uniquely determined from the energy equations. For more than a two-way partition, the transformations are no longer uniquely determined by the energy equations alone. For example, in a three-way partition it is always possible to add arbitrarily a "circulating" energy transformation, Ξ , which does not alter the energy equations.

$$\begin{aligned}\frac{\partial \mathcal{E}_1}{\partial t} &= (\langle \mathcal{E}_2 * \mathcal{E}_1 \rangle + \Xi) + (\langle \mathcal{E}_3 * \mathcal{E}_1 \rangle - \Xi) \\ \frac{\partial \mathcal{E}_2}{\partial t} &= -(\langle \mathcal{E}_2 * \mathcal{E}_1 \rangle + \Xi) + (\langle \mathcal{E}_3 * \mathcal{E}_2 \rangle + \Xi) \\ \frac{\partial \mathcal{E}_3}{\partial t} &= -(\langle \mathcal{E}_3 * \mathcal{E}_1 \rangle - \Xi) - (\langle \mathcal{E}_3 * \mathcal{E}_2 \rangle + \Xi)\end{aligned}$$

Therefore for lack of a closing condition, we shall have to appeal to intuitive heuristic arguments to arrive at the energy transformations corresponding to our partitioning.

To determine the energy transformations among the seven energy components in (8.12) and their external sources and sinks, we shall first form the energy equations for $[\bar{K}_x]$, $[\hat{K}_x]$, $[\hat{K}_y]$, $[\mathcal{P}]$, \bar{K} , \hat{K} , \mathcal{P} . We shall make free use of the identities (8.2), (8.3), (8.4), (8.10), and (8.12) without necessarily referring to them explicitly.

To form the equation for $[\bar{K}_x]$ we take the zonal mean of the x component of (2.6), multiply by $[\bar{u}]/2m^2$, integrate with respect to y and apply the boundary conditions (5.1), (5.2), and (5.6). In the above notation, we then have

$$\frac{\partial [\bar{K}_x]}{\partial t} = \langle \mathcal{E} * [\bar{K}_x] \rangle - \langle [\bar{K}_x] * F \rangle \quad (8.17)$$

where

$$\langle [\bar{K}_x] * S \rangle = 0 \quad (8.18)$$

since there are no external sources for $[\bar{K}_x]$,

$$\langle [\bar{K}_x] * F \rangle = \langle [\bar{K}_x] *_{H'} F \rangle + \langle [\bar{K}_x] *_{V'} F \rangle + \langle [\bar{K}_x] *_{V_1} F \rangle \quad (8.19)$$

and

$$\langle [\bar{K}_x] *_{V_1} F \rangle = 0 \quad (8.20)$$

$$\langle [\bar{K}_x] *_{H'} F \rangle = -\frac{1}{2} \left\{ \frac{[\bar{u}]}{m} [{}_H \bar{F}_x] \right\} = \frac{(k_H \Delta)^2}{2} \{ [D] [D_s] [D_s] \} \quad (8.21)$$

$$\langle [\bar{K}_x] *_{V'} F \rangle = -\frac{1}{2} \left\{ \frac{[\bar{u}]}{m} [{}_V \bar{F}_x] \right\} = \left(\frac{g \rho c_d}{2p} \right)_4 \left\{ \frac{[\bar{u}]}{m^3} [V_4] [u_4] \right\} \quad (8.22)$$

$$\begin{aligned}\langle \mathcal{E} * [\bar{K}_x] \rangle &= \frac{1}{2} \left\{ \frac{[\bar{u}]}{m^2} [\bar{v} \eta - \bar{u} D] \right\} \\ &= \frac{1}{2} \left\{ \frac{[\bar{u} \bar{v}]}{m^2} \frac{\partial [\bar{u}]}{\partial y} \right\} = \frac{1}{4} \left\{ \frac{[\bar{u} \bar{v} + \hat{u} \hat{v}]}{m^2} \frac{\partial [\bar{u}]}{\partial y} \right\}\end{aligned} \quad (8.23)$$

Since neither $[\hat{\Phi}]$ nor Φ' appears in (8.23) then

$$\langle [\mathcal{P}] * [\bar{K}_x] \rangle = 0 \quad (8.24)$$

leaving

$$\langle \bar{K} * [\bar{K}_x] \rangle = \frac{1}{4} \left\{ \frac{[\bar{u} \bar{v}]}{m^2} \frac{\partial [\bar{u}]}{\partial y} \right\} \quad (8.26)$$

and

$$\langle \hat{K} * [\bar{K}_x] \rangle = \frac{1}{4} \left\{ \frac{[\hat{u} \hat{v}]}{m^2} \frac{\partial [\bar{u}]}{\partial y} \right\} \quad (8.27)$$

Decomposing both sides of (8.26) and (8.27) into a zonal mean and perturbation correlations according to (C3) and remembering that $[\bar{v}] \equiv 0$, we obtain

$$\langle \bar{K}' * [\bar{K}_x] \rangle = \frac{1}{4} \left\{ \frac{[\bar{u}' \bar{v}']}{{m^2}} \frac{\partial [\bar{u}]}{\partial y} \right\} \quad (8.28)$$

$$\langle [\hat{K}'] * [\bar{K}_x] \rangle = \frac{1}{4} \left\{ \frac{[\hat{u}'] [\hat{v}']}{{m^2}} \frac{\partial [\bar{u}]}{\partial y} \right\} \quad (8.29)$$

$$\langle \hat{K}' * [\bar{K}_x] \rangle = \frac{1}{4} \left\{ \frac{[\hat{u}' \hat{v}']}{{m^2}} \frac{\partial [\bar{u}]}{\partial y} \right\} \quad (8.30)$$

Similarly we may form the equation for $[\hat{K}_x]$ by multiplying the zonal mean x component of (2.2) by $[\hat{u}]/2m^2$ and integrating as before:

$$\frac{\partial [\hat{K}_x]}{\partial t} = \langle \mathcal{E} * [\hat{K}_x] \rangle - \langle [\hat{K}_x] * F \rangle \quad (8.31)$$

where

$$\langle [\hat{K}_x] * S \rangle = 0 \quad (8.32)$$

$$\langle [\hat{K}_x] * F \rangle = \langle [\bar{K}_x] *_{H'} F \rangle + \langle [\hat{K}_x] *_{V'} F \rangle + \langle [\hat{K}_x] *_{V_1} F \rangle \quad (8.33)$$

$$\langle [\hat{K}_x] *_{H'} F \rangle = -\frac{1}{2} \left\{ \frac{[\hat{u}]}{m} [{}_H \hat{F}_x] \right\} = \frac{(k_H \Delta)^2}{2} \left\{ [D] [D_s] [\hat{D}_s] \right\} \quad (8.34)$$

$$\langle [\hat{K}_x] *_{V'} F \rangle = \frac{1}{2} \left\{ \frac{[\hat{u}]}{m} [{}_V \bar{F}_x] \right\} = -\left(\frac{g \rho c_d}{2p} \right)_4 \left\{ \frac{[\hat{u}]}{m^3} [V_4] [u_4] \right\} \quad (8.35)$$

$$\langle [\hat{K}_x] *_{\nu} F_1 \rangle = -\frac{1}{2} \left\{ \frac{[\hat{u}]}{m} [2_{\nu} F_{x_1}] \right\} = \left(\frac{g\rho}{p} \right)_2^2 K_2 \left\{ \frac{[\hat{u}]^2}{m^2} \right\} \quad (8.36)$$

$$\langle \mathcal{E} * [\hat{K}_x] \rangle = \frac{1}{2} \left\{ \frac{[\hat{u}]}{m^2} [\hat{v}\eta] \right\}$$

$$= \frac{1}{4} \left\{ \frac{[\bar{u}\hat{v} + \bar{v}\hat{u}]}{m^2} \frac{\partial[\hat{u}]}{\partial y} + \frac{[\hat{u}][\hat{D}\bar{u}]}{m^2} + \frac{2f[\hat{u}][\hat{v}]}{m^2} \right\} \quad (8.37)$$

$$\langle [\mathcal{P}] * [\hat{K}_x] \rangle = 0 \quad (8.38)$$

$$\langle \mathcal{P}' * [\hat{K}_x] \rangle = 0 \quad (8.39)$$

$$\begin{aligned} \langle ([\bar{K}_z] + [\hat{K}_y]) * [\hat{K}_z] \rangle &= \frac{1}{2} \left\{ \frac{[\hat{u}][\hat{v}]}{m^2} \left(f - \frac{m^2}{2} \frac{\partial[\bar{u}]/m^2}{\partial y} \right) \right\} \\ &= \frac{1}{2} \left\{ \frac{[\hat{u}][\hat{v}]}{m^2} \left(f + \frac{\alpha}{a} [\bar{u}] \right) \right\} - \frac{1}{4} \left\{ \frac{[u][\hat{v}]}{m^2} \frac{\partial[\bar{u}]}{\partial y} \right\} \\ &= \frac{1}{2} \left\{ \frac{[\bar{u}][\hat{v}]}{2m^2} \frac{\partial[\hat{u}]}{\partial y} + \frac{[\bar{u}][\hat{u}][\hat{D}]}{2m^2} + \frac{f[\hat{u}][\hat{v}]}{m^2} \right\} \quad (8.40) \end{aligned}$$

$$\begin{aligned} \langle K' * [\hat{K}_z] \rangle &= \frac{1}{2} \left\{ \widehat{[v'\zeta']} \frac{[\hat{u}]}{m^2} \right\} \\ &= \frac{1}{4} \left\{ \frac{[\bar{u}'\hat{v}' + \bar{v}'\hat{u}']}{{m^2}} \frac{\partial[\hat{u}]}{\partial y} + \frac{[\hat{u}][\hat{D}'\bar{u}']}{{m^2}} \right\} \quad (8.41) \end{aligned}$$

Comparing (8.40) with (8.29) we have that

$$\langle [\hat{K}_y] * [\hat{K}_x] \rangle = \frac{1}{2} \left\{ \frac{[\hat{u}][\hat{v}]}{m^2} \left(f + \frac{\alpha}{a} [\bar{u}] \right) \right\} \quad (8.42)$$

$$\langle [\hat{K}_x] * [\bar{K}_x] \rangle = \frac{1}{4} \left\{ \frac{[\hat{u}][\hat{v}]}{m^2} \frac{\partial[\bar{u}]}{\partial y} \right\} \quad (8.43)$$

$$\langle [\hat{K}_y] * [\bar{K}_x] \rangle = 0 \quad (8.44)$$

By multiplying the zonal mean y component of (2.2) by $[\hat{v}]/2m^2$ and integrating as before we have

$$\frac{\partial[\hat{K}_y]}{\partial t} = \langle \mathcal{E} * [\hat{K}_y] \rangle - \langle [\hat{K}_y] * F \rangle \quad (8.45)$$

in which

$$\langle [\hat{K}_y] *_{\nu} F \rangle = -\frac{1}{2} \left\{ \frac{[\hat{v}]}{m} [{}_{\nu} \hat{F}_y] \right\} = \frac{(k_H \Delta)^2}{2} \{ \widehat{[D] D_T] [\hat{D}_T]} \} \quad (8.46)$$

$$\langle [\hat{K}_y] *_{\nu} \bar{F} \rangle = \frac{1}{2} \left\{ \frac{[\hat{v}]}{m} [{}_{\nu} \bar{F}_y] \right\} = -\left(\frac{g\rho c_d}{2p} \right)_4 \left\{ \frac{[\hat{v}][|\nabla_d| v_d]}{m^3} \right\} \quad (8.47)$$

$$\langle [\hat{K}_y] *_{\nu} F_1 \rangle = -\frac{1}{2} \left\{ \frac{[\hat{v}]}{m} [2_{\nu} F_{y_1}] \right\} = \left(\frac{g\rho}{p} \right)_2^2 K_2 \left\{ \frac{[\hat{v}]^2}{m^2} \right\} \quad (8.48)$$

and

$$\langle \mathcal{E} * [\hat{K}_y] \rangle = -\frac{1}{2} \left\{ \frac{[\hat{v}]}{m^2} \left[\widehat{u\eta} + m^2 \frac{\partial[\hat{B}]}{\partial y} \right] \right\} \quad (8.49)$$

The available potential energy conversions must be due
673039-63—3

to the $\hat{\Phi}$ part of \hat{B} :

$$\langle \mathcal{P} * [\hat{K}_y] \rangle = \langle [\mathcal{P}] * [\hat{K}_y] \rangle = -\frac{1}{2} \left\{ [\hat{v}] \frac{\partial[\hat{\Phi}]}{\partial y} \right\} = \frac{1}{2} \left\{ [\hat{\Phi}] [\hat{D}] \right\}$$

$$(8.50)$$

$$\langle \mathcal{P}' * [\hat{K}_y] \rangle = 0 \quad (8.51)$$

The remainder of (8.49) only involving mean quantities is:

$$\langle [K] * [\hat{K}_y] \rangle = \langle [K_x] * [\hat{K}_y] \rangle = -\frac{1}{2} \left\{ \frac{[\hat{u}][\hat{v}]}{m^2} \left(f + \frac{\alpha}{a} [\bar{u}] \right) \right\} \quad (8.52)$$

which is identical with (8.42). Finally

$$\langle K' * [\hat{K}_y] \rangle = -\frac{1}{2} \left\{ \widehat{[u'\zeta']} \frac{[\hat{v}]}{m^2} - \frac{[\bar{u}'^2 + \bar{v}'^2]}{2m^2} [\hat{D}] \right\} \quad (8.53)$$

The equation for the fourth and remaining zonal mean energy component $[\mathcal{P}]$ is obtained by multiplying the zonal mean of (3.10) by $[\hat{\Phi}]/2\gamma^2$ and integrating as before:

$$\frac{\partial[\mathcal{P}]}{\partial t} = \langle \mathcal{E} * [\mathcal{P}] \rangle - \langle [\mathcal{P}] * F \rangle + \langle S * [\mathcal{P}] \rangle \quad (8.54)$$

$$\langle S * [\mathcal{P}] \rangle = \langle Q_R * [\mathcal{P}] \rangle = \frac{\kappa}{2\gamma^2} \{ [\hat{\Phi}] [Q_R] \}$$

$$= \frac{\kappa g}{p_4 2\gamma^2} \{ [\hat{\Phi}] [c_R - \frac{b}{R} \hat{\Phi}] \} \quad (8.55)$$

$$\langle [\mathcal{P}] * F \rangle = \langle [\mathcal{P}] * H \rangle = -\frac{1}{2\gamma^2} \{ [\hat{\Phi}] [H] \}$$

$$= \left(\frac{\kappa_H \Delta}{2\gamma} \right)^2 \left\{ m^2 \left[|\bar{D}| \frac{\partial[\hat{\Phi}]}{\partial y} \right] \frac{\partial[\hat{\Phi}]}{\partial y} \right\} \quad (8.56)$$

$$\langle \mathcal{E} * [\mathcal{P}] \rangle = \frac{1}{2} \left\{ \frac{[\hat{\Phi}]}{2} \frac{\partial}{\partial y} \frac{[\hat{\Phi}]}{\gamma^2} - [\hat{\Phi}] [\hat{D}] \right\} \quad (8.57)$$

The mean part of (8.57) is consistent with (8.24), (8.38), and (8.50). Since the perturbation part involves $\hat{\Phi}'$ then

$$\langle K' * [\mathcal{P}] \rangle = 0 \quad (8.58)$$

and

$$\langle \mathcal{E}' * [\mathcal{P}] \rangle = \langle \mathcal{P}' * [\mathcal{P}] \rangle = \frac{1}{2} \left\{ \frac{[\hat{\Phi}'v']}{2} \frac{\partial}{\partial y} \frac{[\hat{\Phi}]}{\gamma^2} \right\} \quad (8.59)$$

To form the equation for \bar{K} , we take the scalar product of $\bar{\nabla}/2m^2$ and (2.6), integrate over the domain, while applying the boundary conditions (5.1), (5.2), and (5.6).

$$\frac{\partial \bar{K}}{\partial t} = \langle \mathcal{E} * \bar{K} \rangle - \langle \bar{K} * F \rangle + \langle S * \bar{K} \rangle \quad (8.60)$$

where

$$\langle S * \bar{K} \rangle = 0 \quad (8.61)$$

$$\langle \bar{K}^* F \rangle = \langle \bar{K}^* {}_H F \rangle + \langle \bar{K}^* {}_v F \rangle + \langle \bar{K}^* {}_{F_1} \rangle \quad (8.62)$$

$$\langle \bar{K}^* {}_{F_1} \rangle = 0 \quad (8.63)$$

$$\begin{aligned} \langle \bar{K}^* {}_H F \rangle &= -\frac{1}{2} \left\{ \left[\frac{\nabla}{m} \cdot {}_H \bar{F} \right] \right\} \\ &= \frac{(k_H \Delta)^2}{2} \{ [D] D_s \bar{D}_s + [D] D_T \bar{D}_T \} \end{aligned} \quad (8.64)$$

$$\langle \bar{K}^* {}_v F \rangle = -\frac{1}{2} \left\{ \left[\frac{\nabla}{m} \cdot {}_v \bar{F} \right] \right\} = \left(\frac{g \rho c_d}{2p} \right)_4 \left\{ \frac{[|\nabla|] (uu_4 + vv_4)}{m^3} \right\} \quad (8.65)$$

and

$$\langle \mathcal{E}^* \bar{K} \rangle = \frac{1}{2} \left\{ \left[\frac{\hat{u}\hat{v} - \hat{u}\bar{v}}{2m^2} \hat{\zeta} - \frac{\hat{u}^2 + v^2}{2m^2} \hat{D} \right] \right\} \quad (8.66)$$

Since $\hat{\Phi}$ does not appear then

$$\langle P^* \bar{K} \rangle = 0 \quad (8.67)$$

and

$$\langle \mathcal{E}^* \bar{K} \rangle = \langle \hat{K}^* \bar{K} \rangle \quad (8.68)$$

Upon expanding (8.68) into zonal mean and perturbation parts we have

$$\langle \hat{K}^* \bar{K} \rangle = \langle \hat{K}^* [\bar{K}_x] \rangle + \langle \hat{K}^* \bar{K}' + \hat{K}'^* [\bar{K}_x] \rangle + \langle \hat{K}'^* \bar{K}' \rangle \quad (8.69)$$

Therefore that part of (8.66) involving only transformations between mean partitions, $\langle \hat{K}^* [\bar{K}_x] \rangle$ is given by (8.29). The interaction between zonal mean and perturbation partitions (the middle term on the right side of (8.69)) is obtained by expanding (8.66) and extracting:

$$\begin{aligned} \langle \hat{K}^* \bar{K}' + \hat{K}'^* [\bar{K}_x] \rangle &= \\ &- \frac{1}{4} \left\{ -[\bar{u}' \hat{\zeta}'] \frac{[\hat{v}]}{m^2} + \frac{[\hat{u}^2 + v'^2]}{m^2} \hat{D} \right\} + [\bar{v}' \hat{\zeta}'] \frac{[\hat{u}]}{m^2} \\ &- \frac{[\hat{v}' \bar{u}' - \hat{u}' \bar{v}']}{m^2} \hat{\zeta} + 2[\hat{u}' \hat{D}'] \frac{[\hat{u}]}{m^2} + 2[\hat{v}' \hat{D}'] \frac{[\hat{v}]}{m^2} \\ &- \frac{[\hat{u}' \hat{v}']}{{m^2}} \frac{\partial [\bar{u}]}{\partial y} \} \end{aligned} \quad (8.70)$$

Upon subtracting (8.30) we have

$$\begin{aligned} \langle \bar{K}'^* [\hat{K}] \rangle &= \langle K'^* [\hat{K}_x] \rangle + \langle K'^* [\hat{K}_y] \rangle - \langle \hat{K}'^* [\hat{K}] \rangle \\ &= \frac{1}{4} \left\{ -[\bar{u}' \hat{\zeta}'] \frac{[\hat{v}]}{m^2} + \frac{[\hat{u}^2 + v'^2]}{m^2} \hat{D} \right\} + [\bar{v}' \hat{\zeta}'] \frac{[\hat{u}]}{m^2} \\ &- \frac{[\hat{v}' \bar{u}' - \hat{u}' \bar{v}']}{{m^2}} \hat{\zeta} + 2[\hat{u}' \hat{D}'] \frac{[\hat{u}]}{m^2} + 2[\hat{v}' \hat{D}'] \frac{[\hat{v}]}{m^2} \} \end{aligned} \quad (8.71)$$

Since $\langle K'^* [\hat{K}_x] \rangle$ and $\langle K'^* [\hat{K}_y] \rangle$ are known from (8.41) and (8.53) then

$$\begin{aligned} \langle \hat{K}'^* [\hat{K}] \rangle &= \frac{1}{4} \left\{ [\bar{v}' \hat{\zeta}'] \frac{[\hat{u}]}{m^2} - [\hat{u}' \bar{\zeta}'] \frac{[\hat{v}]}{m^2} \right. \\ &\left. + \frac{[\hat{v}' \bar{u}' - \hat{u}' \bar{v}']}{{m^2}} \hat{\zeta} - 2[\hat{u}' \hat{D}'] \frac{[\hat{u}]}{m^2} - 2[\hat{v}' \hat{D}'] \frac{[\hat{v}]}{m^2} \right\} \end{aligned} \quad (8.72)$$

Those parts of (8.71) and (8.72) due to $[\hat{K}_x]$ must involve $[\hat{u}]$ and $[\hat{\zeta}] = -m^2 \partial([\hat{u}]/m^2)/\partial y$ while those due to $[\hat{K}_y]$ must involve $[\hat{v}]$ and $[\hat{D}] = m^2 \partial([\hat{v}]/m^2)/\partial y$ from which we conclude that

$$\langle \bar{K}'^* [\hat{K}_x] \rangle = \frac{1}{4} \left\{ [\bar{v}' \hat{\zeta}'] \frac{[\hat{u}]}{m^2} - \frac{[\hat{v}' \bar{u}' - \hat{u}' \bar{v}']}{{m^2}} \hat{\zeta} + 2[\hat{u}' \hat{D}'] \frac{[\hat{u}]}{m^2} \right\} \quad (8.73)$$

$$\langle \bar{K}'^* [\hat{K}_y] \rangle = \frac{1}{4} \left\{ -[\bar{u}' \hat{\zeta}'] \frac{[\hat{v}]}{m^2} + \frac{[u^2 + v'^2]}{m^2} \hat{D} \right\} + 2[\hat{v}' \hat{D}'] \frac{[\hat{v}]}{m^2} \quad (8.74)$$

$$\langle \hat{K}'^* [\hat{K}_x] \rangle = \frac{1}{4} \left\{ [\hat{v}' \bar{\zeta}'] \frac{[\hat{u}]}{m^2} + \frac{[\hat{v}' \bar{u}' - \hat{u}' \bar{v}']}{{m^2}} \hat{\zeta} - 2[\hat{u}' \hat{D}'] \frac{[\hat{u}]}{m^2} \right\} \quad (8.75)$$

$$\langle \hat{K}'^* [\hat{K}_y] \rangle = \frac{1}{4} \left\{ -[\hat{u}' \bar{\zeta}'] \frac{[\hat{v}]}{m^2} - 2[\hat{v}' \hat{D}'] \frac{[\hat{v}]}{m^2} \right\} \quad (8.76)$$

Upon comparing (8.73) with (8.75) we note some terms in common but with opposite signs. These must represent an *indirect* transformation between \hat{K}' and \bar{K}' through $[\hat{K}_x]$, for if it were direct $[\hat{u}]$ and $[\hat{\zeta}]$ would not appear. Hence $[\hat{K}_x]$ acts *catalytically*, i.e. it is not changed despite its participation in the transformation.

If two transformations $\langle A^* C \rangle$ and $\langle C^* B \rangle$ are catalytic with respect to their common energy component C then each may be expressed as the sum of a catalytic part and a non-catalytic part:

$$\begin{aligned} \langle A^* C \rangle &= \langle A^* C \rangle_c + \langle A^* C \rangle_{NC} \\ \langle C^* B \rangle &= \langle C^* B \rangle_c + \langle C^* B \rangle_{NC} \end{aligned} \quad (8.77)$$

Since by definition the catalytic parts satisfy

$$\langle A^* C \rangle_c = \langle C^* B \rangle_c \quad (8.78)$$

we may define

$$\langle A^* C^* B \rangle \equiv -\langle B^* C^* A \rangle \equiv \frac{\langle A^* C \rangle_c + \langle C^* B \rangle_c}{2} \quad (8.79)$$

Also by subtracting (8.77) and (8.78) we have

$$\langle A^* C \rangle - \langle C^* B \rangle = \langle A^* C \rangle_{NC} - \langle C^* B \rangle_{NC} \quad (8.80)$$

Hence (8.73) and (8.75) give

$$\begin{aligned} \langle \bar{K}'^* [\hat{K}_x]^* \hat{K}' \rangle &\equiv -\langle \hat{K}'^* [\hat{K}_x]^* \bar{K}' \rangle \\ &= -\frac{1}{2} \left\{ \frac{[\hat{v}' \bar{u}' - \hat{u}' \bar{v}']}{{m^2}} \hat{\zeta} - [\hat{u}' \hat{D}'] \frac{[\hat{u}]}{m^2} \right\} \end{aligned} \quad (8.81)$$

$$\langle \bar{K}'^* [\hat{K}_x] \rangle_{NC} = \frac{1}{4} \left\{ [\bar{v}' \hat{\zeta}'] \frac{[\hat{u}]}{m^2} \right\} \quad (8.82)$$

$$\langle \hat{K}'^* [\hat{K}_x] \rangle_{NC} = \frac{1}{4} \left\{ [\hat{v}' \bar{\zeta}'] \frac{[\hat{u}]}{m^2} \right\} \quad (8.83)$$

Similarly a comparison of (8.74) and (8.76) yields the catalytic eddy kinetic energy exchange through \hat{K}_v :

$$\langle \bar{K}' * \hat{K}_v * \hat{K}' \rangle = -\langle \hat{K}' * [\hat{K}_v] * \bar{K}' \rangle = \frac{1}{2} \left\{ \widehat{[v' D']} \frac{[\hat{v}]}{m^2} \right\} \quad (8.84)$$

$$\langle \bar{K}' * [\hat{K}_v] \rangle_{NC} = \frac{1}{4} \left\{ -[\bar{u}' \hat{\zeta}'] \frac{[\hat{v}]}{m^2} + \widehat{[u'^2 + v'^2]} [\hat{D}] \right\} \quad (8.85)$$

$$\langle \hat{K}' * [\hat{K}_v] \rangle_{NC} = \frac{1}{4} \left\{ -[\hat{u}' \bar{\zeta}'] \frac{[\hat{v}]}{m^2} \right\} \quad (8.86)$$

We now go to the *direct* transformation between \hat{K}' and \bar{K}' which follows from the pure perturbation terms of the expansion of (8.66) according to (8.68) and (8.69):

$$\langle \hat{K}' * \bar{K}' \rangle = \frac{1}{4} \left\{ \frac{1}{m^2} [(\bar{u}' \hat{v}' - \hat{u}' \bar{v}') \hat{\zeta}' - \widehat{(u'^2 + v'^2)} \hat{D}'] \right\} \quad (8.87)$$

The equation for the total shear kinetic energy \hat{K} is formed by the scalar multiplication of $\hat{V}/2m^2$ and (2.2), and integrating as before:

$$\frac{\partial \hat{K}}{\partial t} = \langle \mathcal{E} * \hat{K} \rangle - \langle \hat{K} * F \rangle + \langle S * \hat{K} \rangle \quad (8.88)$$

in which

$$\langle S * \hat{K} \rangle = 0 \quad (8.89)$$

Also

$$\langle \hat{K} * F \rangle = \langle \hat{K}_{*H} F \rangle + \langle \hat{K}_{*v} \bar{F} \rangle + \langle \hat{K}_{*v} F_1 \rangle \quad (8.90)$$

where

$$\begin{aligned} \langle \hat{K}_{*H} F \rangle &= -\frac{1}{2} \left\{ \left[\frac{\hat{V}}{m} \cdot H \hat{F} \right] \right\} \\ &= \frac{(k_H \Delta)^2}{2} \left\{ \left[\widehat{D} \widehat{D_s} \hat{D}_s + \widehat{D} \widehat{D_t} \hat{D}_t \right] \right\} \end{aligned} \quad (8.91)$$

$$\begin{aligned} \langle \hat{K}_{*v} \bar{F} \rangle &= \frac{1}{2} \left\{ \left[\frac{\hat{V}}{m} \cdot v \bar{F} \right] \right\} \\ &= -\left(\frac{g \rho c_d}{2p} \right)_4 \left\{ \left[\frac{|\mathbf{V}_4| (\hat{u} u_4 + \hat{v} v_4)}{m^3} \right] \right\} \end{aligned} \quad (8.92)$$

$$\begin{aligned} \langle \hat{K}_{*v} F_1 \rangle &= -\frac{1}{2} \left\{ \left[\frac{\hat{V}}{m} \cdot 2v F_1 \right] \right\} \\ &= \left(\frac{g \rho}{p} \right)_2 K_2 \left\{ \left[\left(\frac{\hat{u}}{m} \right)^2 + \left(\frac{\hat{v}}{m} \right)^2 \right] \right\} \end{aligned} \quad (8.93)$$

$$\langle \mathcal{E} * \hat{K} \rangle = \frac{1}{2} \left\{ \left[\hat{\Phi} \hat{D} \right] \right\} - \frac{1}{2} \left\{ \left[\frac{\bar{u} \hat{v} - \hat{u} \bar{v}}{2m^2} \hat{\zeta} - \widehat{\frac{u^2 + v^2}{2m^2}} \hat{D} \right] \right\} \quad (8.94)$$

Comparison of (8.94) with (8.66) and (8.68) requires that

$$\langle \mathcal{P} * \hat{K} \rangle = \frac{1}{2} \left\{ \left[\hat{\Phi} \hat{D} \right] \right\} \quad (8.95)$$

Expanding both sides into zonal mean and perturbation components gives upon using (8.38), (8.39), (8.50), and (8.51) that

$$\langle [\mathcal{P}] * \hat{K}' + \mathcal{P}' * \hat{K}' \rangle = \frac{1}{2} \left\{ \left[\hat{\Phi}' \hat{D}' \right] \right\} \quad (8.96)$$

Since the right side involves only perturbation correlations

$$\langle [\mathcal{P}] * \hat{K}' \rangle = 0 \quad (8.97)$$

$$\langle \mathcal{P}' * \hat{K}' \rangle = \frac{1}{2} \{ \hat{\Phi}' \hat{D}' \} \quad (8.98)$$

Equation (8.97) with (8.58) gives

$$\langle [\mathcal{P}] * \bar{K}' \rangle = 0 \quad (8.99)$$

Finally we multiply (3.10) by $\hat{\Phi}/2\gamma^2$ and integrate over the domain as before giving:

$$\frac{\partial \mathcal{P}}{\partial t} = \langle \mathcal{E} * \mathcal{P} \rangle - \langle \mathcal{P} * F \rangle + \langle S * \mathcal{P} \rangle \quad (8.100)$$

where

$$\langle S * \mathcal{P} \rangle = \langle Q_R * \mathcal{P} \rangle = \frac{\kappa}{2\gamma^2} \{ [\hat{\Phi} Q_R] \} = \frac{\kappa g}{2\gamma^2 p_4} \{ [\hat{\Phi} (c_R - \frac{b}{R} \hat{\Phi})] \} \quad (8.101)$$

$$\langle \mathcal{P} * F \rangle = \langle \mathcal{P} * H \rangle = -\frac{1}{2\gamma^2} \{ [\hat{\Phi} H] \} = \left(\frac{k_H \Delta}{2\gamma} \right)^2 \{ |\bar{D}| (\nabla \hat{\Phi})^2 \} \quad (8.102)$$

$$\langle \mathcal{E} * \mathcal{P} \rangle = -\frac{1}{2} \{ [\hat{\Phi} \hat{D}] \} \quad (8.103)$$

From (8.95) we therefore have that

$$\langle \mathcal{E} * \mathcal{P} \rangle = \langle \hat{K} * \mathcal{P} \rangle \quad (8.104)$$

so that

$$\langle \bar{K} * \mathcal{P} \rangle = 0 \quad (8.105)$$

Therefore by (8.24), (8.25), and (8.99) we have

$$\langle \mathcal{P}' * \bar{K}' \rangle = 0 \quad (8.106)$$

To obtain the losses and gains of energy by the perturbation components we use the identity

$$\langle F_j * \mathcal{E}_i' \rangle \equiv \langle F_j * \mathcal{E}_i \rangle - \langle F_j * [\mathcal{E}_i] \rangle \quad (8.107)$$

and similarly for $\langle S_k * \mathcal{E}_i' \rangle$.

The non-zero transformations derived in this sub-section are diagrammatically summarized in figure 8.1.

Our transformations $\langle [\mathcal{P}] * \mathcal{P}' \rangle, \langle \mathcal{P}' * K' \rangle = \langle \mathcal{P}' * \hat{K}' \rangle$, and

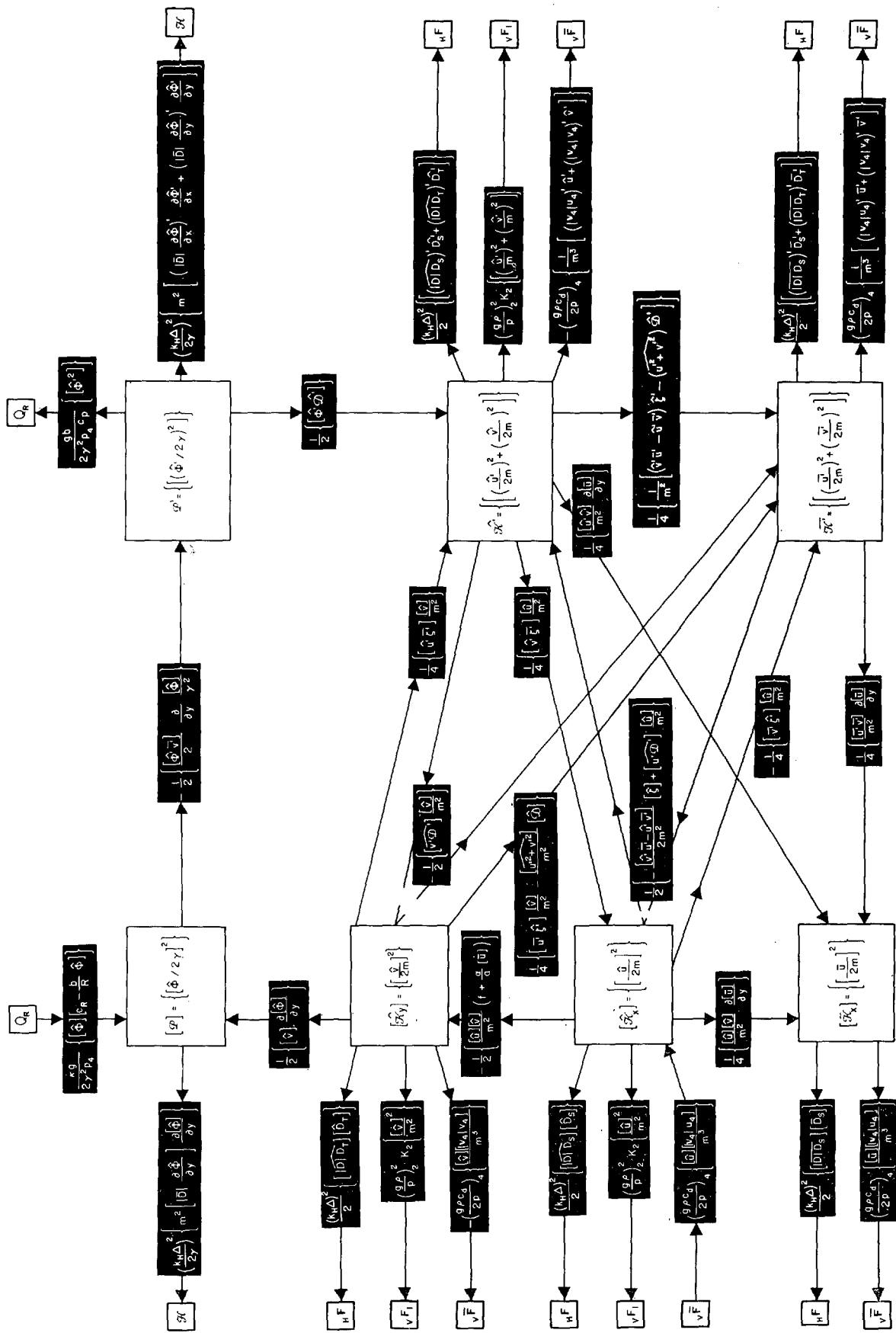


FIGURE 8.1.—The energy partitions (white interior boxes), sources (white boxes across top), and sinks (white boxes on left and right sides), and the transformations between them (black boxes). The left half of the diagram involves the zonal mean partitions and the right half the perturbations.

$\langle [K] * [\mathcal{P}] \rangle = \langle \hat{K}_v * [\mathcal{P}] \rangle$ as given by (8.59), (8.98) and (8.50), respectively, are the same form as Phillips', with his requirement that the geostrophic wind and vertical velocity be used. On the other hand our $\langle K' * [K] \rangle$, obtained by adding (8.41), (8.120), (8.121):

$$\begin{aligned} \langle K' * [K] \rangle &= \left\{ \frac{[u'v']}{{m^2}} \frac{\partial[\bar{u}]}{\partial y} \right\} + \frac{1}{2} \left\{ \frac{[\hat{u}]}{{m^2}} \overbrace{[\mathcal{D}'u']} \right\} \\ &\quad - \frac{1}{2} \left\{ \overbrace{[u']\hat{s}'} \frac{[\hat{v}]}{{m^2}} - \frac{[u'^2+v'^2]}{2m^2} [\hat{\mathcal{D}}] \right\} \end{aligned} \quad (8.107a)$$

differs from Phillips' in form. On the right side only the first term corresponds to that of Phillips, being the sum of $\langle K' * [\bar{K}_x] \rangle$ and part of $\langle K' * [\hat{K}_v] \rangle$. The second term is the remainder of $\langle K' * [\hat{K}_z] \rangle$ and the last is $\langle K' * [\hat{K}_v] \rangle$. The last two terms are essentially ageostrophic and their relative magnitudes will be discussed in Section 8f.

Before analyzing our experimental results in terms of the energy transformation functions, we shall examine the properties of the transformations in terms of the observed atmosphere.

c. PROPERTIES OF THE TRANSFORMATIONS INVOLVING ONLY THE ZONALLY SYMMETRIC CIRCULATION

From (8.55) we see that for the zonal mean external energy sources to create zonal mean available potential energy requires $\{\hat{\Phi}[Q_R]\} > 0$. Since $\{\hat{\Phi}\} = \{[Q_R]\} = 0$, then by (C10) the requirement is that

$$\{\hat{\Phi}[Q_R]\} = \{\hat{\Phi}[Q'_R]\} > 0$$

i.e., the variations in heating must be positively correlated with those of temperature.

We note from the difference of (8.42) and (8.50)

$$\langle \hat{K}_v * [\hat{K}_x] \rangle - \langle [\mathcal{P}] * \hat{K}_v \rangle = \frac{1}{2} \left\{ [\hat{v}] \left(\frac{\partial[\hat{\Phi}]}{\partial y} + \frac{[\hat{u}]}{{m^2}} \left(f + \frac{\alpha}{a} [\bar{u}] \right) \right) \right\} \quad (8.108)$$

that in the absence of other transformations with \hat{K}_v , a direct meridional circulation ($[\hat{v}] > 0$) will suffer a decrease in kinetic energy if $[\hat{u}]$ is super-geostrophic, but will increase its kinetic energy if $[\hat{u}]$ is sub-geostrophic. The opposite is true for an indirect circulation ($[\hat{v}] < 0$). Hence in order to maintain the mean meridional circulation against frictional dissipation, $[\hat{u}]$ must be sub-geostrophic in a direct circulation and super-geostrophic in an indirect circulation. Since $f + \alpha[\bar{u}]/a = 2\alpha(\Omega + [\lambda]/2)$, then it represents an absolute Coriolis parameter with respect to the vertically integrated motion of the atmospheric shell. On the other hand, if $[\hat{u}]$ is geostrophic, then \hat{K}_v is catalytic with respect to transformations between $[\mathcal{P}]$ and $[\bar{K}_x]$ so that by (8.79),

$$\langle [\mathcal{P}] * \hat{K}_v * [\hat{K}_x] \rangle = -\frac{1}{2} \left\{ [\hat{v}] \frac{\partial[\hat{\Phi}]}{\partial y} \right\} = \frac{1}{2} \left\{ \frac{[\hat{u}][\hat{v}]}{{m^2}} \left(f + \frac{\alpha}{a} [\bar{u}] \right) \right\} \quad (8.109)$$

for the typical atmospheric case of $\partial[\hat{\Phi}]/\partial y < 0$, then (8.109) is positive in a direct meridional circulation and negative in an indirect.

From the difference between (8.43) and (8.42)

$$\langle \hat{K}_x * [\bar{K}_x] \rangle - \langle \hat{K}_v * [\hat{K}_x] \rangle = -\frac{1}{4} \left\{ \frac{[\hat{u}][\hat{v}]}{{m^2}} [\bar{\eta}] \right\} \quad (8.110)$$

we see that with $[\hat{u}] > 0$ and the absolute vorticity of the zonal mean vertically integrated current (the barotropic component) $[\bar{\eta}]/2 > 0$ the combined contribution from $[\bar{K}_x]$ and \hat{K}_v will be to increase $[\hat{K}_x]$ in a direct circulation and to decrease it in an indirect circulation. Whether there is a net domain increase or decrease of $[\hat{K}_x]$ will depend on whether the Hadley circulation has low or high intensity. If $[\bar{\eta}]$ were zero then \hat{K}_x is catalytic with respect to \hat{K}_v and $[\bar{K}_x]$ so that

$$\langle \hat{K}_v * [\hat{K}_x] * [\bar{K}_x] \rangle = \frac{1}{2} \left\{ \frac{[\hat{u}][\hat{v}]}{{m^2}} \left(f + \frac{\alpha}{a} [\bar{u}] \right) \right\} = \frac{1}{4} \left\{ \frac{[\hat{u}][\hat{v}]}{{m^2}} \frac{\partial[\bar{u}]}{\partial y} \right\} \quad (8.111)$$

Observationally we know the atmosphere does not behave this way.

Finally if \hat{v} were geostrophic ($= \frac{m^2}{f} \frac{\partial \hat{\Phi}}{\partial x}$), then $[\hat{v}] \equiv 0$, $[\hat{K}_v] \equiv 0$ and

$$\langle [\mathcal{P}] * \hat{K}_v \rangle = \langle \hat{K}_v * [\hat{K}_x] \rangle = \langle \hat{K}_x * [\bar{K}_x] \rangle = 0 \quad (8.112)$$

Hence in the absence of zonal perturbations, a zonally symmetric circulation can be maintained against dissipation only by a non-geostrophic meridional circulation.

d. PROPERTIES OF THE TRANSFORMATIONS INVOLVING ONLY ZONAL PERTURBATIONS

From (8.55) and (8.101) we see that zonal asymmetries of heating, Q'_R , can transform only with \mathcal{P}' . For the moment regarding the generalized heating function Q , then

$$\langle Q \mathcal{P}'_d \rangle = \frac{\kappa}{2\gamma_s^2} \{ [Q' \hat{\Phi}'] \} \quad (8.113)$$

Infrared radiation from the atmosphere requires larger cooling rates to occur in connection with higher temperatures and hence makes (8.113) negative. On the other hand the large-scale release of latent heat of condensation in middle latitudes occurs at relatively high temperatures, and contributes toward making (8.113) positive. The effect of eddy conduction between the earth's surface and the atmosphere depends on the conductivity of the surface. Bare land surfaces, which have small conductivity, come

into relatively rapid adjustment with the atmosphere and give rise to little systematic correlation between Q' and $\hat{\Phi}'$. The sea surface, especially the western ocean in winter, heats the atmosphere where it is coldest and thus contributes to making (8.113) negative. Thus the net effect of eddy conduction between the atmosphere and the oceans and continents is the same as that of infrared radiation. In the present model only infrared cooling as a function of temperature is assumed, and hence $\langle Q'_x * P' \rangle \propto -\{[\hat{\Phi}^2]\} < 0$.

For the same reason that condensation occurs at relatively high temperatures, $\{[\hat{\Phi}' \hat{D}']\} > 0$ in middle latitudes, so that $\langle P' * \hat{K}' \rangle > 0$ in (8.98). This sinking of cold air and rising of warm air is a result of quasi-geostrophic thermally direct circulations in zonal planes associated with baroclinic waves. The growth of such waves, and the amplification of the vertical component of motion, is analogous to the action of the pressure forces in simple turbulence tending to establish 3-dimensional isotropy [3]; i.e., the increase of the transverse turbulent components ω' and v' at the expense of the zonal component u' . In classical turbulence however this tendency toward isotropy increases with wave number, being predominant in the molecular dissipative range. On the other hand, the earth's rotation and the atmosphere's small but positive static stability demand a rather small wave number of maximum baroclinic instability, and so the atmospheric energy spectrum possesses at least one other point of maximum tendency toward isotropy. As the wave amplifies, the adiabatic heating to the west of the trough and the cooling to the east increase the eastward phase speed of the isotherms relative to that of the streamlines, creating in the occlusion stage a more barotropic, and hence a less 3-dimensionally isotropic, wave disturbance. This represents a transformation $\langle \hat{K}' * \bar{K}' \rangle > 0$, which may be viewed as a spectral exchange of zonal eddy kinetic energy from vertical wave number one to zero. This, we found, could be accomplished along any of three distinct paths:

(i) Equation (8.87) gives a direct transformation which depends on triple correlations. It is not immediately apparent what its sign is since compensations along a latitude circle would make the correlations small in magnitude.

(ii) Equation (8.84) gives the indirect transformation which is catalytic with respect to $[\hat{K}_y]$. In middle latitudes a typical baroclinic wave requires $\overline{[v' D']} > 0$ and since here $\hat{v} < 0$ then $\langle \hat{K}' * [\hat{K}_y] * \bar{K}' \rangle > 0$. This transformation is non-geostrophic and small because of \hat{v} .

(iii) Equation (8.81) gives the indirect transformation which is catalytic with respect to $[\hat{K}_z]$. For the purpose of discussion we evaluate \hat{V}' in the first term geostrophically, hence we have approximately

$$\frac{1}{4} \left\{ \frac{[\hat{v}' \bar{u}' - \hat{u}' \bar{v}']}{m^2} [\hat{\xi}] \right\} \approx -\frac{1}{4} \left\{ [\bar{v}' \hat{\Phi}'] \frac{\partial [\hat{\xi}]/f}{\partial y} \right\} \quad (8.114)$$

For a poleward eddy heat transport $[\bar{v}' \hat{\Phi}'] > 0$ and in the vicinity of the jet stream $\frac{\partial [\hat{\xi}]/f}{\partial y} > 0$, hence its quasi-geostrophic contribution is to make $\langle \hat{K}' * [\hat{K}_z] * \bar{K}' \rangle < 0$. For a baroclinic wave the second term also gives a negative contribution since $\overline{[u' D']} > 0$ and $[\hat{u}] > 0$.

Thus it appears unlikely that any of the above three transformations could adequately account for the increase of \bar{K}' during the occlusion process. One would conclude that non-catalytic interactions with the zonal mean flow perform the necessary function.

e. PROPERTIES OF THE TRANSFORMATIONS BETWEEN THE ZONAL PERTURBATIONS AND THE ZONALLY SYMMETRIC CIRCULATION

It will be remembered that the non-catalytic part of $\langle \bar{K}' * [\hat{K}_z] \rangle$, (8.82), is $\frac{1}{4} \left\{ [\bar{v}' \hat{\xi}'] \frac{[\hat{u}]}{m^2} \right\}$. Approximating $[\hat{u}]$ and $\hat{\xi}'$ geostrophically and assuming sinusoidal temperature perturbations of wave number n/a , so that $\nabla^2 \hat{\Phi}' \approx -(n/a)^2 \hat{\Phi}'$, then we have approximately that

$$\langle \bar{K}' * [\hat{K}_z] \rangle_{NC} \approx \frac{1}{4} \left\{ \left(\frac{n}{af} \right)^2 [\bar{v}' \hat{\Phi}'] \frac{\partial [\hat{\Phi}]}{\partial y} \right\} \quad (8.115)$$

Upon comparing with (8.59) we see that the ratio

$$\frac{\langle [\hat{K}_z] * \bar{K}' \rangle_{NC}}{\langle P' * P' \rangle} \approx \left(\frac{\gamma n}{fa} \right)^2$$

i.e., the square of the ratio of the speed of long internal gravity waves to that of long inertial waves. From the definition of R in Appendix B, we have with (B5) that

$$\frac{\langle [\hat{K}_z] * \bar{K}' \rangle_{NC}}{\langle P' * P' \rangle} \approx \left(\frac{\gamma}{\gamma_s} \right)^2 \frac{R}{\sqrt{2}} = \frac{1}{2} \left(\frac{n\gamma}{\gamma_s} \right)^2 R_i R_{ot}^2 \quad (8.116)$$

which for maximum instability ($R=1$) has a value of $\gamma^2 / \gamma_s^2 2^{1/2}$. For a poleward temperature decrease and a poleward eddy heat transport, $\{[\hat{\Phi}' \bar{v}'] \partial [\hat{\Phi}]/\partial y\} < 0$, so that $\langle P' * P' \rangle > 0$, and quasi-geostrophically $\langle [\hat{K}_z] * \bar{K}' \rangle_{NC}$ is also positive and 0.57 as large, the two transformations taking place in phase.

Hence $\langle [\hat{K}_z] * \bar{K}' \rangle_{NC}$ is really an integral part of the quasi-geostrophic baroclinic instability process. We therefore have found a substantial means for systematically creating barotropic perturbation energy. According to (8.41) the net transfer between $K' = \hat{K}' + \bar{K}'$ and $[\hat{K}_z]$ is proportional to $\overline{[v' \hat{\xi}']}$. For a typical mid-latitude tilted

trough $[v'\zeta'] > 0$ and for perturbations which increase in intensity upward we then have that $\langle K' * [\hat{K}_x] \rangle > 0$, so that the net effect of K' is to maintain $[\hat{K}_x]$ against dissipation. From (8.82) and (8.83) we then have that

$$\langle \hat{K}' * [\hat{K}_x] \rangle_{NC} > \langle [\hat{K}_x] * \bar{K}' \rangle_{NC} > 0 \quad (8.117)$$

The catalytic transfer $\langle \bar{K}' * [\hat{K}_x] * \hat{K}' \rangle$ is analytically related to $\langle \hat{K}' * [\hat{K}_x] \rangle_{NC}$ and $\langle [\hat{K}_x] * \bar{K}' \rangle_{NC}$ by (8.81), (8.82), (8.83), and (8.41):

$$\langle K' * [\hat{K}_x] \rangle - \langle \bar{K}' * [\hat{K}_x] * \hat{K}' \rangle = -\frac{1}{2} \left\{ \frac{[\hat{u}'\bar{v}']}{{m^2}} [\hat{\zeta}] + \widehat{[u'v']} \frac{2\alpha}{a} \frac{[\hat{u}]}{{m^2}} \right\} \quad (8.118)$$

If we ignore the last term which depends on spherical kinematics, then the difference on the left side depends on the meridional correlation of $[\hat{u}'\bar{v}']$ with the thermal vorticity of the zonal current $[\hat{\zeta}]$. Since the effect of vorticity of the zonal current is normally small compared with f we should expect that the right side of (8.118) is small. This condition together with (8.117) yields

$$\langle \hat{K}' * [\hat{K}_x] \rangle_{NC} > \langle [\hat{K}_x] * \bar{K}' \rangle_{NC} \gg \langle K' * [\hat{K}_x] \rangle \approx \langle \bar{K}' * [\hat{K}_x] * \hat{K}' \rangle > 0 \quad (8.119)$$

The analogous non-catalytic transformations involving $[\hat{K}_y]$ are given by (8.53), (8.85), and (3.86)

$$\begin{aligned} \langle K' * [\hat{K}_y] \rangle &= \langle \bar{K}' * [\hat{K}_y] \rangle_{NC} + \langle \hat{K}' * [\hat{K}_y] \rangle_{NC} \\ &= -\frac{1}{2} \left\{ \widehat{[u'\zeta']} \frac{[\hat{v}]}{{m^2}} - \frac{[\hat{u}'^2 + \hat{v}'^2]}{2m^2} [\hat{D}] \right\} \quad (8.120) \end{aligned}$$

In mid-latitudes in the indirect circulation, $\widehat{[u'\zeta']} > 0$ for tilted waves, so that the first term increases $[\hat{K}_y]$ at the expense of K' . The second term, which represents the vertical advection of eddy kinetic energy by the meridional circulation, also increases $[\hat{K}_y]$ in the upward limb of the meridional circulation, giving $\langle K' * [\hat{K}_y] \rangle < 0$ in the downward limb. The net effect will depend on the relative magnitudes of the contributing transformations.

The remaining energy exchanges involve interactions of \hat{K}' and \bar{K}' with $[\bar{K}_x]$. The latter, a purely barotropic spectral exchange, has been discussed by a number of writers [35], [14]. It depends on the quasi-horizontal character and finite amplitude of the eddies, which are therefore non-isotropic 3-dimensionally and hence do not give a net transfer of energy to higher wave numbers through an inertial cascade. In fact, since the finite amplitude disturbances tend to conserve the vertical component of absolute vorticity there is a net transfer

to larger waves and ultimately to zonal wave number zero, i.e. $[\bar{K}_x]$. This can be seen by noting that south of the jet stream where $\partial[\bar{u}]/\partial y > 0$, there is a NE-SW tilt of the disturbances, $[\bar{u}'\bar{v}'] > 0$, so that $\langle \bar{K}' * [\bar{K}_x] \rangle > 0$ in (8.28). North of the jet $\partial[\bar{u}]/\partial y < 0$ and the momentum transfer is much weaker northward, that is $[\bar{u}'\bar{v}']$ is slightly positive and may even be negative for a NW-SE orientation of the eddies. Hence there may be a small negative or even a positive contribution to $\langle \bar{K}' * [\bar{K}_x] \rangle$. One must conclude that the net effect of large-scale barotropic disturbances is to increase the energy of the mean westerlies.

The same may be argued for the transfer from the baroclinic component of the eddy energy, i.e., $\langle \hat{K}' * [\bar{K}_x] \rangle > 0$ in (8.30). In fact the sum

$$\langle K' * [\bar{K}_x] \rangle = \frac{1}{2} \left\{ \frac{\widehat{[u'v']}}{m^2} \frac{\partial[\bar{u}]}{\partial y} \right\} > 0 \quad (8.121)$$

f. THE EXPERIMENTAL RESULTS

Table 8.1 and figure 8.2 give the seven energy components as a function of time. $[\hat{K}_y]$ is of the order of 5×10^{-5} joule gm.⁻¹, that is, approximately two orders of magnitude less than \hat{K}' , \bar{K}' , or \mathcal{P}' , and is not perceptible in figure 8.2. The ratio $\hat{K}/\bar{K} \approx 2$ is close to the observed partitioning of kinetic energy.

An 11- to 12-day cycle is quite evident in all the components, but to a lesser extent in $[\hat{K}_x]$ which is weaker with a somewhat more erratic period. The three eddy energy components and $[\bar{K}_x]$ are approximately in phase, whereas $[\mathcal{P}]$ is approximately a day short of being exactly out of phase. The variations of $[\hat{K}_x]$ can be identified with the phase of $[\mathcal{P}]$, which might have been expected from the quasi-geostrophic coupling of the transformations with their respective perturbation energy components (8.115). $[\hat{K}_x]$ also has a secondary phase which we shall see is associated with the high frequency oscillations of the meridional circulation.

It will be noted that within the first 36 days, $[\mathcal{P}]$ has a decreasing trend, during which the index cycle is well defined. Beyond this point a quasi-equilibrium in $[\mathcal{P}]$ is attained, and the cycles are longer and smaller in amplitude. It can be shown (Appendix B) that the geostrophic baroclinic stability criterion predicts an equilibrium meridional temperature gradient and hence a corresponding equilibrium value of $[\mathcal{P}]$ which is proportional to the static stability (see equation B18). Since we started the experiment with $[\mathcal{P}]$ definitely larger than necessary for instability of the most unstable wave number, the behavior of the trend in $[\mathcal{P}]$ over the 60-day period is not surprising.

In earlier subsections we have been able from observed properties of the atmosphere to deduce the sign and relative magnitudes of most of the possible energy trans-

TABLE 8.1.—Energy components (unaveraged) in $\text{2 joule gm.}^{-1} \sim 488 \text{ ly.}$

DAY	$[\bar{\mathcal{K}}]$	$[\hat{\mathcal{K}}_x]$	$[\hat{\mathcal{K}}_y]$	$[\mathcal{P}]$	$\bar{\mathcal{K}}'$	$\hat{\mathcal{K}}'$	\mathcal{P}'
0	0.0347	0.0493	0.0000	0.5271	0.0000	0.0000	0.0195
1	0.0456	0.0482	0.0001	0.5248	0.0004	0.0084	0.0055
2	0.0536	0.0491	0.0001	0.5228	0.0004	0.0068	0.0047
3	0.0594	0.0495	0.0001	0.5274	0.0005	0.0058	0.0039
4	0.0638	0.0496	0.0001	0.5314	0.0007	0.0050	0.0037
5	0.0675	0.0494	0.0000	0.5358	0.0011	0.0046	0.0033
6	0.0708	0.0487	0.0000	0.5392	0.0019	0.0046	0.0034
7	0.0744	0.0501	0.0000	0.5376	0.0031	0.0047	0.0043
8	0.0778	0.0505	0.0000	0.5341	0.0050	0.0050	0.0054
9	0.0811	0.0499	0.0001	0.5286	0.0070	0.0058	0.0067
10	0.0841	0.0483	0.0001	0.5215	0.0091	0.0066	0.0082
11	0.0869	0.0459	0.0000	0.5134	0.0108	0.0070	0.0093
12	0.0900	0.0471	0.0000	0.5039	0.0111	0.0071	0.0093
13	0.0925	0.0470	0.0000	0.4985	0.0102	0.0070	0.0080
14	0.0941	0.0480	0.0000	0.4956	0.0087	0.0061	0.0065
15	0.0944	0.0464	0.0001	0.4987	0.0068	0.0054	0.0029
16	0.0940	0.0458	0.0000	0.5034	0.0052	0.0043	0.0038
17	0.0929	0.0461	0.0000	0.5079	0.0045	0.0035	0.0032
18	0.0915	0.0478	0.0000	0.5095	0.0049	0.0033	0.0035
19	0.0902	0.0485	0.0000	0.5085	0.0067	0.0037	0.0049
20	0.0895	0.0479	0.0000	0.5041	0.0090	0.0047	0.0073
21	0.0896	0.0459	0.0000	0.4968	0.0117	0.0061	0.0096
22	0.0907	0.0450	0.0000	0.4861	0.0135	0.0074	0.0113
23	0.0924	0.0446	0.0000	0.4759	0.0144	0.0081	0.0117
24	0.0941	0.0454	0.0000	0.4679	0.0136	0.0082	0.0105
25	0.0950	0.0445	0.0000	0.4659	0.0122	0.0075	0.0085
26	0.0948	0.0440	0.0000	0.4672	0.0105	0.0064	0.0068
27	0.0941	0.0435	0.0000	0.4705	0.0091	0.0056	0.0055
28	0.0930	0.0440	0.0000	0.4732	0.0085	0.0050	0.0053
29	0.0919	0.0444	0.0000	0.4723	0.0086	0.0049	0.0064
30	0.0908	0.0444	0.0000	0.4730	0.0100	0.0057	0.0083
31	0.0903	0.0440	0.0000	0.4684	0.0117	0.0068	0.0109
32	0.0904	0.0432	0.0000	0.4616	0.0140	0.0080	0.0132
33	0.0912	0.0425	0.0000	0.4535	0.0153	0.0091	0.0146
34	0.0922	0.0419	0.0000	0.4459	0.0158	0.0097	0.0148
35	0.0933	0.0416	0.0000	0.4410	0.0152	0.0096	0.0133
36	0.0939	0.0415	0.0000	0.4400	0.0132	0.0088	0.0109
37	0.0937	0.0416	0.0000	0.4423	0.0109	0.0076	0.0087
38	0.0926	0.0416	0.0000	0.4460	0.0094	0.0068	0.0076
39	0.0912	0.0418	0.0000	0.4499	0.0085	0.0061	0.0071
40	0.0899	0.0422	0.0000	0.4532	0.0081	0.0056	0.0066
41	0.0890	0.0427	0.0000	0.4557	0.0084	0.0053	0.0064
42	0.0885	0.0430	0.0000	0.4580	0.0080	0.0049	0.0057
43	0.0883	0.0432	0.0000	0.4600	0.0084	0.0046	0.0053
44	0.0881	0.0431	0.0000	0.4617	0.0082	0.0046	0.0051
45	0.0880	0.0433	0.0000	0.4625	0.0086	0.0043	0.0048
46	0.0878	0.0435	0.0000	0.4624	0.0091	0.0046	0.0052
47	0.0876	0.0437	0.0000	0.4612	0.0097	0.0047	0.0054
48	0.0876	0.0435	0.0000	0.4599	0.0101	0.0048	0.0057
49	0.0878	0.0433	0.0000	0.4588	0.0105	0.0050	0.0060
50	0.0880	0.0432	0.0000	0.4580	0.0100	0.0048	0.0061
51	0.0881	0.0433	0.0000	0.4570	0.0105	0.0048	0.0064
52	0.0883	0.0434	0.0000	0.4561	0.0101	0.0049	0.0065
53	0.0885	0.0435	0.0000	0.4558	0.0100	0.0048	0.0063
54	0.0885	0.0434	0.0000	0.4565	0.0096	0.0047	0.0060
55	0.0883	0.0436	0.0000	0.4581	0.0089	0.0045	0.0055
56	0.0880	0.0438	0.0000	0.4605	0.0083	0.0042	0.0052
57	0.0878	0.0441	0.0000	0.4634	0.0075	0.0040	0.0049
58	0.0875	0.0443	0.0000	0.4669	0.0073	0.0038	0.0047
59	0.0874	0.0446	0.0000	0.4702	0.0063	0.0037	0.0047
60	0.0874	0.0448	0.0000	0.4731	0.0070	0.0036	0.0047

formation functions including some that are essentially non-geostrophic. However the fact that time cycles exist is more difficult to deduce because the index cycle is essentially non-linear ([2], [27]).

To discuss further the maintenance of the general circulation we must calculate the transformation functions derived in Section 8b for our experiment. Since internal gravity-inertial wave propagation is admissible in our model, we must expect that some of the transformation functions, in particular those involving the meridional circulation $\langle v \rangle$, will undergo high frequency variations. This is easily demonstrated in figure 8.3 by a plot of $\langle [\mathcal{P}]*[\hat{\mathcal{K}}_y] \rangle$ as a function of time with a resolution of 2 hours. In this particular instance there are

TABLE 8.2.—Energy components (2-day average) in $\text{2 joule gm.}^{-1} \sim 488 \text{ ly.}$

DAY	$[\bar{\mathcal{K}}]$	$[\hat{\mathcal{K}}_x]$	$[\hat{\mathcal{K}}_y]$	$[\mathcal{P}]$	$\bar{\mathcal{K}}'$	$\hat{\mathcal{K}}'$	\mathcal{P}'
11	0.0871	0.0479	0.0001	0.5120	0.0105	0.0070	0.0090
12	0.0899	0.0471	0.0001	0.5044	0.0109	0.0072	0.0090
13	0.0922	0.0465	0.0000	0.4995	0.0101	0.0069	0.0080
14	0.0937	0.0464	0.0000	0.4976	0.0086	0.0062	0.0065
15	0.0943	0.0466	0.0000	0.4986	0.0069	0.0053	0.0050
16	0.0939	0.0470	0.0000	0.5018	0.0054	0.0043	0.0039
17	0.0928	0.0472	0.0000	0.5059	0.0047	0.0036	0.0034
18	0.0914	0.0474	0.0000	0.5083	0.0051	0.0033	0.0037
19	0.0901	0.0473	0.0000	0.5085	0.0067	0.0037	0.0051
20	0.0896	0.0471	0.0000	0.5038	0.0049	0.0047	0.0072
21	0.0898	0.0467	0.0000	0.4953	0.0114	0.0060	0.0094
22	0.0908	0.0460	0.0000	0.4851	0.0133	0.0072	0.0109
23	0.0923	0.0452	0.0000	0.4759	0.0139	0.0079	0.0112
24	0.0938	0.0445	0.0000	0.4697	0.0134	0.0079	0.0102
25	0.0947	0.0442	0.0000	0.4670	0.0120	0.0073	0.0085
26	0.0948	0.0441	0.0000	0.4675	0.0105	0.0064	0.0067
27	0.0941	0.0443	0.0000	0.4699	0.0091	0.0055	0.0056
28	0.0930	0.0444	0.0000	0.4726	0.0086	0.0050	0.0055
29	0.0918	0.0444	0.0000	0.4739	0.0083	0.0050	0.0064
30	0.0908	0.0442	0.0000	0.4724	0.0101	0.0057	0.0084
31	0.0904	0.0438	0.0000	0.4676	0.0120	0.0068	0.0109
32	0.0906	0.0434	0.0000	0.4602	0.0139	0.0080	0.0132
33	0.0914	0.0428	0.0000	0.4520	0.0154	0.0091	0.0146
34	0.0924	0.0422	0.0000	0.4448	0.0158	0.0097	0.0146
35	0.0934	0.0416	0.0000	0.4404	0.0150	0.0095	0.0131
36	0.0939	0.0414	0.0000	0.4396	0.0131	0.0087	0.0108
37	0.0936	0.0415	0.0000	0.4414	0.0112	0.0077	0.0090
38	0.0926	0.0418	0.0000	0.4446	0.0096	0.0068	0.0078
39	0.0912	0.0420	0.0000	0.4481	0.0088	0.0061	0.0072
Mean	0.0921	0.0442	0.0000	0.4702	0.0109	0.0066	0.0083
17-39	0.0921	0.0442	0.0000	0.4702	0.0109	0.0066	0.0083

periods of 8 to 24 hours. This transformation at 20-min. intervals reveals no shorter periods. In order to get a measure of the net effect of the non-geostrophic motions on a synoptic time scale, all of the integrals were averaged using 2-hourly values for a 2-day period centered at the day of interest. The averaged energy components are to be found in table 8.2. The energy transformations, sources, and sinks for each day unaveraged and averaged are given in tables 8.3 and 8.4, respectively.

The time averaged $\langle \hat{\mathcal{K}}_z \rangle$ has a much more regular variation since the high frequency effects of the meridional circulation have been filtered. The period and phase of $\langle \hat{\mathcal{K}}_z \rangle$ more or less coincides with that of $\langle \mathcal{P} \rangle$. Figure 8.4 gives a plot of the averaged transformation functions except those with maximum magnitude less than 1.5×10^{-3} joule gm. $^{-1}$ day $^{-1}$, i.e., those which are more than 20 times smaller than $\langle Q_R * [\mathcal{P}] \rangle$, which is shown for reference. However, the dissipations, some of which are large, are not given in this figure.

The only significant transformations involving the meridional circulations are $\langle [\mathcal{P}] * [\hat{\mathcal{K}}_y] \rangle$ and $\langle [\hat{\mathcal{K}}_y] * [\hat{\mathcal{K}}_x] \rangle$ which are nearly identical because of strong geostrophic coupling, and by our definition $\langle \hat{\mathcal{K}}_y \rangle$ is virtually catalytic with respect to $\langle \mathcal{P} \rangle$ and $\langle \hat{\mathcal{K}}_z \rangle$. They are also the only significant transformations to change sign with time. In fact over a complete index cycle their average value is almost zero (see fig. 8.7) having no net effect on the transfer of energy. This has been suggested by the measurements of White and Saltzman [59] in comparing $\langle [\mathcal{P}_e] * [K] \rangle$ and $\langle [\mathcal{P}_d] * K' \rangle$ for a portion of the atmosphere.

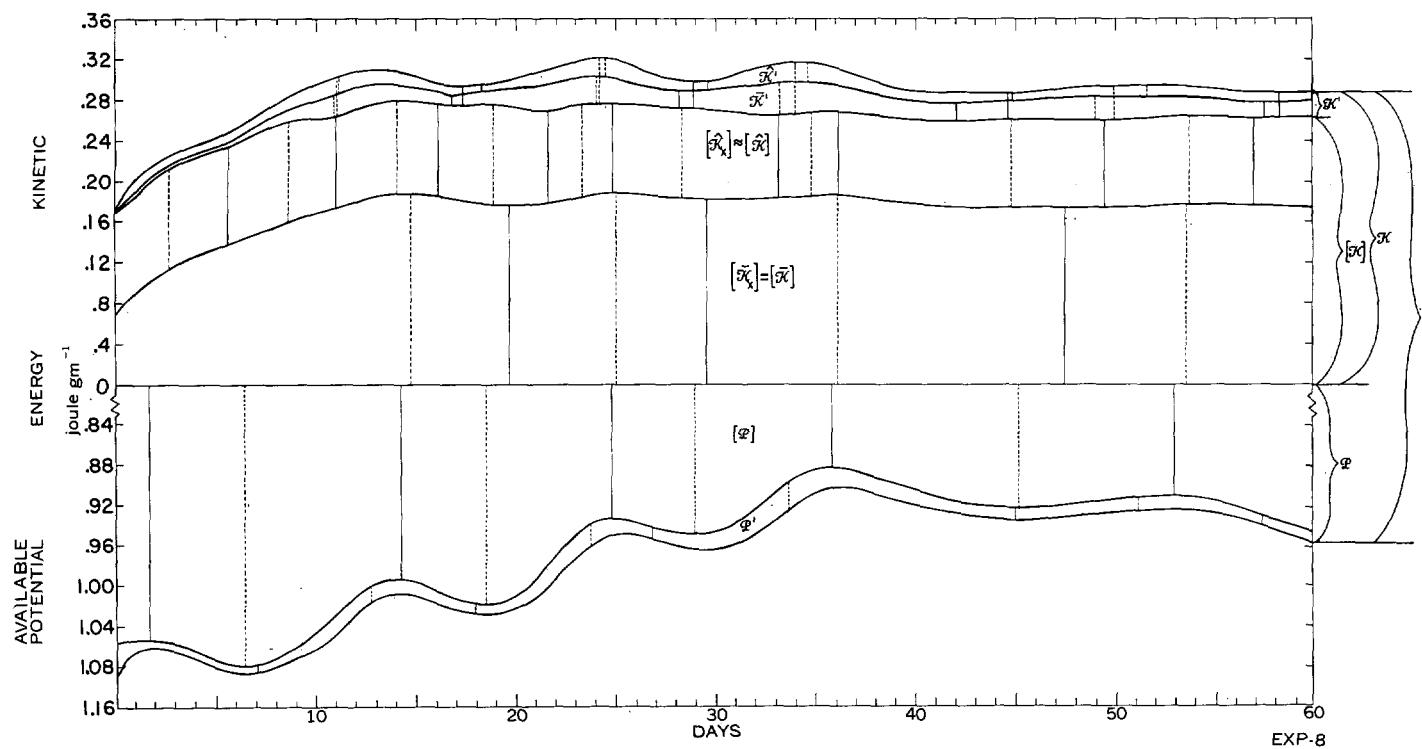


FIGURE 8.2.—The experimental energy partitions as a function of time (unaveraged) corresponding to table 8.1. The thin solid vertical lines mark the minima and the dashed lines the maxima.

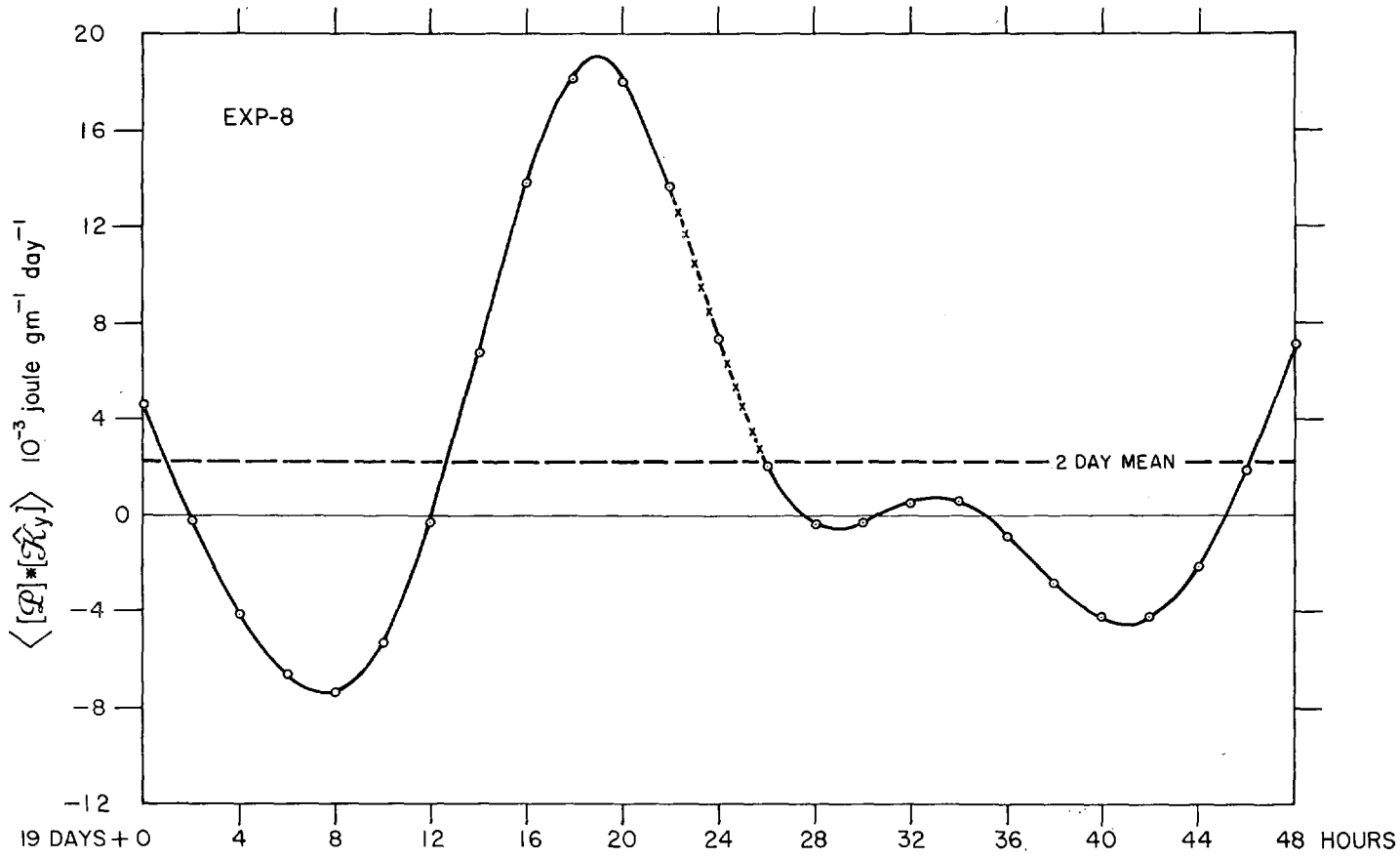


FIGURE 8.3.—A fine time resolution plot of the transformation of zonal available potential energy $[P]$ to that of the meridional circulation \hat{K}_y to show the high-frequency non-geostrophic transformations. The resolution is 2 hours (every 6 time steps) except between 19 days + 22 hours and 19 days + 26 hours where the resolution is 20 min. (every time step).

TABLE 8.3.—*Energy transformations, generations, and dissipations (unaveraged) $\times 10^{-3}$ joule gm.⁻¹ day⁻¹ ~0.244 ly. day⁻¹.*

TABLE 8.3.—Continued.

TABLE 8.4.—Energy transformations, generations, and dissipations (2-day averaged) $\times 10^{-8}$ joule gm.⁻¹ day⁻¹ ~ 0.244 ly. day⁻¹.

DAY	$\langle \bar{E}_1^{\text{gen}} \cdot \bar{E}_2^{\text{gen}} \rangle$	$\langle \bar{E}_1^{\text{diss}} \cdot \bar{E}_2^{\text{diss}} \rangle$	$\langle \bar{E}_1^{\text{gen}} \cdot \bar{E}_2^{\text{diss}} \rangle_{\text{av}}$	$\langle \bar{E}_1^{\text{diss}} \cdot \bar{E}_2^{\text{gen}} \rangle_{\text{av}}$	$\langle \bar{E}_1^{\text{gen}} \cdot \bar{E}_2^{\text{gen}} \rangle_{\text{av}}$	$\langle \bar{E}_1^{\text{diss}} \cdot \bar{E}_2^{\text{diss}} \rangle_{\text{av}}$	$\langle \bar{E}_1^{\text{gen}} \cdot \bar{E}_2^{\text{diss}} \rangle_{\text{av}}$	$\langle \bar{E}_1^{\text{diss}} \cdot \bar{E}_2^{\text{gen}} \rangle_{\text{av}}$	$\langle \bar{E}_1^{\text{gen}} \cdot \bar{E}_2^{\text{gen}} \rangle$	$\langle \bar{E}_1^{\text{diss}} \cdot \bar{E}_2^{\text{diss}} \rangle$	$\langle \bar{E}_1^{\text{gen}} \cdot \bar{E}_2^{\text{gen}} \rangle$	$\langle \bar{E}_1^{\text{diss}} \cdot \bar{E}_2^{\text{diss}} \rangle$	DAY					
11	3.1.02	0.0284	0.5589	13.5672	0.0609	0.0871	10.6620	2.5543	1.2907	0.1967	0.0302	17.3818	14.7969	0.2048	14.7224	0.3579	11	
12	3.4.84	0.0290	0.6331	13.5981	0.0593	0.1220	10.2979	3.2260	1.6412	0.1636	-0.0637	16.1891	14.7285	0.2071	14.7723	0.3542	12	
13	3.3958	0.0262	0.5338	12.5365	0.0418	0.1231	9.0325	3.4710	1.8127	1.0364	0.8228	13.5924	13.0093	0.1876	14.7917	0.3146	13	
14	3.0086	0.0173	0.3411	10.1846	0.0209	0.0621	5.0441	2.3095	1.6942	1.9451	1.7778	10.4178	10.3959	0.1928	14.7938	0.2381	14	
15	2.2658	0.0106	0.1979	7.5793	0.0093	0.0316	3.2016	2.5803	1.3887	2.0813	2.0027	7.1903	7.4501	0.1719	14.7918	0.1993	15	
16	1.3591	0.0023	0.2505	4.8459	0.0092	0.0316	1.6482	0.9879	0.0285	0.0020	4.7284	4.8159	0.1119	14.7740	0.1532	16		
17	0.5405	-0.0012	0.3831	2.9950	0.0880	0.0175	2.2898	0.7042	0.5809	-3.4878	-5.5222	3.9074	0.5268	0.0747	14.7511	0.1327	17	
18	0.1070	-0.0014	0.4660	2.7876	0.0070	0.0125	2.7169	0.2090	0.3264	-3.7625	5.4621	4.0014	0.0854	14.7339	0.1477	18		
19	0.3046	0.0023	0.4412	4.5146	0.1169	0.0142	4.4811	0.2091	0.3036	-2.8701	-2.9164	9.2020	6.4378	0.1642	14.7234	0.2018	19	
20	1.0586	0.0130	0.4243	7.6071	0.0404	0.0194	7.0286	0.6713	0.5249	-0.9834	-1.0720	13.9149	10.1980	0.3037	14.7332	0.2842	20	
21	2.0936	0.0254	0.5095	10.9718	0.0683	0.0476	9.4935	1.4518	0.9508	0.1554	0.0248	13.8831	12.8263	0.4168	14.7878	0.3706	21	
22	3.0528	0.0324	0.6059	13.5469	0.0892	0.1059	11.0840	2.5066	1.4683	0.6248	0.4076	19.5842	16.1810	0.4622	14.8268	0.4311	22	
23	3.6335	0.0286	0.5801	14.6013	0.0893	0.1619	11.3440	3.5564	1.8725	1.1822	0.8919	18.7320	16.5938	0.3639	14.8612	0.4439	23	
24	3.6715	0.0228	0.3788	13.8776	0.0634	0.1855	10.3490	4.0636	1.9372	2.2564	1.9038	14.9953	12.4659	0.2327	14.8872	0.4048	24	
25	3.2057	0.0191	0.1394	11.8479	0.0339	0.1593	8.6169	3.8847	1.6397	3.0289	2.7964	12.0243	0.0890	14.9039	0.3353	25		
26	2.5095	0.0120	0.0345	9.3013	0.0211	0.1080	6.7222	3.2138	1.6116	2.2972	2.1534	8.9751	9.0057	-0.0139	14.9102	0.2669	26	
27	1.8222	0.0052	0.0495	7.0722	0.0176	0.0670	5.2603	2.3674	0.7100	0.7238	0.6248	7.1145	6.7614	-0.0314	14.9076	0.2227	27	
28	1.3400	0.0012	0.1080	10.0137	0.0137	0.0401	4.6300	1.6627	0.4174	-0.7224	5.0798	5.8149	0.0250	14.9003	0.2158	28		
29	1.2010	0.0011	0.1419	5.8504	0.0103	0.0244	5.0776	1.2633	0.3159	-1.1292	-1.1741	9.0916	6.6227	0.1298	14.8991	0.2527	29	
30	1.4085	0.0030	0.1776	7.2131	0.0143	0.216	6.3934	2.2226	0.4390	-0.7081	-0.7614	5.0431	8.8977	0.2877	14.9088	0.3335	30	
31	1.8463	0.0093	0.2359	9.4101	0.0327	0.0362	8.0796	1.5744	0.8090	0.3286	0.2992	16.2264	11.9370	0.4397	14.9297	0.4325	31	
32	2.3365	0.0188	0.3191	11.6282	0.0584	0.1674	9.5590	2.2345	1.3467	1.4873	1.3396	18.9550	14.7727	0.5888	14.9485	0.5220	32	
33	2.7311	0.0273	0.4023	10.0209	0.0767	0.1090	2.9792	2.9716	1.9029	2.3575	2.1451	19.9182	16.5554	0.6201	14.9655	0.5788	33	
34	2.9621	0.0302	0.4340	13.1040	0.0744	0.1467	9.9295	3.5968	2.3400	2.9321	1.6692	18.5828	16.6305	0.6559	14.9776	0.5776	34	
35	2.9060	0.0254	0.3929	11.5851	0.0516	0.1560	8.5433	3.8552	2.5264	3.1626	2.9055	15.2847	14.7969	0.6051	14.9839	0.5175	35	
36	2.5829	0.0175	0.3293	9.8038	0.0250	0.1221	6.7661	3.5658	2.3705	2.8632	2.6720	11.6993	11.8202	0.5078	14.9857	0.4292	36	
37	2.0853	0.0101	0.2867	7.5450	0.0885	0.0845	5.1593	2.7661	1.9383	1.7601	1.9011	8.8762	8.8542	0.3978	14.9326	0.3345	37	
38	1.6476	0.0043	0.2950	5.8351	0.0339	0.0587	4.1697	1.9661	1.4168	0.8130	0.7422	7.2223	6.8066	0.2078	14.9705	0.3080	38	
39	1.3691	0.0010	0.3195	5.0330	0.0026	0.0478	3.8449	1.4451	1.0070	-0.2594	-0.3181	6.5273	5.8864	0.1487	14.9672	0.2861	39	
Mean	17-39	2.0181	0.0134	0.3241	8.9223	0.0360	0.0790	7.0364	2.2167	1.2307	0.5783	0.4413	12.3779	10.5655	0.2969	14.8903	0.3500	17-39

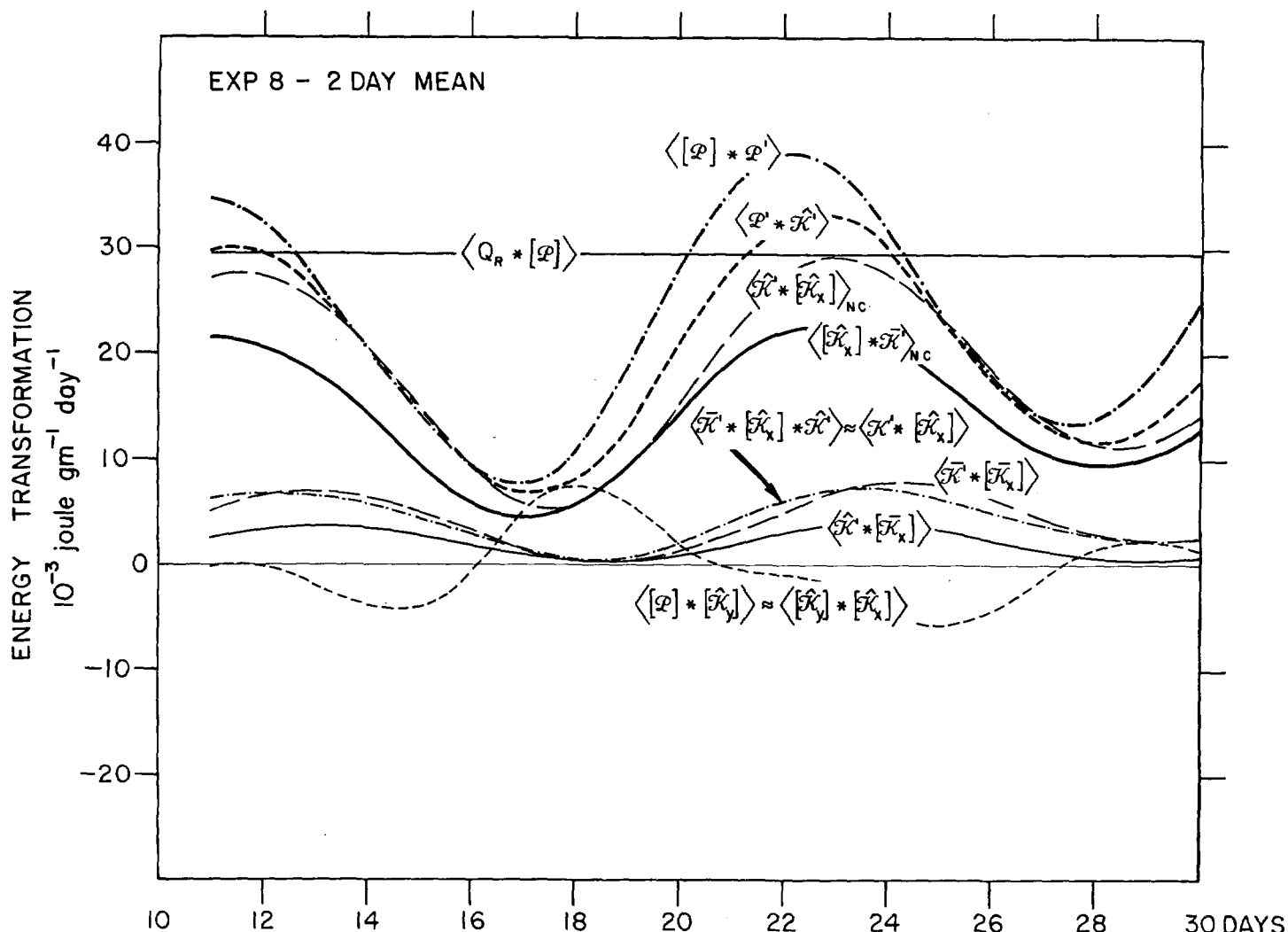


FIGURE 8.4.—The averaged energy transformations as a function of time having a maximum magnitude greater than 1.5×10^{-3} joule gm $^{-1}$ day $^{-1}$. Of the sources and sinks, only the zonal generation of potential energy $\langle Q_R * [P] \rangle$ is given.

Within the cycle, $\langle [P] * [\hat{K}_y] \rangle$ and $\langle P' * \hat{K}' \rangle$ are almost out of phase, $\langle [P] * [\hat{K}_y] \rangle$ tending systematically to compensate the variability of $\langle P' * \hat{K}' \rangle$. $\langle [P] * [\hat{K}_y] \rangle$ may be decomposed into the parts due to the Hadley and Ferrel circulations, the boundary being defined as the latitude where $[\hat{v}] = 0$ or where $[\hat{D}]$ is a minimum. Since $\langle P' * \hat{K}' \rangle$ is virtually all accomplished in the latitude band of the Ferrel circulation $\langle P' * \hat{K}' \rangle + \langle [P] * [\hat{K}_y] \rangle_{\text{Ferrel}}$ represents the net transformation $\langle P * \hat{K} \rangle$ in middle latitudes. A comparison with $\langle P' * \hat{K}' \rangle$ provides a measure of the role played by the non-geostrophic Ferrel circulation in modifying the quasi-geostrophic baroclinic instability process in middle latitudes. From figure 8.5 we see that the net effect is to reduce the maximum quasi-geostrophic transformation by 50 percent and to shift the phase slightly so that extrema occur 1–2 days earlier.

It is also of interest that $\langle [P] * [\hat{K}_y] \rangle_{\text{Hadley}}$ has the period and phase of $\langle P' * \hat{K}' \rangle$ which would lead one to conclude that the small-amplitude low-latitude energy transformation by the mean meridional circulation is induced by the mid-latitude transformation. This will also be evident in the next section where it will be seen that the indirect Ferrel circulation transfers heat equatorward opposite to the direction of the dominant mid-latitude poleward transfer by the quasi-horizontal eddies. One would conclude that a quasi-geostrophic baroclinic model, which mainly accounts for $\langle P' * \hat{K}' \rangle$ would tend to overpredict the potential to kinetic energy transformations for periods which are short compared to the index cycle, i.e., of the order of 1–5 days. Hence the *non-geostrophic modes in mid-latitudes are significantly excited in connection with the baroclinic branches of the energy exchanges*.

Returning to figure 8.4 we note that the quasi-constant energy source $\langle Q_R * [P] \rangle$ gives rise to a cyclic response in

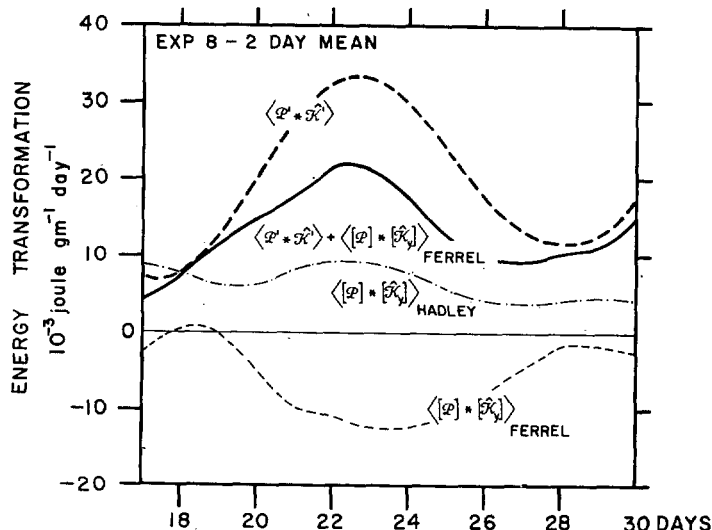


FIGURE 8.5.—A comparison of the quasi-geostrophic energy transformation $\langle P' * \hat{K}' \rangle$, the non-geostrophic transformations $\langle [P] * [\hat{K}_z] \rangle_{\text{Ferrel}}$, and $\langle [P] * [\hat{K}'_z] \rangle_{\text{Hadley}}$; $\langle P' * \hat{K}' \rangle + \langle [P] * [\hat{K}_z] \rangle_{\text{Ferrel}}$ is the total transformation in middle latitudes.

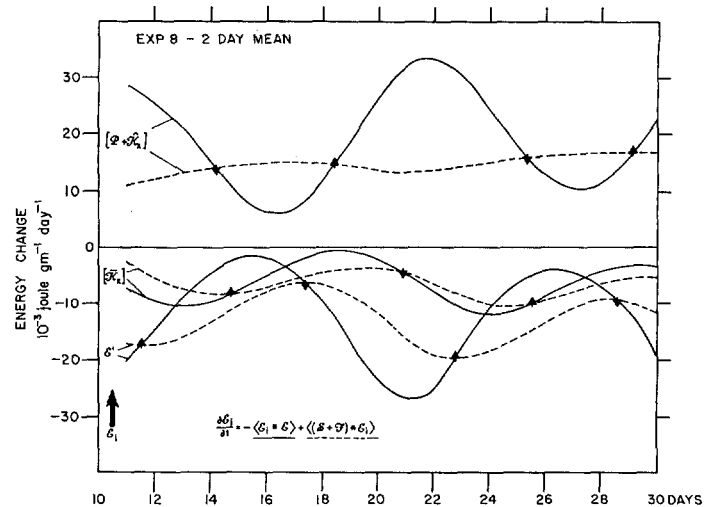


FIGURE 8.6.—The contributions as a function of time to each of $\partial(P+K_z)/\partial t$, $\partial[\bar{K}_z]/\partial t$ and $\partial E'/\partial t$ by sources and dissipation (dashed curves), and by transformations to the other energy partitions (solid curves). The short arrows indicate the maxima and minima (pointing upward and downward, respectively) of $[P+K_z]$, etc.

$\langle [P] * P' \rangle$. Moreover $\langle P' * \hat{K}' \rangle$ and $\langle \hat{K}' * [\hat{K}_z] \rangle_{NC}$ each have later phase and decreased amplitude. This is a result of the viscous dissipations $\langle P' * F \rangle$ and $\langle K' * F \rangle$. On the other hand, because of the strong geostrophic coupling which we deduced between $\langle \hat{K}_z * \bar{K}' \rangle_{NC}$ and $\langle [P] * P' \rangle$ in (8.116), their relative phase and amplitude are less affected by dissipation. From figure 8.7 we see that the ratio $\langle \hat{K}_z * \bar{K}' \rangle_{NC}/\langle [P] * P' \rangle = 0.57$ in (8.116) and the inequalities (8.119) are experimentally verified.

Whereas the phase and amplitude of $\langle [P] * P' \rangle$, $\langle P' * \hat{K}' \rangle$, $\langle \hat{K}' * [\hat{K}_z] \rangle_{NC}$ and $\langle \hat{K}_z * \bar{K}' \rangle_{NC}$ are essentially determined by the baroclinic instability process in the presence of dissipation, that of $\langle \bar{K}' * [\bar{K}_z] \rangle$ and $\langle \hat{K}' * [\bar{K}_z] \rangle$ are determined by the stability of the finite amplitude quasi-horizontal disturbances which exist at the time of occlusion, and are more or less independent of the former.

From figure 8.2 we detect three distinct phases in the significant energy components: $[P+\hat{K}_z]$, E' ($=P'+\hat{K}'+\bar{K}'$), and $[\bar{K}_z]$. Their phases are not directly deducible from the energy transformations alone because of dissipation. Considering only those transformations which we found to be significant, we have that

$$\frac{\partial[P+\hat{K}_z]}{\partial t} \approx -\langle [P] * P' \rangle + \langle K' * [\hat{K}_z] \rangle + \langle Q_R * P \rangle - \langle [P+\hat{K}_z] * F \rangle \quad (8.122)$$

$$\frac{\partial E'}{\partial t} \approx \langle [P] * P' \rangle - \langle K' * [\hat{K}_z] \rangle - \langle K' * [\bar{K}_z] \rangle - \langle P' * Q_R \rangle - \langle E' * F \rangle \quad (8.123)$$

$$\frac{\partial[\bar{K}_z]}{\partial t} \approx \langle \bar{K}_z * F \rangle \quad (8.124)$$

A plot of the experimental results combined according to the above partitioning is given in figure 8.6. Since the dissipation rate is essentially proportional to the energy itself, its phase leads that of the transformations by about 1/4 of a period. This is most evident for E' and $[\bar{K}_z]$, but is obscured for $[P+\hat{K}_z]$ since the dashed curve contains the primary quasi-constant energy source $\langle Q_R * P \rangle$ which dominates the contribution from $-\langle [P+\hat{K}_z] * F \rangle$. For an energy system undergoing stable oscillations we would expect that over an index cycle

$$\frac{\partial \tilde{E}_i}{\partial t} = -\langle \tilde{E}_i * E' \rangle + \langle \tilde{(S+F)*E_i} \rangle \approx 0 \quad (8.125)$$

i.e., there is no net change in any of the energy components E_i . Experimentally this is essentially the case for E' and $[\bar{K}_z]$; however, for $[P+\hat{K}_z]$

$$\langle \widetilde{[P] * P'} \rangle - \langle \widetilde{K' * [\hat{K}_z]} \rangle > \langle \widetilde{Q_R * P} \rangle - \langle \widetilde{[P+\hat{K}_z] * F} \rangle \quad (8.126)$$

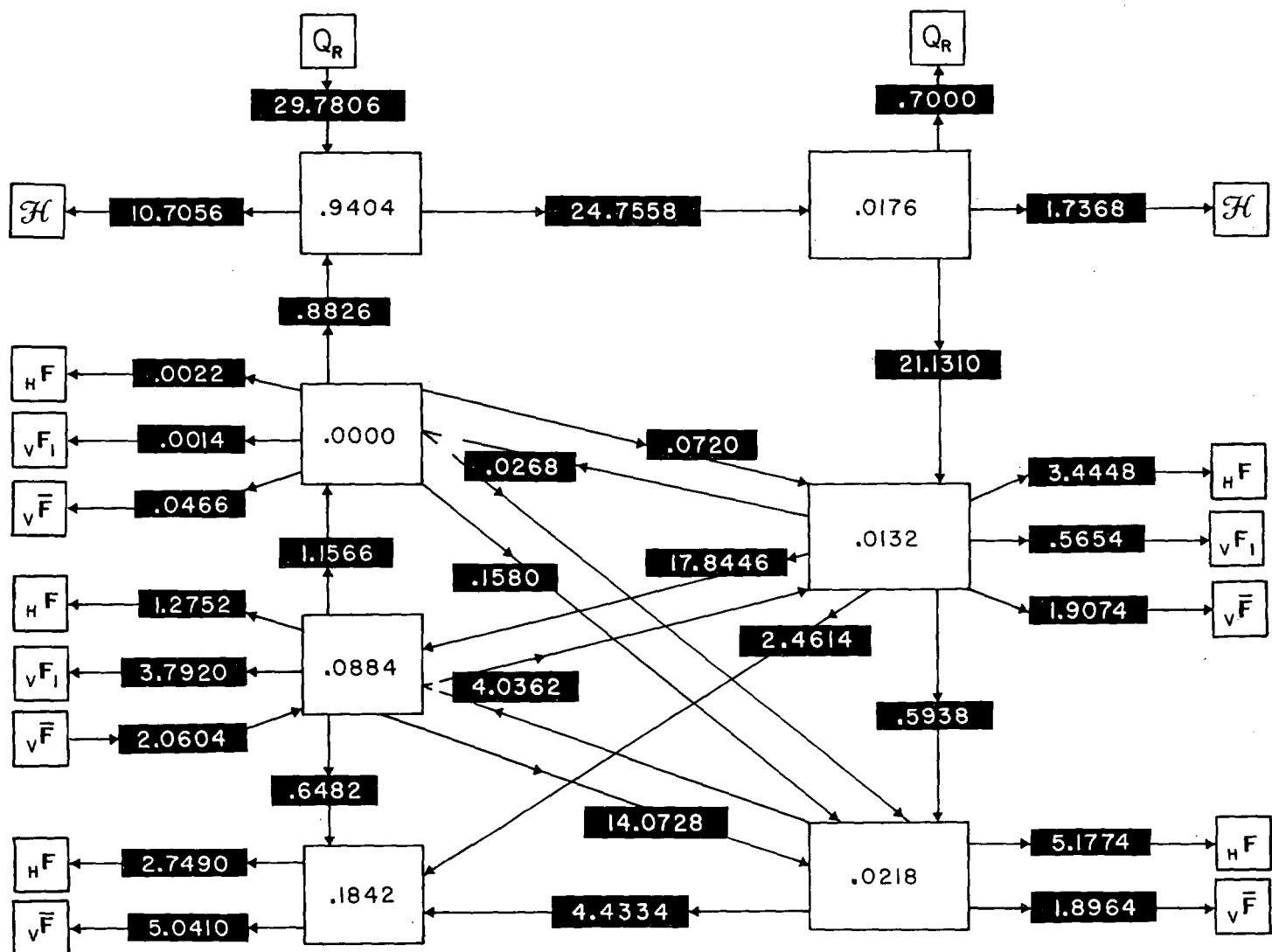


FIGURE 8.7.—A schematic plot of the 17-39 day mean of the 2-day averaged energy partitions (white solid boxes, joule gm.⁻¹), and energy transformations, generation rates, and dissipation rates (black boxes, 10⁻³ joule gm.⁻¹ day⁻¹). The data are taken from tables 8.2 and 8.4 and are given to correspond to the form of figure 8.1.

The resulting systematic decrease of $[\mathcal{P} + \hat{K}_x]$ and particularly $[\mathcal{P}]$ is evident from figure 8.2.

Hence for a particular component, the mean generation-dissipation should balance the net transformation. Since in most instances the transformations are directly measurable from observations, this suggests a direct method for estimating the partitioning of the net generation-dissipation in any of the components, irrespective of the mechanism by which it is accomplished. Since only $[\mathcal{P}]$ and \mathcal{P}' have sources, then the transformations for the kinetic energy components give a measure of pure dissipation.

The arrows at the intersections in figure 8.6 give the time when $d\mathcal{E}_i/dt = 0$ or the extrema in \mathcal{E}_i . The maximum of $[\mathcal{P} + \hat{K}_x]$ is followed by a maximum in \mathcal{E}' in somewhat

over 4 days which in turn is followed by the maximum in the barotropic zonal westerly kinetic energy $[\hat{K}_x]$, the final link in the general circulation, in about 3.5 days. It then takes the radiative gradient about 3.5 days for $[\mathcal{P} + \hat{K}_x]$ to reach its next maximum before being depleted again by baroclinic instability.

Such well-defined cycles in the actual atmosphere are rarely to be found ([49], [64]) since unlike our model the earth's surface asymmetries prevent the wave disturbances occurring in widely separated geographical regions from acting in concert over extended periods of time.

We shall now briefly discuss the magnitudes of our transformations and dissipations as compared with estimates and measurements taken from the atmosphere.

For our comparison we shall use the 17- to 39-day mean of the time-averaged energy integrals in table 8.2. The results are shown in figure 8.7.

The values of generation of available zonal mean and perturbation potential energy are 29.8 and -0.70^* . This ratio of two orders of magnitude is in sharp contrast to that measured by Wiin-Nielsen and Brown [63] using 850- and 500-mb. data for January 1959, 42 and -29 . It is of interest to note that taking the lateral heat diffusive loss into account, the ratio $\langle H^*P \rangle + \langle Q_R^*P' \rangle / \langle Q_R^*[P] \rangle \approx -0.44$ is closer to Wiin-Nielsen and Brown's ratio $\langle Q^*P'_d \rangle / \langle Q^*[P_d] \rangle \approx -0.69$. That is, in our model the lateral heat diffusion plays the role of dissipating available potential energy that is done in the atmosphere by diabatic processes. The essential difference is that the former is accomplished on the zonal mean and grid-size scales whereas the latter is done on the intermediate cyclone- and continental-scales. One, of course, would expect the observed zonal mean generation for winter, 42, to be larger than the annual mean in the calculations, 30. Phillips [40] had a value of 21.

A similar study as a function of time by Winston and Krueger [64] for January using 700-mb. data gave 38 and -25 , which are somewhat smaller in magnitude than Wiin-Nielsen and Brown's measurements. This is possibly due to the low level 700-mb. wind data used. Despite the fact that Winston and Krueger's zonal energy components are about 1/3 of ours in magnitude, their perturbation components are 3 to 8 times larger. Notwithstanding the seasonal difference, in part the former discrepancy is due to their use of 700-mb. data and the fact that our zonal wind shear and speed is excessively large (see Section 11). The latter discrepancy must in part be a seasonal difference. Their ratio of $[P_d]/[K] \approx 0.3$ is quite close to ours. The period they chose to study is distinguished by the unusually well defined time cycle in the energy of about 15 days. Their data show that the maximum K' and P'_d follows that of $[P_d]$ by 6 days or 0.4 of the period, while ours follows in 4 days or 0.36 of the period of 11 days. Furthermore their $\langle Q^*[P_d] \rangle$ has a definite cyclic behavior, while in our case $\langle Q_R^*[P] \rangle$ is quasi-constant. Nevertheless we have seen that a quasi-constant $\langle Q_R^*[P] \rangle$ does give rise to a free cyclic response in the energy components. One must conclude that the variability of $\langle Q^*[P_d] \rangle$ in the actual atmosphere introduces a forced secondary mode to the energy components. Wiin-Nielsen [61] also has calculated $\langle P_d^*K \rangle = 12$ for the same data, as compared with our 20.3. In a more recent study again using the same data, Wiin-Nielsen [62] calculated $\langle \hat{K}^*\bar{K} \rangle$ to be about 3.3. This is to be compared to our $\langle \hat{K}^*\bar{K} \rangle = 13.9$.

Since Wiin-Nielsen and Brown's zonal mean generation $\langle Q^*[P_d] \rangle \approx 42$, then regarding $\langle P_d^*Q \rangle$ as a dissipation,

71 percent is dissipated in the P_d partition, 21 percent in \hat{K} and as a residual 8 percent in \bar{K} . Our results, on the other hand, give that 32 percent is dissipated in P , 21 percent in \hat{K} , and 47 percent in \bar{K} . It is difficult to see why Wiin-Nielsen's results give such a small relative dissipation in the \bar{K} partition, but this may be due to the fact that 850- and 500-mb. data alone underestimate $\langle P_d^*\hat{K} \rangle$ and particularly $\langle \hat{K}^*\bar{K} \rangle$. The former could also be underestimated because geostrophic vertical velocities were used.

As a measure of the energy decay rate we use (8.125) to define the logarithmic decrement:

$$\frac{\widetilde{\langle E_i^*F \rangle}}{\widetilde{\langle E_i \rangle}} \approx \frac{\widetilde{\langle (E+S)*E_i \rangle}}{\widetilde{\langle E_i \rangle}} \quad (8.127)$$

For this purpose, again we shall regard $\langle P^*Q_R \rangle$ as a dissipation $\langle E_i^*F \rangle$ rather than as a negative energy source $\langle E_i^*S \rangle$. For the 17-39-day period the logarithmic decrement for P is $(100 \text{ days})^{-1}$, \hat{K} is $(15.8 \text{ days})^{-1}$, \bar{K} is $(14.8 \text{ days})^{-1}$, $(\hat{K} + \bar{K})$ is $(15.2 \text{ days})^{-1}$, $E = P + \hat{K} + \bar{K}$ is $(42 \text{ days})^{-1}$. Charney and Eliassen [10] estimate the logarithmic decrement of velocity under surface frictional dissipation to be $(12 \text{ days})^{-1}$ for a baroclinic atmosphere. In terms of kinetic energy this becomes $(6 \text{ days})^{-1}$ which is a much faster decay than our $(15.2 \text{ days})^{-1}$. However, the available potential energy reservoir decreases the total energy decay rate by almost a factor of one-third.

We may also compare with observation the relative dissipations of $[K]$ and K' . Our results give: $\langle [K]^*F \rangle = 10.8 \times 10^{-3}$ joule gm. $^{-1}$ day $^{-1}$ and $\langle K'^*F \rangle = 13.0$. On the other hand, Saltzman [47] estimates from winter observations, 2.0 and 29.1, respectively, in the same units. Although our total annual mean kinetic energy dissipation, 23.8, is understandably less than Saltzman's 31.1, our ratio $\langle [K]^*F \rangle / \langle K'^*F \rangle$ is an order of magnitude larger than Saltzman's. The reason for this discrepancy in the partitioning of dissipation is not clear at this time. The dissipation formulation of our model is naturally suspect.

Actually our mean total dissipation over the 17-39-day period, 36.3, is larger than the net generation, 29.1, so that our system is not in equilibrium during this period, as we have already observed. These values lie between independent estimates by Brunt [6], 41, and Lettau [20], 12. Moreover, the ratio of dissipation by surface stresses, $\langle K_{\nu}^*F \rangle = 6.8$, to the total dissipation, $\langle E^*F \rangle = 36.3$, is 1/3 of Brunt's estimate of 0.6.

We may reduce our seven partitions of energy to Phillips' four partitions. A comparison of magnitudes is given in figure 8.8. It was pointed out at the end of Section 8b that our $\langle K'^*[K] \rangle$ (8.107a) differs from Phillips' by additional terms. We find that the common geostrophic term

*Note that the units in this discussion and in figure 8.7 are 10^{-3} joule gm. $^{-1}$ day $^{-1}$, whereas the data of table 8.4 are in 2×10^{-3} joule gm. $^{-1}$ day $^{-1}$.

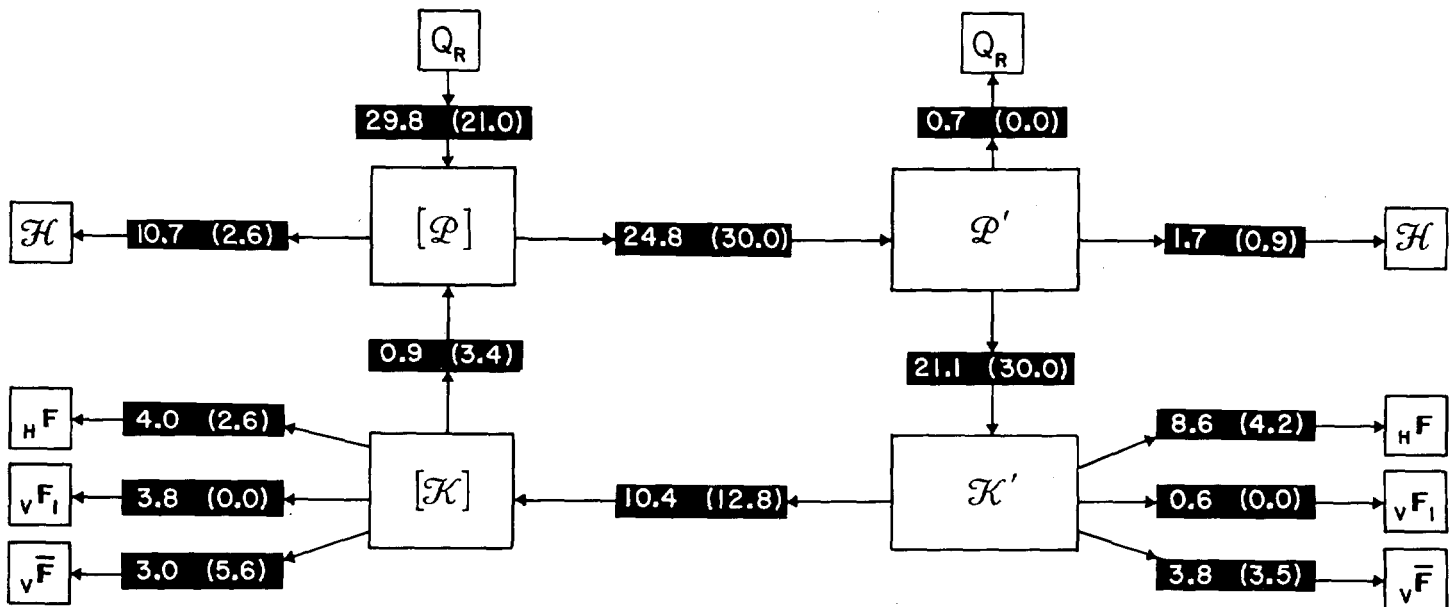


FIGURE 8.8.—A comparison of the mean energy transformations, generation rates, and dissipation rates of the present calculations with those of Phillips [40] (in parentheses). Units are in 10^{-3} joule gm. $^{-1}$ day $^{-1}$.

$$\left\{ \frac{\overline{[u'v']}}{m^2} \frac{\partial \overline{[u]}}{\partial y} \right\} = 9.4$$

whereas the additional non-geostrophic terms are

$$\frac{1}{2} \left\{ \frac{\overline{[\hat{u}]}}{m^2} \overline{[\hat{D}' \hat{u}']} \right\} = 1.2$$

$$\frac{1}{2} \left\{ \overline{[\hat{u}' \hat{\zeta}']} \frac{\overline{[\hat{v}']}}{m^2} \right\} - \left\{ \frac{\overline{[u'^2 + v'^2]}}{4m^2} \overline{[\hat{D}]} \right\} = 0.2$$

Hence the error in ignoring the non-geostrophic terms is to underestimate $\langle K' * [K] \rangle$ by approximately 10 percent.

The comparison of our energy flow with that of Phillips can be characterized by noting that despite his smaller generation, his transformations are all larger. This obviously is mainly due to the fact that our dissipations are systematically larger except for that by surface friction. Also his total energy is increasing during this period whereas ours is decreasing.

g. EFFECTS OF TRUNCATION ERROR

The differencing technique was devised to preserve the dependence of the domain integral of zonal angular momentum on surface stresses only, as well as to identically maintain thermal equilibrium. On the other hand, the kinetic and available potential energies are quadratic functions of the dependent variables. No attempt has been made to insure that the difference scheme is energy

invariant for the effects not representing the energy source or sinks in the continuous equations, that is in

$$\frac{\partial \mathcal{E}}{\partial t} = \langle \mathcal{E} * \mathcal{E} \rangle \equiv 0 \quad (8.128)$$

We may however assess the effects of the resulting truncation error.

To do this we compare the left and right sides of (8.16) over the 17- to 39-day period, i.e.,

$$\frac{(\mathcal{E}_i)_{39 \text{ days}} - (\mathcal{E}_i)_{17 \text{ days}}}{22 \text{ days}} \text{ and } \langle \widetilde{(\mathcal{E} + S + F) * \mathcal{E}_i} \rangle$$

The difference represents the rate of energy gain by each of the partitions due to truncation error. The percentage rate of gain is then

$$\frac{(\mathcal{E}_i)_{39 \text{ days}} - (\mathcal{E}_i)_{17 \text{ days}}}{22 \text{ days}} - \langle \widetilde{(\mathcal{E} + S + F) * \mathcal{E}_i} \rangle$$

These quantities were evaluated for each of the partitions and are tabulated in table 8.5.

We first of all note that there is a gain in all the kinetic energy partitions, while the available potential energy loses in both its partitions. For the total energy there is a net gain. Furthermore, the predominant percentual truncation error occurs in the perturbation partitions, \mathcal{E}'_i . This is not only because the perturbation energy is small compared with the zonal mean energy but also one might expect the truncation error to increase with reduced scale.

TABLE 8.5.—A measure of the truncation error in the energy partitions over the 17-39-day period. Column 4 gives the average percentage energy gain per day.

ε_i	1 $(\varepsilon_i)_{39} - (\varepsilon_i)_{17/22}$ days 10^{-3} joule gm $^{-1}$ day $^{-1}$	2 $\langle \varepsilon \cdot s \cdot \vartheta \rangle \cdot \varepsilon_i$ 10^{-3} joule gm $^{-1}$ day $^{-1}$	3 $\bar{\varepsilon}_i$ joule gm $^{-1}$	4 $(1)-(2)/(3)$ % day $^{-1}$
[$\bar{\kappa}_x$]	-0.15	-0.25	.1842	.05
[$\hat{\kappa}_x$]	-0.47	-1.04	.0884	.64
[$\hat{\kappa}_y$]	.00	-0.01	.0000	> 2.
[φ]	-5.25	-4.80	.9404	- .05
$\bar{\kappa}'$.37	-0.69	.0218	4.9
$\hat{\kappa}'$	0.23	-1.61	.0132	14.0
φ'	0.35	1.19	.0176	- 4.8
[κ]	-0.62	-1.29	.2726	.25
κ'	0.60	-2.30	.0350	8.3
κ	-0.02	-3.59	.3076	1.16
φ	-4.90	-3.61	.9580	- .14
[ε]	-5.87	-6.09	1.2130	.02
ε'	0.95	-1.11	.0526	3.92
ε	-4.92	-7.20	1.2656	.18

9. THE HEAT BALANCE

It was pointed out earlier that the highly simplified thermal structure of this model required an a priori constraint of thermal equilibrium in the large—i.e., the static stability and the domain mean temperature enter as constant parameters. However, the means by which this equilibrium is maintained are self-determined by the physical mechanisms inherent in the model. One may calculate the contributions to the heat flux divergence across each latitudinal surface extending through the depth of the atmosphere by integrating (3.10) with respect to x :

$$\frac{\partial[\hat{\Phi}]}{\partial t} = -m^2 \frac{\partial}{\partial y} \left[\frac{\hat{v}\hat{\Phi}}{2m^2} \right] - m^2 \gamma^2 \frac{\partial}{\partial y} \left[\frac{\hat{v}}{m^2} \right] + [H] + \kappa [Q_R] \quad (9.1)$$

Since $\hat{\Phi} = RT'_2$, then if we divide (9.1) by R , the flux divergences of heat may be expressed in terms of the changes in $[T'_2]$. The terms on the right side represent, in order, the temperature change due to the large-scale

quasi-horizontal eddies (since $[\hat{v}\hat{\Phi}] = [\hat{v}'\hat{\Phi}']$), the meridional circulation (including the effect of latent heat), the small-scale lateral diffusion, and the radiative heating gradient. These are shown in figures 9.1 to 9.4 as a function of latitude and time.

We note that the index cycle is particularly evident in the changes due to the large-scale eddies and the meridional circulation in subtropical and middle latitudes. The large-scale eddies give rise to temperature increases in high latitudes which vary between 0.5 and 1.5°C. day $^{-1}$ whereas falls in the subtropics are less than half as large—the two together imply a northward heat flux. On the other hand, the meridional circulation gives changes in the opposite sense which are smaller in magnitude in middle latitudes. This southward heat transfer is obviously due to the Hadley indirect cell which tends to compensate the large-scale eddy transfer. It is seen that the contribution due to the small-scale eddies is much smaller, of the order of 0.1°C. day $^{-1}$, except in the vicinity

of the north boundary. The time variation due to radiative heating is due to that part which simulates the outgoing radiation, since it depends on the local temperature. The mean changes at the south and north boundaries are respectively approximately $+0.1$ and $-0.5^\circ \text{C. day}^{-1}$.

Returning to figure 9.1 we see that the maximum intensity of the mid-latitude flux divergence by the large-scale eddies coincides with the time of maximum $\langle P' * \hat{K}' \rangle$ (fig. 8.4). However, the phase of the temperature change due to the meridional circulation (fig. 9.2) follows that due to the large-scale eddies by approximately 1 day and is of opposite sign so that the compensation is not complete. This is reflected in the net temperature change, i.e., the left side of (9.2) which is shown in figure 9.5. The result is a well pronounced lag of about 4 days between $\partial[\hat{\Phi}]/\partial t$ at middle and at subtropical latitudes. It is to be noted that at equatorial latitudes, the flux divergence due to the meridional circulation (fig. 9.2), and reflected in the net change (fig. 9.5), has a period of 6 days, just half that at mid-latitudes. The amplitude of this period is only noticeable before 35 days. The zonal mean temperature $[T_2]$ as a function of time is given in figure 9.6.

One may also calculate the heat flux through a latitude circle. Multiplying (9.1) by $c_p/R = \kappa^{-1}$ gives the heating rate per unit mass and, since p_4/g is the mass per unit area, then operating with $(p_4L/g) \int_0^y (\) dy/m^2$ gives the heating rate for the zone from the equator to y . Upon using (4.26) we then have

$$\begin{aligned} \frac{p_4L}{\kappa g} \int_0^y \frac{\partial[\hat{\Phi}]}{\partial t} \frac{dy}{m^2} &= \frac{p_4L}{\kappa g} \left(-\frac{[\bar{v}\hat{\Phi}]}{2m^2} - \gamma^2 \frac{[\hat{v}]}{m^2} \right. \\ &\quad \left. + (k_H\Delta)^2 \left[\frac{|\bar{D}|}{2} \frac{\partial\hat{\Phi}}{\partial y} \right] \right)_0^y + \frac{p_4L}{g} \int_0^y [Q_R] \frac{dy}{m^2} \quad (9.2) \end{aligned}$$

By virtue of our boundary conditions there is no heat flux through $y=0, Y$. In order to compare our results with annual mean observations, it is necessary to deal with a quasi-steady state. This is done by taking a time mean of our results over an integral number of index cycles. In particular a mean was taken over the 2 cycles encompassed by 17–39 days. Then according to the notation of (C4), (9.2) becomes

$$\begin{aligned} \frac{p_4L}{\kappa g} \left(\frac{\tilde{\bar{v}}\hat{\Phi}}{2m^2} + \gamma^2 \frac{\tilde{\hat{v}}}{m^2} - (k_H\Delta)^2 \frac{|\bar{D}|}{2} \frac{\partial\hat{\Phi}}{\partial y} \right)_y \\ + \frac{p_4L}{\kappa g} \int_0^y \frac{\partial\hat{\Phi}}{\partial t} \frac{dy}{m^2} - \frac{p_4L}{g} \int_0^y \tilde{Q}_R \frac{dy}{m^2} = 0 \quad (9.3) \end{aligned}$$

in which we take $Rp_4L\Delta/g\kappa = 5.42 \times 10^{19} \text{ cal. deg.}^{-1}$. The last two terms were evaluated numerically according to (C6). The poleward fluxes at y by the various components are given in figure 9.7, the curves being

A: $\frac{p_4L}{\kappa g} \left(\frac{\tilde{\bar{v}}\hat{\Phi}}{2m^2} \right)_y$	Flux by large-scale quasi-horizontal eddies
B: $\frac{p_4L}{\kappa g} \gamma^2 \left(\frac{\tilde{\hat{v}}}{m^2} \right)_y$	Flux by the mean meridional circulation (including the effects of condensation)
C: $-\frac{p_4L}{\kappa g} (k_H\Delta)^2 \left(\frac{ \bar{D} }{2} \frac{\partial\hat{\Phi}}{\partial y} \right)_y$	Flux by small-scale quasi-horizontal eddies
D: $\frac{p_4L}{\kappa g} \int_0^y \frac{\partial\hat{\Phi}}{\partial t} \frac{dy}{m^2}$	Effective flux due to non-steadiness
E: $-\frac{p_4L}{g} \int_0^y \frac{\tilde{Q}_R}{m^2} dy$	Effective flux due to radiative heating

We note that the northward flux required by the net radiation has a maximum of $4.6 \times 10^{19} \text{ cal. day}^{-1}$ which corresponds more closely to Albrecht's [1] estimate than to Houghton's [19] $11.4 \times 10^{19} \text{ cal. day}^{-1}$. As we have seen in Section 3 the linearization and particularly the normalization are responsible for a reduction of Houghton's maximum by almost 40 percent (fig. 3.3). Moreover, as will be seen, the meridional temperature gradient of our calculations is larger than in the atmosphere. Thereby we overestimate the latitudinal cooling gradient due to long wave radiation. The flux required by the net radiation gradient is thus further reduced to a maximum of $4.6 \times 10^{19} \text{ cal. day}^{-1}$ rather than $7.2 \times 10^{19} \text{ cal. day}^{-1}$ (compare curve E in figure 9.7 with the normalized curve in figure 3.3). Fortunately, our maximum due to Q_R corresponds in magnitude to the maximum meridional sensible heat transport demanded of the atmosphere when evaporation, condensation, and ocean transports as well as radiation are taken into account (see Appendix A and fig. A6). The latitude of our maximum, however, lies in between the double maxima of the net heating shown in figure A6.

Our dynamical calculations in figure 9.7 show that the major mechanism for the northward heat flux in mid-latitudes is that of the large-scale eddies. The meridional circulation dominates south of 32° latitude and actually gives a significantly large southward heat transfer in mid-latitudes, as one would expect, by the Ferrel circulation. The small-scale eddies seem to contribute too heavily to the northward transfer.

A comparison of the calculated large-scale eddy transfer with observations [56], [31] shows a good correspondence in the latitudinal variation, that is a maximum at about 48°N . and a rapid reduction south of 30°N . The magnitude is somewhat less than the observed transfer, particularly the sensible plus latent heat transfer measured by Starr and White which is probably a more valid comparison with our heating function. If the small-scale diffusion mechanism were adjusted to give a smaller

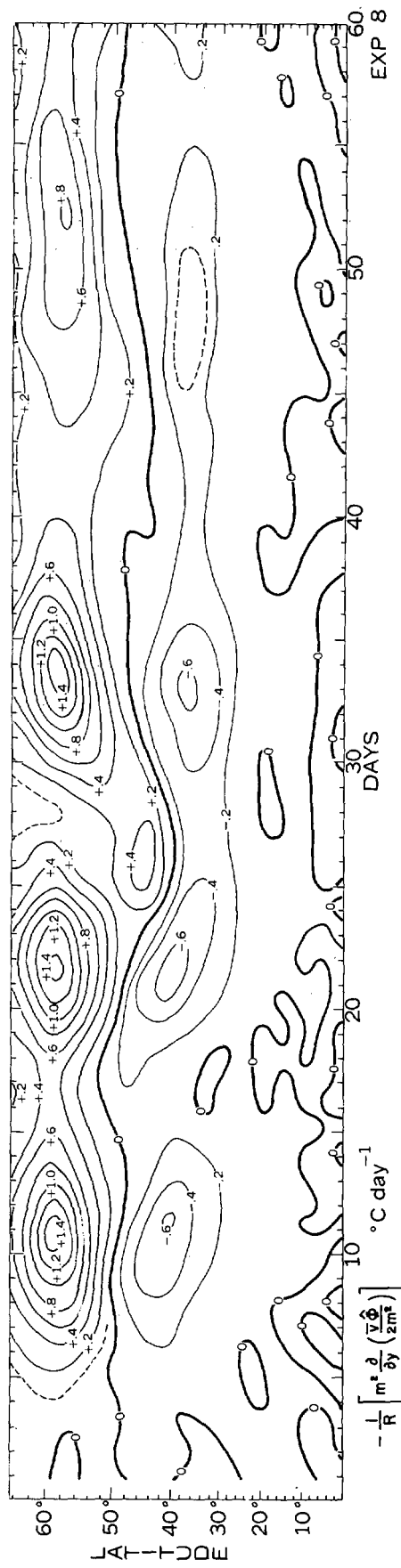


FIGURE 9.1.—The contribution to the meridional heat flux divergence by the large-scale eddies as a function of time and latitude.

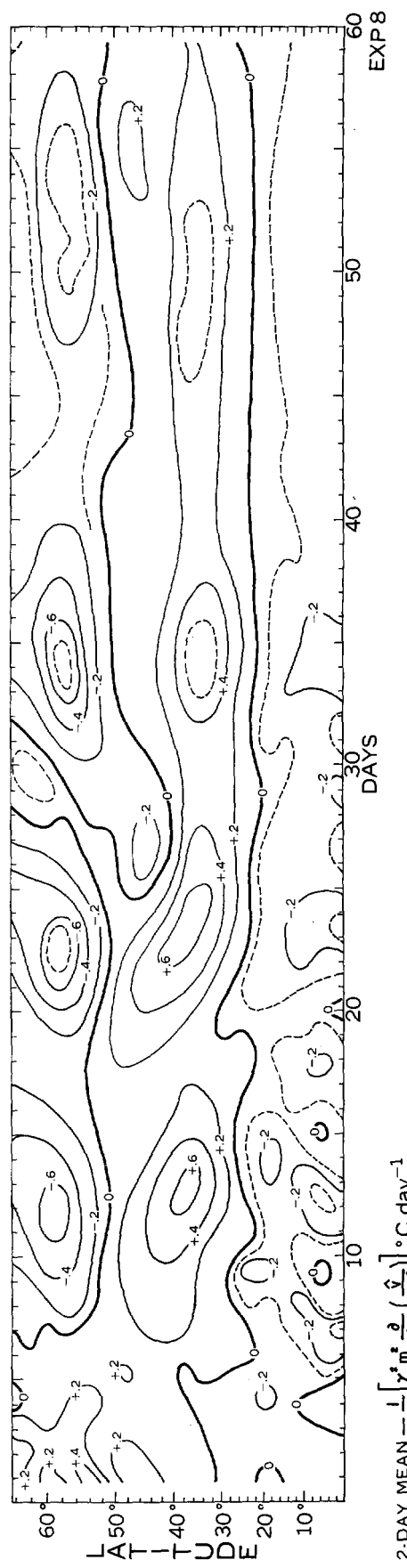


FIGURE 9.2.—The contribution to the meridional heat flux divergence by the meridional circulation (a running average over 2-day intervals to eliminate the high frequency variations).

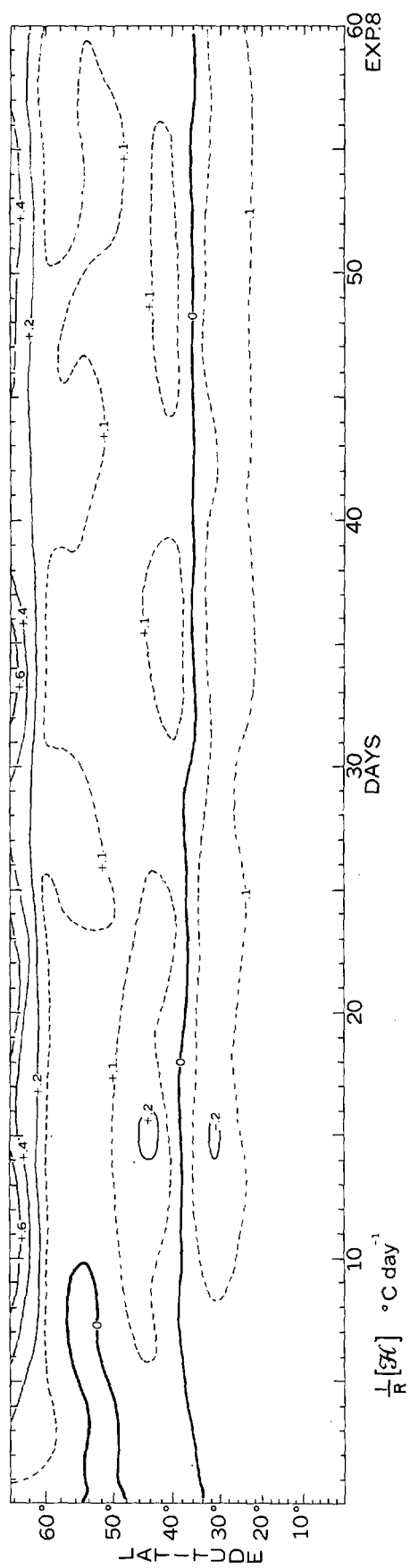


FIGURE 9.3.—The contribution to the meridional heat flux divergence by small-scale lateral heat diffusion.

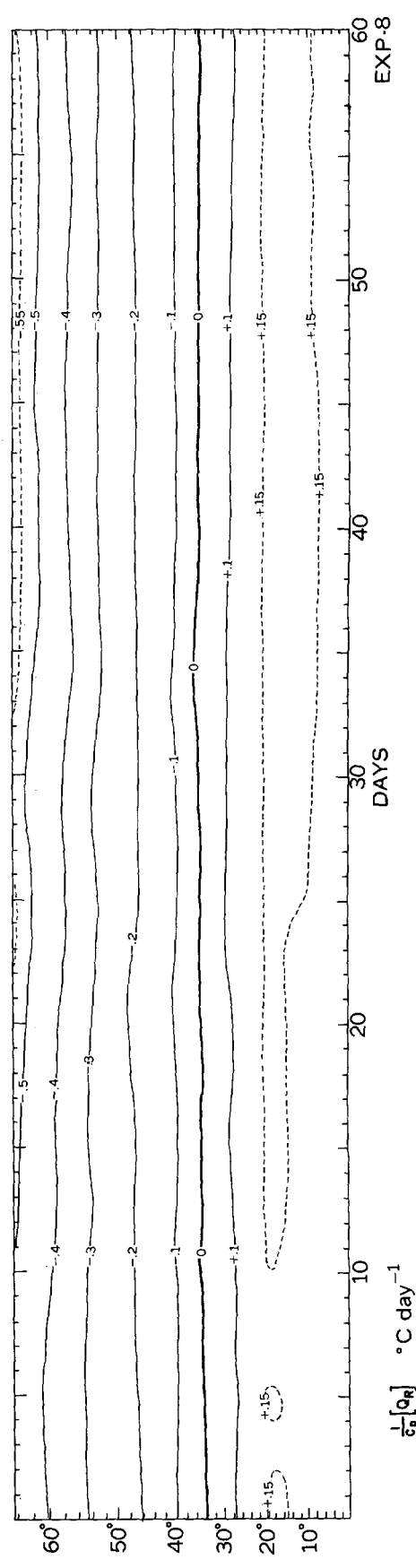


FIGURE 9.4.—The contribution to the meridional heat flux divergence by the radiative heating gradient.

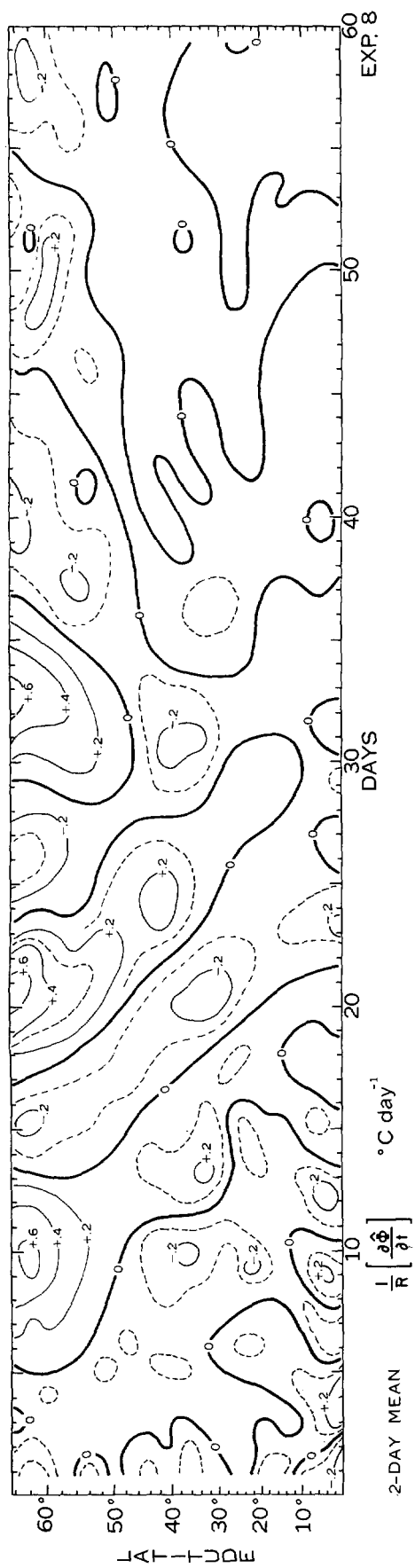


FIGURE 9.5.—The sum of the contributions given in figures 9.1 to 9.4 (averaged over 2-day intervals).

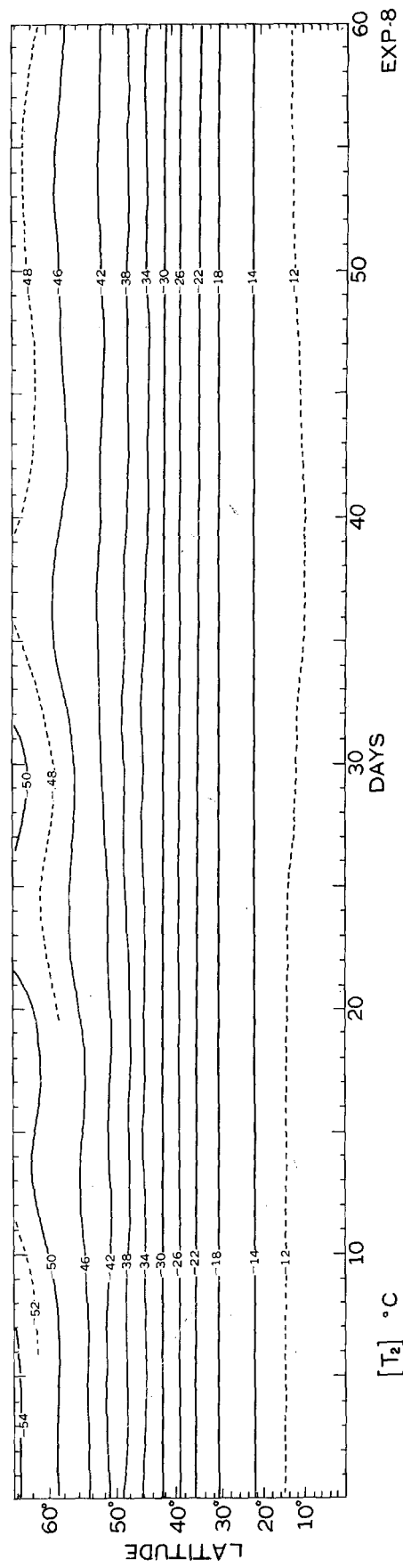


FIGURE 9.6.—The zonal mean temperature as a function of time and latitude.

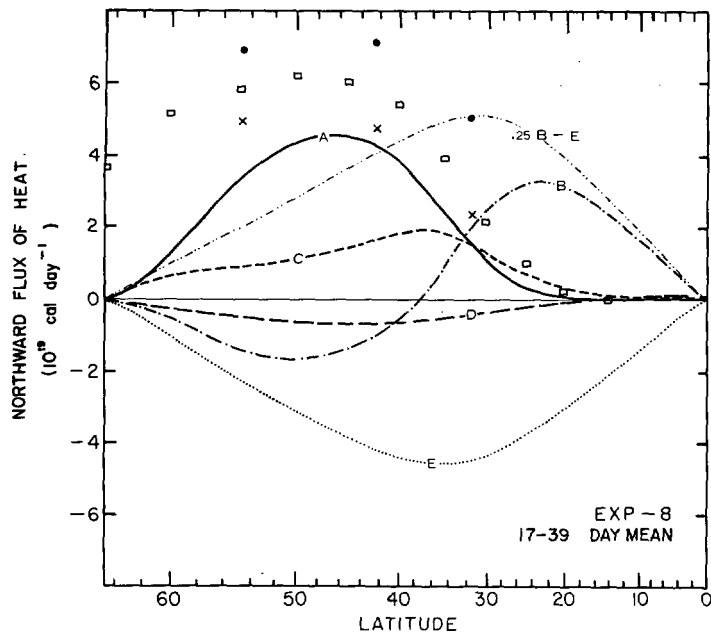


FIGURE 9.7.—The net contributions to poleward heat flux as a function of latitude for the 17-39 day mean: Curve A corresponds to figure 9.1 (large-scale eddies), B to 9.2 (meridional circulation), C to 9.3 (small-scale eddies), D to 9.5 (net), and E to 9.4 (radiative heating). The observed annual mean large-scale eddy flux through a latitude surface (to be compared with curve A) are given by: □ sensible—Mintz [31]; × sensible—Starr and White [56]; • sensible and latent—Starr and White [56].

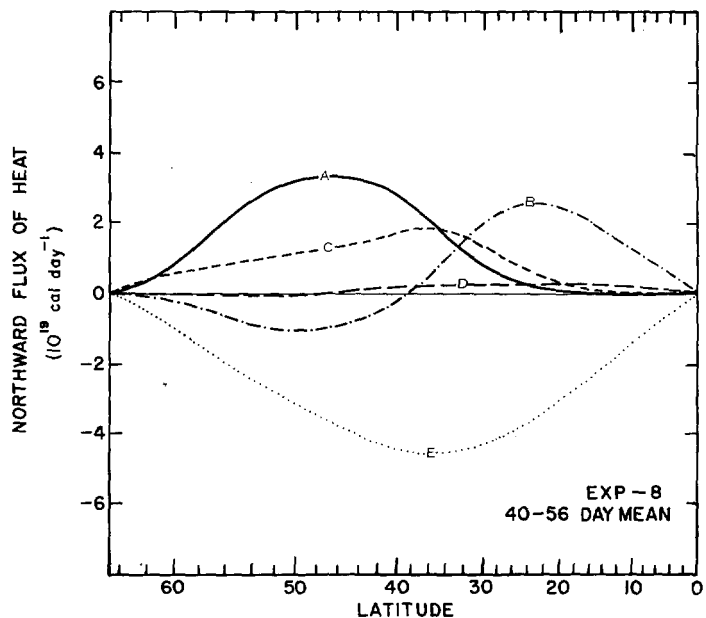


FIGURE 9.8.—Same as figure 9.7, but for the 40-56 day mean.

flux, the large-scale eddies would have to increase in intensity to satisfy the radiative flux requirements. Since the Hadley circulation would also increase and compensate, just a small reduction in the small-scale eddy transfer could give rise to a much larger increase in the large-scale eddy transfer. Furthermore during this period the net heat flux was somewhat negative (as reflected by the non-steady contribution), so that a balance was not quite maintained. In addition, since we have simplified the radiative transfer and the heating by the hydrologic cycle and the oceans, detailed qualitative comparison of the present results with observation is unwarranted.

The flux required by the net non-adiabatic heating in the present model due to radiation and condensation is found from (3.2). In terms of the fluxes in (9.3) it is

$$\frac{p_4 L}{g} \int_0^y \tilde{Q} dy = \frac{p_4 L}{g} \int_0^y \tilde{Q}_R dy + 0.25 \frac{p_4 L}{\kappa g} \gamma^2 \left(\frac{\hat{v}}{m^2} \right)_y \quad (9.4)$$

since $\gamma^2 = 0.8 \gamma_s^2$. The flux required by non-adiabatic heating is therefore shown in figure 9.7 as (0.25 B-E). For all practical purposes this curve has a single maximum at 31° latitude in contrast to the flux corresponding to $p_4 Q/g$ in figure A6. That is, the non-adiabatic heating used here is monotonic; the reason lies in our assumption

that the remaining non-adiabatic heat sources and sinks balance each other, particularly assumption (3.1). We must therefore conclude that the meridional scale of the motions is primarily determined by the adiabatic dynamics and that the reduced heating scale due to the condensation part is mainly in response to the dynamics.

Although direct atmospheric measurements of the heat transfer by the meridional circulation are not available, since it is essentially ageostrophic, its character may be deduced indirectly by noting the discrepancy between the integral of the non-adiabatic heating calculated in Appendix A (fig. A7) and observed large-scale eddy fluxes. The present results (compare curve B in fig. 9.7 with curve (A-B) in fig. A7) bear this out.

The energy partitions as a function of time (fig. 8.2) indicated a quasi-equilibrium in the energy levels beyond 40 days. This was marked by a lengthening of the cycle period and a reduction in the energy fluctuations about the equilibrium state. To see what changes occurred in the poleward heat transfer mechanisms we have calculated northward heat flux for the single cycle 40-56 days (fig. 9.8). Upon comparing with the 17-39 day mean (fig. 9.7), we note a reduction of the intensity of the transfer by the large-scale eddies and the meridional circulation of approximately 20 percent, whereas the small-scale eddy transfer is about the same. The latter is therefore playing a relatively larger role in the heat transfer than during the earlier period. However, the qualitative character of the transfer by the different mechanisms is intact.

10. THE ZONAL ANGULAR MOMENTUM BALANCE

Unlike the case of heat, there is no a priori constraint to insure a balance in the angular momentum, i.e., that the domain integral of the total zonal angular momentum be identically constant. The model must not only determine the partitioning amongst the allowable angular momentum transport mechanisms but also the degree of balance. This, as we shall see, will be determined by the surface wind distribution.

The angular momentum flux divergence per unit mass across a latitude circle at each level may be calculated by multiplying the equation of motion by am^{-2} and integrating with respect to x :

$$a \frac{\partial}{\partial t} \frac{[u_1]}{m^2} = -a \left(m^2 \frac{\partial}{\partial y} \frac{[u_1 v_1]}{m^4} - \frac{[H F_{x1}]}{m} \right) + a \left(\frac{[\hat{D}\bar{u}]}{4m^2} + \frac{f[\hat{v}]}{2m^2} + \frac{[v F_{x1}]}{m} \right) \quad (10.1)$$

$$a \frac{\partial}{\partial t} \frac{[u_3]}{m^2} = -a \left(m^2 \frac{\partial}{\partial y} \frac{[u_3 v_3]}{m^4} - \frac{[H F_{x3}]}{m} \right) - a \left(\frac{[\hat{D}\bar{u}]}{4m^2} + \frac{f[\hat{v}]}{2m^2} + \frac{[v F_{x3}]}{m} \right) + a \frac{[v \bar{F}_x]}{m} \quad (10.2)$$

The two terms in the first parenthesis on the right side represent the meridional flux divergence of relative angular momentum resulting from large-scale motions and from small-scale lateral diffusion. The three terms in the second parenthesis are the internal vertical flux divergence resulting from the transfer of relative angular momentum by the large-scale vertical motions, from the transfer of the earth's angular momentum by the meridional circulation, and the transfer of relative angular momentum by small-scale vertical eddy diffusion. The last term of (10.2) is the vertical exchange of angular momentum between the lower boundary and the lower half of the atmosphere.

By adding (10.1) and (10.2) and dividing by 2 we have the equation for the change of vertically integrated zonal angular momentum per unit mass:

$$a \frac{\partial}{\partial t} \frac{[\bar{u}]}{2m^2} = -am^2 \frac{\partial}{\partial y} \frac{[\bar{u}v]}{2m^4} + \frac{a[H \bar{F}_x]}{2m} + \frac{a[v \bar{F}_x]}{2m} \quad (10.3)$$

The three contributions on the right side are shown (aside from a factor of a) in figures 10.1, 10.2, and 10.3 as a function of time and latitude. Aside from the transients during the first 8 or 9 days, the large-scale eddies (fig. 10.1) give an increase of angular momentum in middle latitudes and a decrease in subtropical latitudes. Its maximum intensity occurs approximately 2 days after the corresponding maximum flux divergence of heat (fig. 9.1). As might be expected the small-scale lateral diffusion (fig. 10.2) increases the angular momentum at high and low latitudes at the expense of that of the jet stream, but quantitatively the contributions are considerably less than that of the large-scale flux divergence. Of course,

the surface stresses (fig. 10.3) increase the atmosphere's angular momentum in the surface easterlies and decrease it in the westerlies. The upward flux divergence of angular momentum from earth to atmosphere also shows a strong correlation with the index cycle, its maximum occurring at the transition from low to high index.

The zonal angular momentum itself, $[\bar{u}]/2m^2$, resulting from these contributions, is shown in figure 10.4. This too is periodic but with small amplitude, attaining its maximum during the transition from low to high index. It is at this time that the maximum gradient of zonal angular momentum occurs south of the jet stream and one should therefore expect a minimum in the inertial stability.

In order to examine the degree of balance in the zonal angular momentum, we form the domain integral from (10.3)

$$\frac{\partial}{\partial t} \left\{ \frac{a[\bar{u}]}{2m^2} \right\} = \left\{ \frac{a[v \bar{F}_x]}{2m} \right\} \quad (10.4)$$

by virtue of the lateral boundary conditions. Hence $\{[\bar{u}]/2m^2\}$ can change only as a result of the non-vanishing of the right side, that is, if the zonal surface stresses exert a net torque on the atmosphere. Figure 10.5 shows $\{[\bar{u}]/2m^2\}$ as a function of time. We note that during the first 20 days there is a steady increase accompanying the transition from surface easterly winds everywhere to the generation of westerlies in middle latitudes. Beyond this point the total zonal angular momentum becomes quasi-constant. The variations, which show very little correlation with the index cycle, are within ± 2 percent of their mean. This is a well known equilibrium property of the atmosphere, aside from seasonal changes. Just as in the atmosphere, the model accomplishes this equilibrium through adjustments in the surface wind distribution. This is quite evident from figure 10.3 from which we see that changes of mid-latitude westerly torques are accompanied by compensating tropical easterly torques.

In order to examine the fluxes themselves in somewhat greater detail, we shall deal with a time mean for an integral number of index cycles to attain conditions approximating a steady state, as was done in the case of heat flux.

For this purpose we shall consider the budget for zonal rings bounded by the latitudes y_{j-1} and y_{j+1} and by the pressure surfaces p_{k-1} and p_{k+1} . Taking the normalized area-weighted integral of (10.1) and (10.2), i.e., operating with $(m_j^2/2\Delta) \int_{y_{j-1}}^{y_{j+1}} (\) dy/m^2$, and then multiplying by the mass of a zonal ring, $-\hat{p}2\Delta L/gm_j^2$, we have that the change of angular momentum of a zonal ring is

$$\begin{aligned} -\frac{\hat{p}La2\Delta}{g} \left(\frac{\partial [u_1]}{\partial t} \right)_j &= \\ -\frac{\hat{p}La}{g} \left(-\frac{[u_1 v_1]}{m^4} + \left(\frac{k_H \Delta}{m} \right)^2 [D_1 D_{S1}] \right)_{j-1}^{j+1} & \\ -\frac{\hat{p}La2\Delta}{g} \left(\frac{[\hat{D}\bar{u}]}{4m^4} + \frac{f[\hat{v}]}{2m^4} + \frac{[v F_{x1}]}{m^3} \right)_j & \end{aligned} \quad (10.5)$$

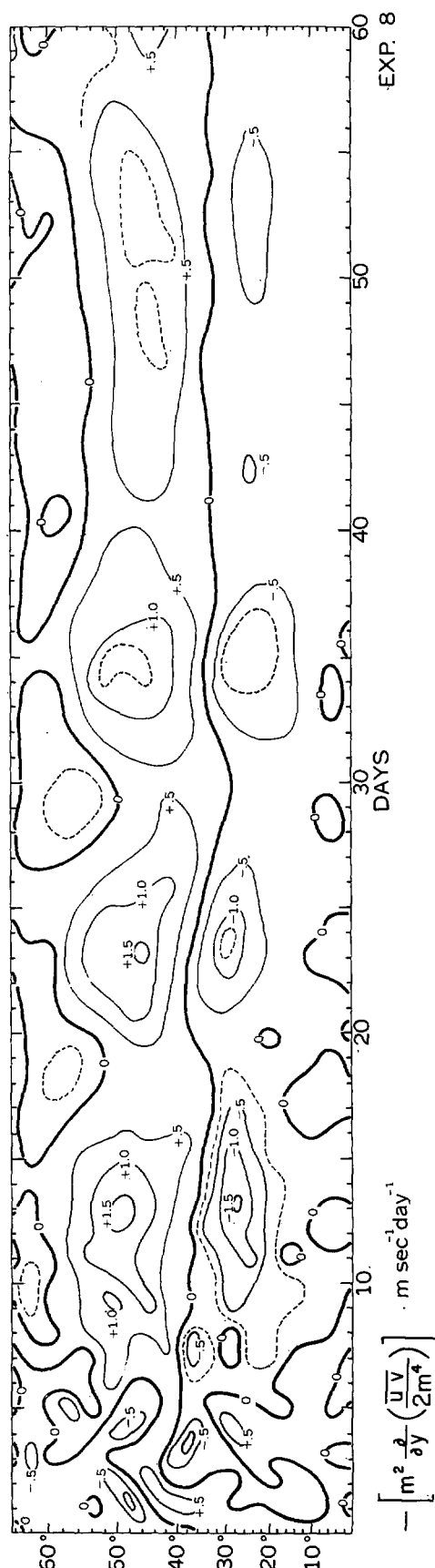


FIGURE 10.1.—The contribution to the meridional flux divergence of vertically integrated zonal angular momentum by the large-scale eddies and the meridional circulation.

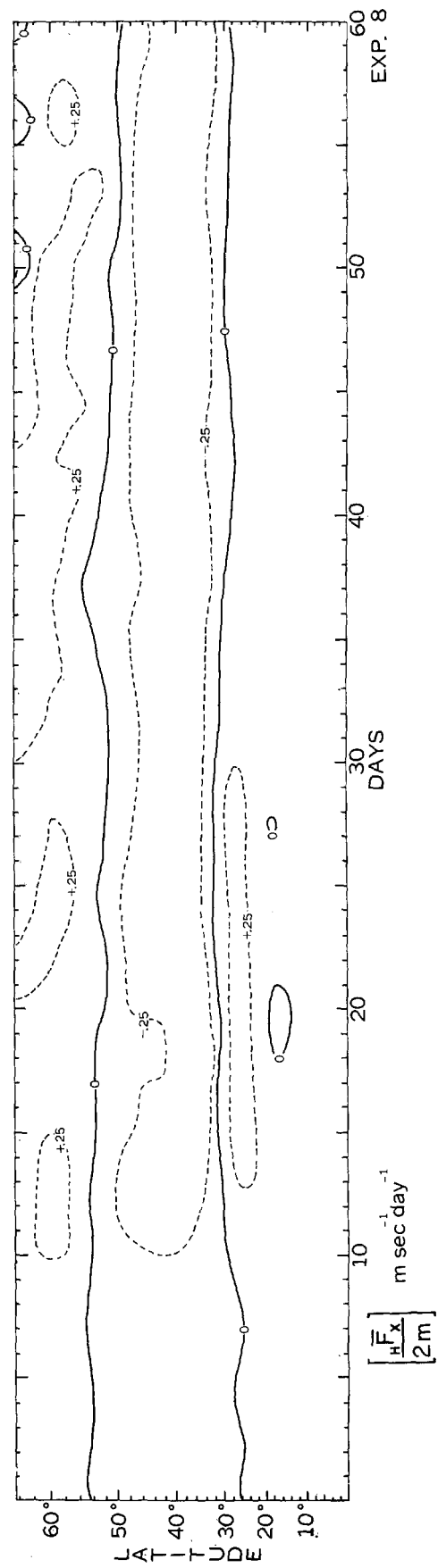


FIGURE 10.2.—The contribution to the meridional flux divergence of vertically integrated zonal angular momentum by the small-scale lateral diffusion.

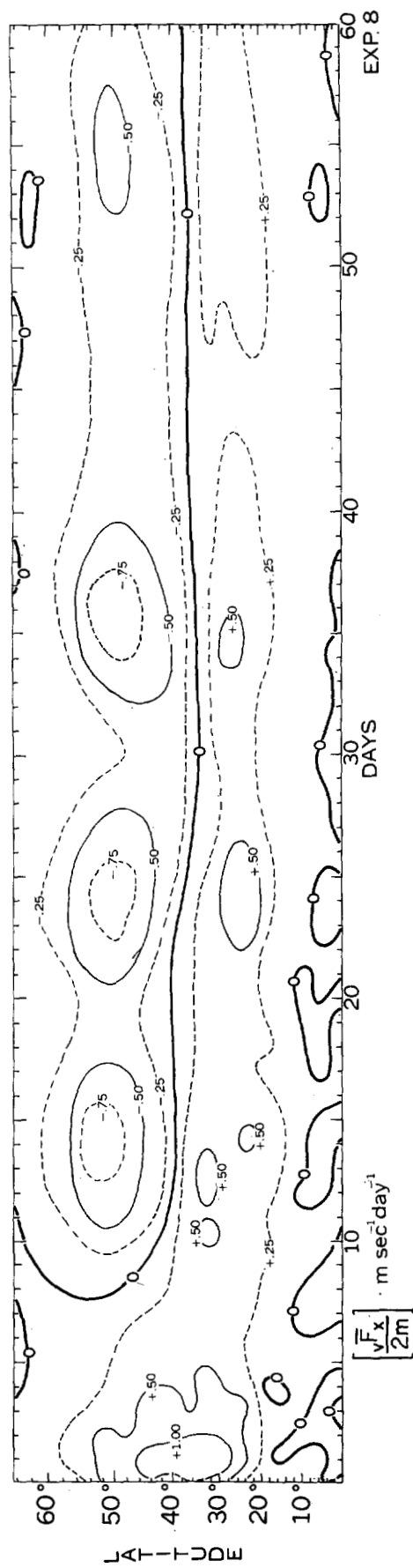


FIGURE 10.3.—The contribution to the meridional flux divergence of vertically integrated zonal angular momentum by the surface stresses.

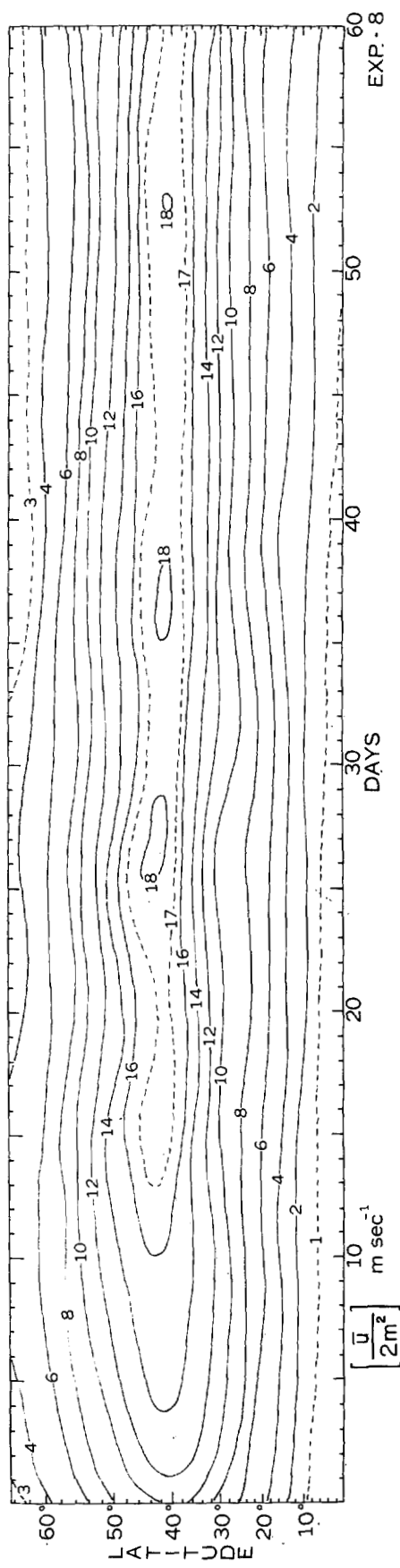


FIGURE 10.4.—The longitudinal mean vertically integrated zonal angular momentum as a function of time and latitude.

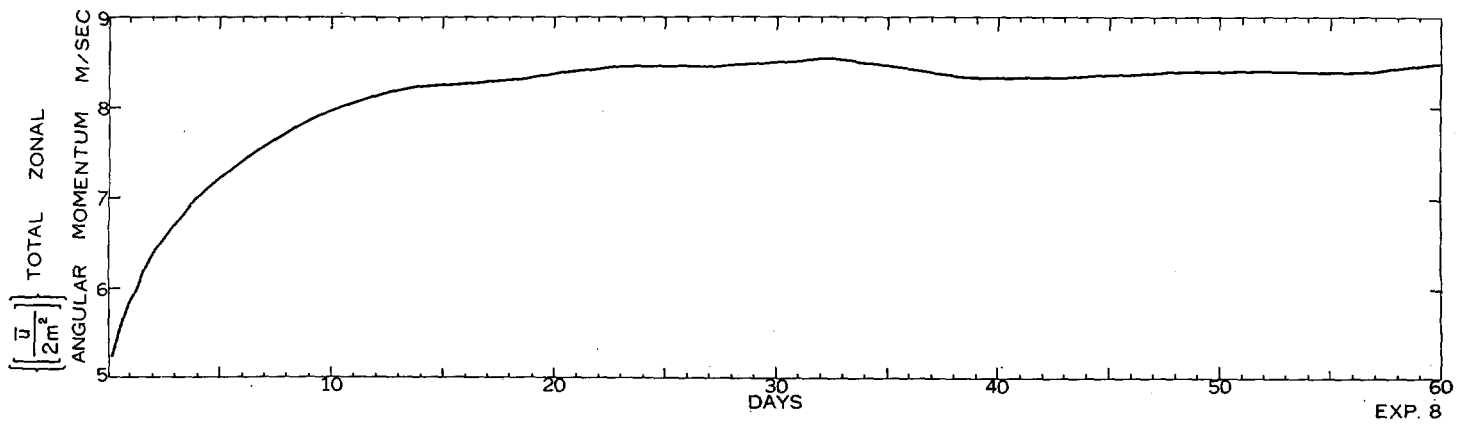


FIGURE 10.5.—The domain mean vertically integrated zonal angular momentum as a function of time.

$$\begin{aligned}
 -\frac{\hat{p}La2\Delta}{g} \left(\frac{\partial[u_3]/m^4}{\partial t} \right)_j = & \\
 -\frac{\hat{p}La}{g} \left(-\frac{[u_3v_3]}{m^4} + \left(\frac{k_H\Delta}{m} \right)^2 [D_3|D_{S3}] \right)_{j-1}^{j+1} & \\
 + \frac{\hat{p}La2\Delta}{g} \left(\frac{\hat{D}\bar{u}}{4m^4} + \frac{f[\hat{v}]}{2m^4} + \frac{[v\bar{F}_{x1}]}{m^3} \right)_j & \\
 - \frac{\hat{p}La2\Delta}{g} \left(\frac{[v\bar{F}_x]}{m^3} \right)_j & \quad (10.6)
 \end{aligned}$$

Taking a time mean and introducing deviations from the mean for the large-scale non-linear eddy transfers according to the notation (C4), (C5):

$$\begin{aligned}
 0 = -\frac{\hat{p}La2\Delta}{g} \left(\frac{\partial\tilde{u}_l/m^4}{\partial t} \right)_j, & \\
 -\frac{\hat{p}La}{g} \left(\frac{\tilde{u}_l\tilde{v}_1}{m^4} + \frac{\tilde{u}_l^*v_1^*}{m^4} - \left(\frac{k_H\Delta}{m} \right)^2 \widetilde{|D_1|D_{S1}} \right)_{j-1}^{j+1} & \\
 + \frac{\hat{p}La2\Delta}{g} \left(\frac{\tilde{\hat{D}}\tilde{u}}{4m^4} + \frac{\hat{D}^*\tilde{u}^*}{4m^4} + \frac{f\tilde{v}}{2m^4} + \frac{v\tilde{F}_{x1}}{m^3} \right)_j & \quad (10.7)
 \end{aligned}$$

$$\begin{aligned}
 0 = -\frac{\hat{p}La2\Delta}{g} \left(\frac{\partial\tilde{u}_3/m^4}{\partial t} \right)_j + \frac{\hat{p}La2\Delta}{g} \left(\frac{\tilde{v}\bar{F}_x}{m^3} \right)_j & \\
 -\frac{\hat{p}La}{g} \left(\frac{\tilde{u}_3\tilde{v}_3}{m^4} + \frac{\tilde{u}_3^*v_3^*}{m^4} - \left(\frac{k_H\Delta}{m} \right)^2 \widetilde{|D_3|D_{S3}} \right)_{j-1}^{j+1} & \\
 -\frac{\hat{p}La2\Delta}{g} \left(\frac{\tilde{\hat{D}}\tilde{u}}{4m^4} + \frac{\hat{D}^*\tilde{u}^*}{4m^4} + \frac{f\tilde{v}}{2m^4} + \frac{v\tilde{F}_{x1}}{m^3} \right)_j & \quad (10.8)
 \end{aligned}$$

The fluxes may therefore be calculated upon applying the boundary conditions (5.2) and (5.6). The components are plotted in figure 10.6 for the period 17–39 days. The plotted values must be multiplied by $-\hat{p}La2\Delta/g = 1.44 \times 10^{31}$ gm. cm.² m.⁻¹ = 1.67×10^6 ton m. day sec.⁻¹ in order to get them into the units of equations (10.7) and (10.8). The double arrows denote the total fluxes. Although the angular momentum is somewhat

non-steady locally (the numbers in parentheses), an attempt has been made to depict the flow by introducing a stream function, which is shown in figure 10.7. The predominant flow, upward from the subtropical surface westerlies, maximum northward just south of the angular momentum maximum and then downward in the surface westerlies, is in excellent qualitative agreement with similar charts of observed angular momentum streamlines by Widger [60] and Lorenz [25]. Even such features as the weak return circulations at equatorial and high latitudes are evident. However, the artificial boundaries in the present model preclude detailed comparison with observations in their vicinity.

For further comparison with observations wherever possible, the components of the northward flux in the upper and lower half of the atmosphere are graphed in figures 10.8 and 10.9 and the upward flux at 500 mb. and at the surface are graphed in figures 10.10 and 10.11. It is evident that the total northward transfer (curve D) is predominantly accomplished by the large-scale eddies (curve A). Comparison with Starr and White's [56] calculations from observations (using appropriately averaged

data, i.e., what corresponds to \tilde{u}^*v^*) and those of Mintz [31] shows excellent agreement in the magnitude and distribution of the large-scale eddy flux in the 500–0 mb. layer. Buch's [7] data do not differ materially from those of Starr and White. As in the case of northward heat flux our calculations are somewhat smaller in magnitude. But in the case of angular momentum a direct comparison with observations is somewhat more valid since observation gives a very small flux across 64.4° latitude. The percentage deviation of our results from observation in the 1000–500-mb. layer is much larger than in the upper layer, but the absolute deviation is about the same. The significance of our result is that we predict that the large-scale eddy flux in the lower atmosphere is almost an order of magnitude smaller than that in the upper half. The transfer by the meridional circulation (curve B) is virtually

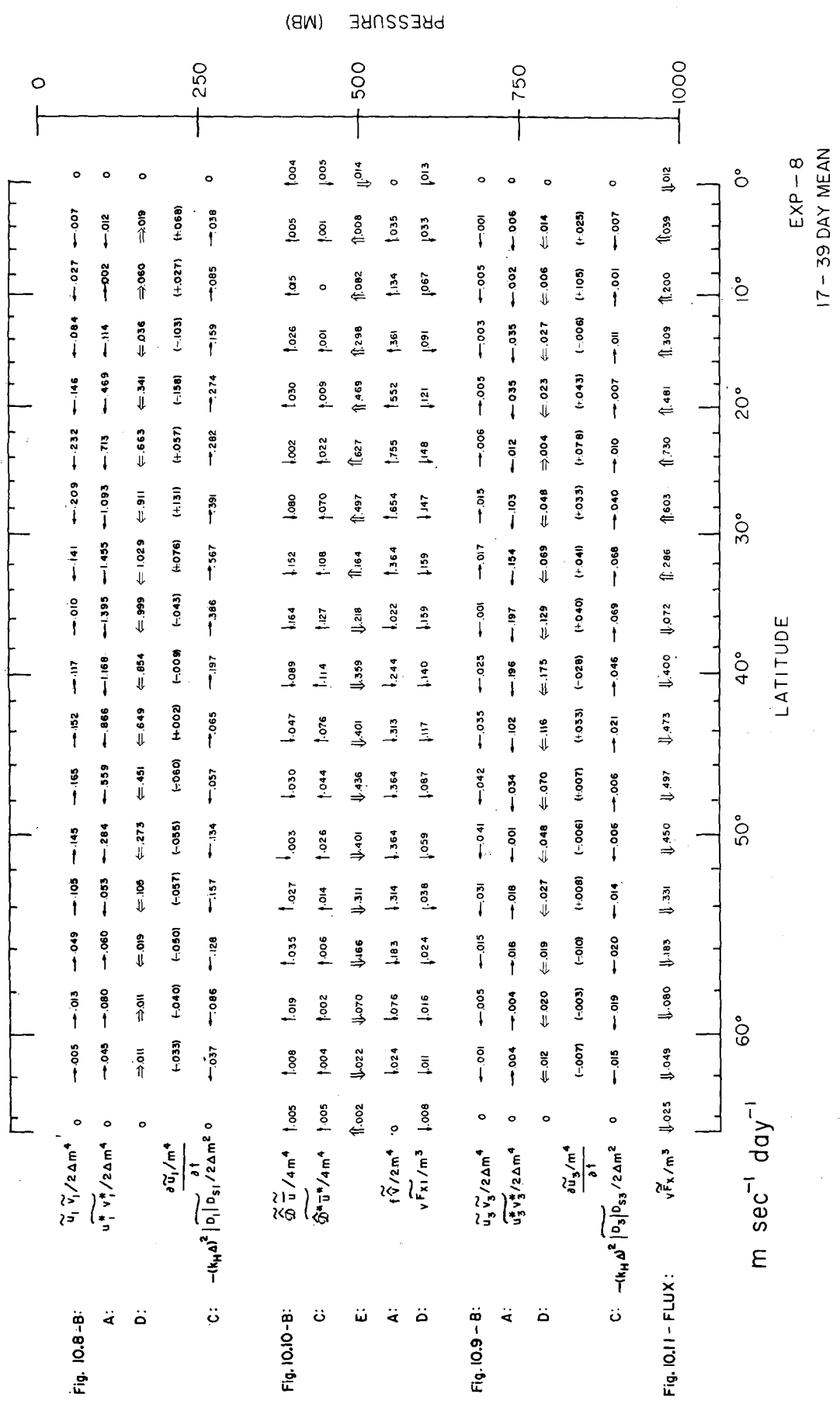


FIGURE 10.6.—The contributions to the meridional and vertical flux of zonal angular momentum for the 17-39 day mean. The double arrows are the resultants.

negligible at all latitudes. The net upward transfer at 500 mb. in figure 10.10 (curve E) is for the most part a result of the transfer of the earth's angular momentum by the meridional circulation (curve A). Since this is essentially ageostrophic, direct measurements are extremely difficult. The fact that the transports by the large-scale vertical advection terms are small (curves B and C) is a reflection of the quasi-geostrophic character of the motion, i.e., that the vertical advection of momentum in the equations of motion is negligible. More direct verification of this will be given in Section 12. The flux between the ground and the atmosphere is given in figure 10.11. Since the corresponding stress is more familiar we also show

$$\tilde{\tau}_{z4} = -\frac{\hat{p}}{g} \tilde{v} \tilde{F}_x \quad (10.9)$$

Here we have plotted the annual mean stress over the oceans from Priestley [44] and Mintz's [31] deduced surface stress from the geostrophic poleward eddy flux of angular momentum.

As in the case of the heat transfer, we have calculated the angular momentum fluxes during the quasi-equilibrium period, 40–56 days, in figures 10.12, 10.13, 10.14, and 10.15. Here too we note that there has been a reduction of the transfer by the large-scale eddies, the meridional circulation, and the surface stresses, but that the general character of the latitudinal distribution is intact.

11. THE MEAN ZONAL WIND AND MERIDIONAL CIRCULATION

The mean zonal wind over the 17–39 day period, \tilde{u}/m , is shown in figure 11.1. The most striking failure is in predicting the maximum. Our value of 40 m. sec.^{-1} is larger than that of Mintz [31] who had 27 m. sec.^{-1} at a somewhat lower latitude and much larger than Buch's measurements [7] of 19 m. sec.^{-1} . Our discrepancy is however smaller than the theoretical calculations of Phillips [40] who had 50 m. sec.^{-1} . The southward tilt with height of the axis of maximum zonal wind is in good agreement with observation. Our subtropical easterlies are in close agreement with observation except that they do not extend above the 500-mb. level. There is only a faint suggestion of a secondary maximum of zonal easterlies at 20° latitude in contradistinction to Phillips' [40] and Charney's [9] results. Although Mintz's [30] observations show such a double structure during each season with the predominant maximum occurring at low latitudes, his annual mean [32] does not. On the other hand, Buch's data [7] show only a single maximum at all seasons as well as for the annual mean. Cold core, flat base dishpan experiments [15], [17] also show the instantaneous existence of a weak double jet. The reality of a double jet as a feature of the annual mean is therefore in question since it may tend to be wiped out by averaging over

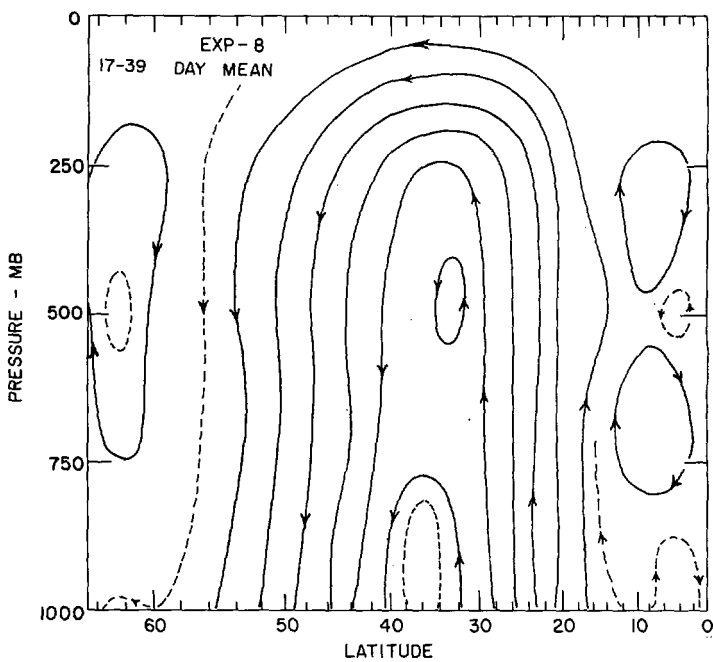


FIGURE 10.7.—The "streamlines" of the zonal angular momentum flux corresponding to the resultants in figure 10.6.

latitudinal shifts with season. Its significance as a feature of the annual mean flow is even more questionable. It is quite possible that any stronger tendency for a double jet structure in our calculations may have been wiped out by too great a small-scale lateral diffusion coefficient.

The discrepancy in the magnitude of the maximum zonal wind reflects an error in both the vertical mean and the vertical shear. The vertical wind shear or alternatively the meridional temperature gradient is much too large. As is discussed in Appendix B, the equilibrium vertical shear as well as the zonal wave number of maximum instability are essentially determined by the effective static stability. Hence for a reduction of the effective static stability the wave number of maximum instability is increased and the equilibrium meridional temperature gradient is reduced. This would suggest that an effective static stability of 0.8 standard is too large. For example, figure 6.3 indicates that a reduction of the effective static stability to 0.6 standard would decrease the equilibrium vertical shear by 75 percent or the zonal wind maximum to about 30 m. sec.^{-1} . It is not clear how much such a reduction would increase our large-scale eddy transfer of heat, which is also smaller than observed. If the net heating were not to be altered, any such increase would have to be accompanied by a corresponding increase in the southward heat transfer by the Ferrel cell.

The mean meridional circulation averaged over the 17- to 39-day period is shown in figure 11.2. As was evident in Section 9 only the subtropical Hadley and mid-latitude

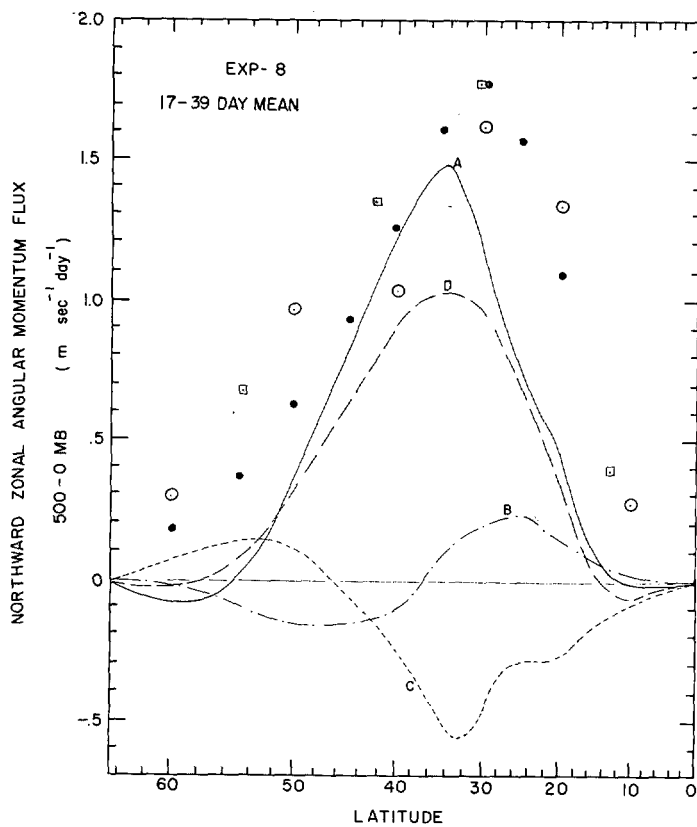


FIGURE 10.8.—The contributions to the meridional flux of zonal angular momentum between 500 and 0 mb. for the 17-39 day mean corresponding to figure 10.6. The observed annual mean large-scale eddy flux: ● Mintz [31]; □ Starr and White [56]; ○ Buch [7].

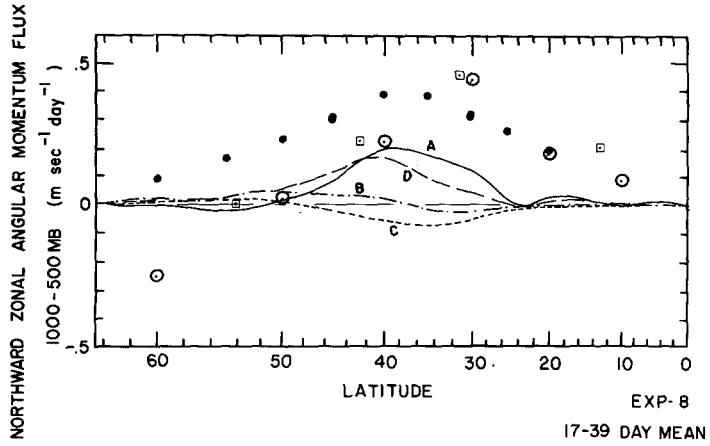


FIGURE 10.9.—The contributions to the meridional flux of zonal angular momentum between 1000 and 500 mb. for the 17-39 day mean corresponding to figure 10.6.

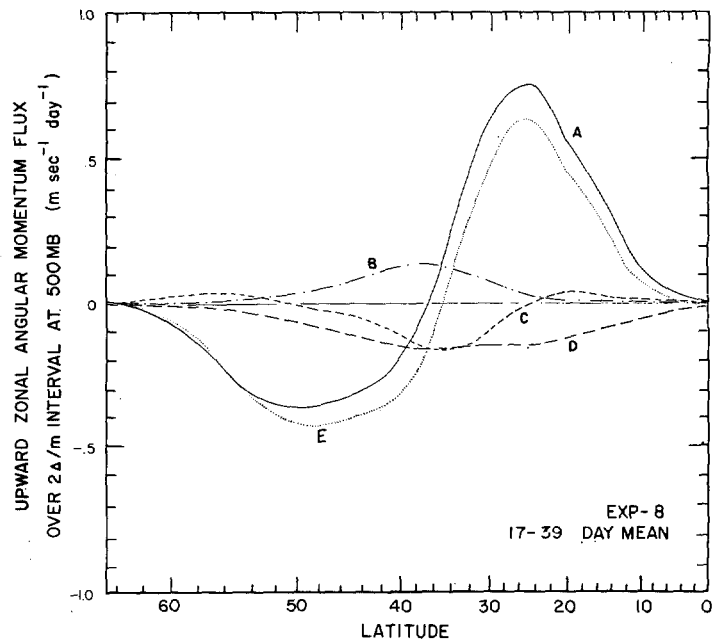


FIGURE 10.10.—The contributions to the upward flux of zonal angular momentum through 500 mb. for the 17-39 day mean corresponding to figure 10.6.

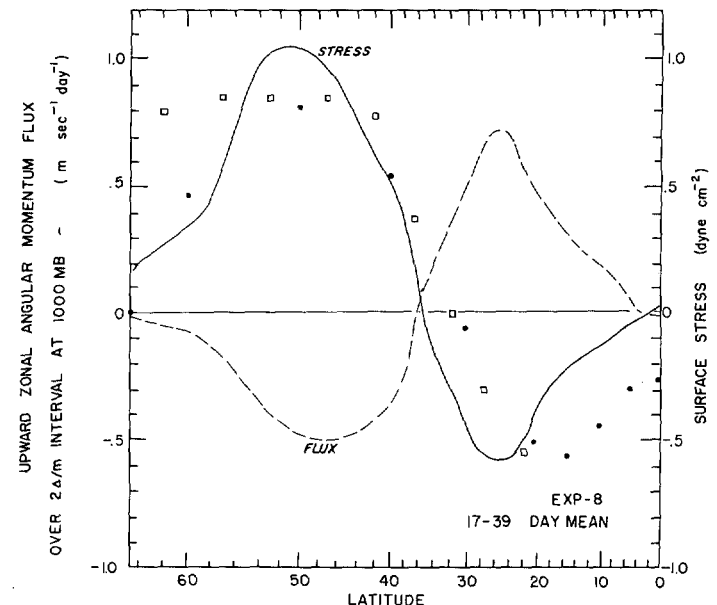


FIGURE 10.11.—The upward flux of zonal angular momentum through the lower boundary for the 17-39 day mean due to surface friction corresponding to figure 10.6 (dashed curve) and the associated stress (solid curve). The "observed" surface stress for the annual mean: ● Priestley [44]; □ Mintz [31].

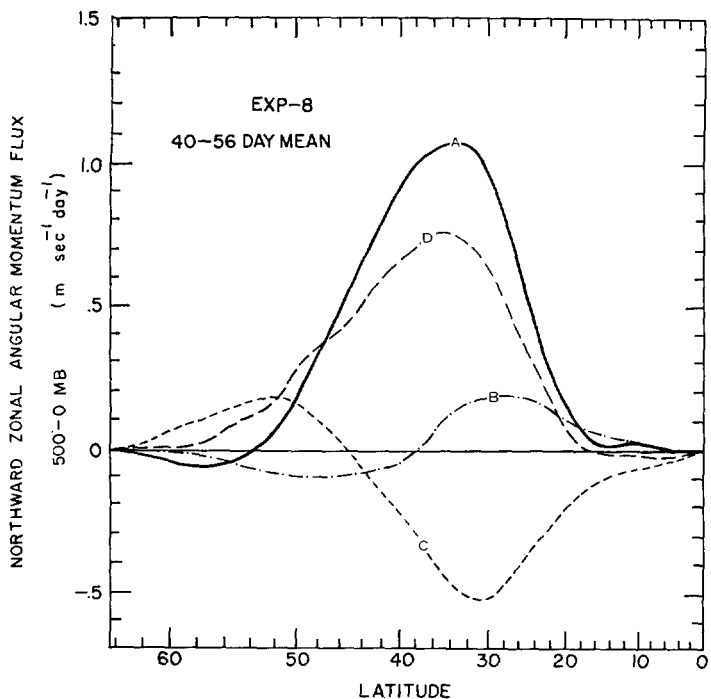


FIGURE 10.12.—Same as figure 10.8 but for the 40-56 day mean.

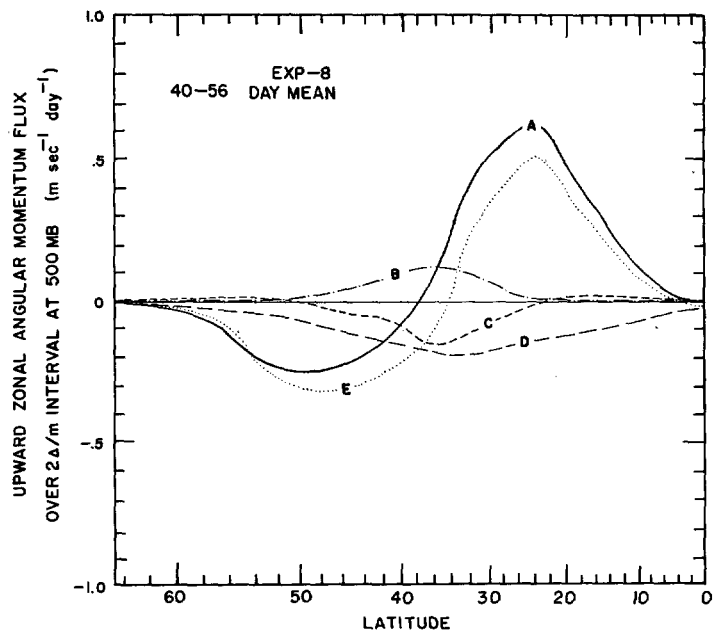


FIGURE 10.14.—Same as figure 10.10 but for the 40-56 day mean.

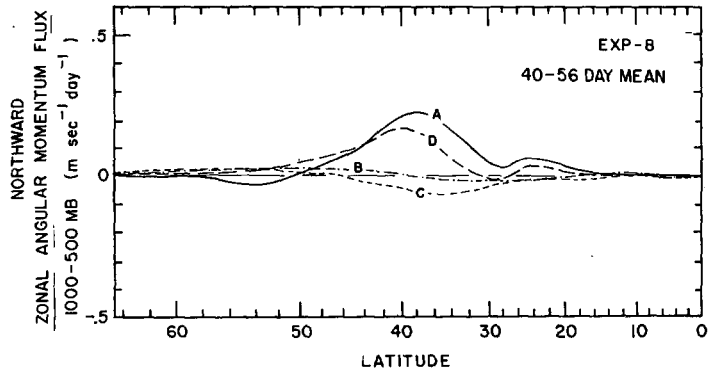


FIGURE 10.13.—Same as figure 10.9 but for the 40-56 day mean.

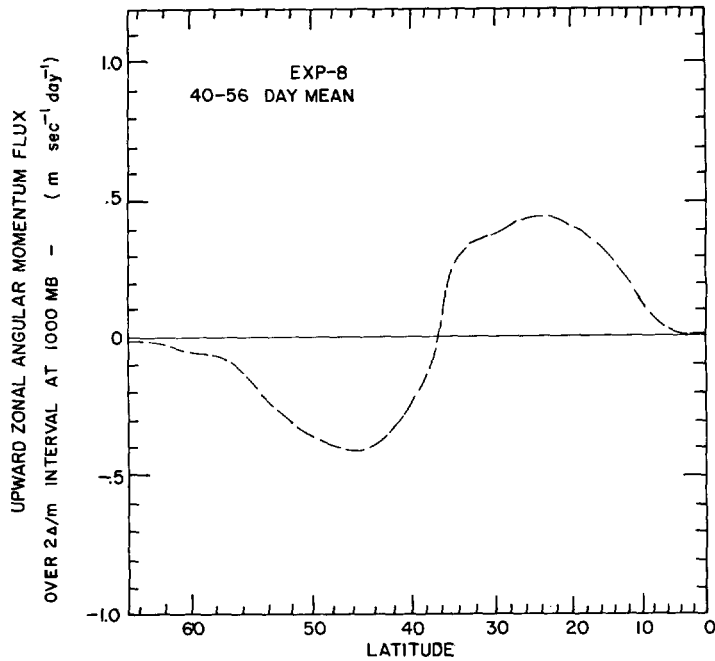


FIGURE 10.15.—Same as figure 10.11 but for the 40-56 day mean.

Ferrel cells appear. The artificial boundary at 64.4° latitude precludes our detecting a third polar cell if it were a dynamical consequence. The vertical velocities associated with these meridional cells (1 mm. sec.^{-1}) are an order of magnitude smaller than the large-scale synoptic vertical velocities. These certainly are not directly observable, but have been deduced by a number of investigators. Mintz and Lang's [33] calculations of \tilde{w}_z agree fairly well in magnitude and latitudinal distribution. On the other hand Buch's ([7], p. 33) data do not appear accurate enough for a comparison since they give a substantial net meridional mass transfer for the annual mean.

Tucker [58] made calculations for winter and summer. In both seasons his method gives maximum vertical velocities at the tropopause of $1-10 \text{ mm. sec.}^{-1}$. One would expect the maximum at mid-troposphere with a minimum at the tropopause. Nevertheless the cellular structure

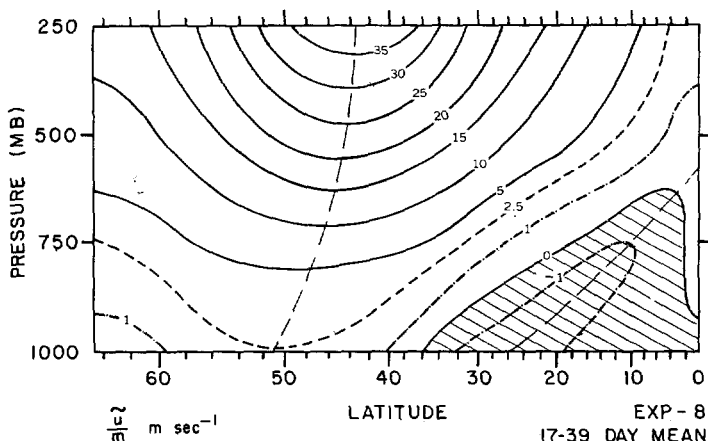


FIGURE 11.1.—The longitudinal mean of zonal wind averaged over 17-39 days. The negative values (hatched area) are easterly winds.

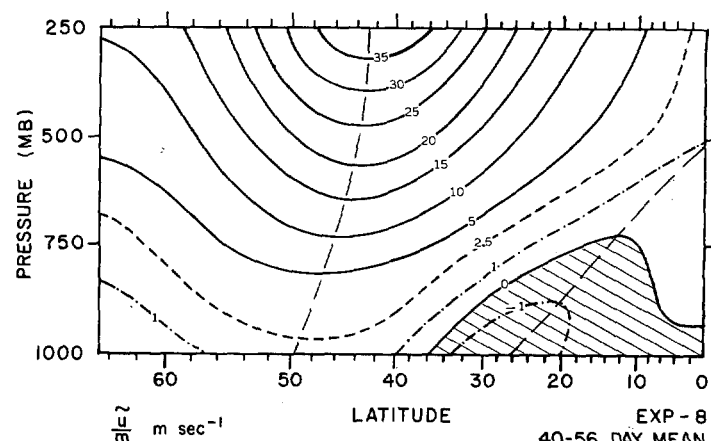


FIGURE 11.3.—The same as figure 11.1 but for 40-56 days.

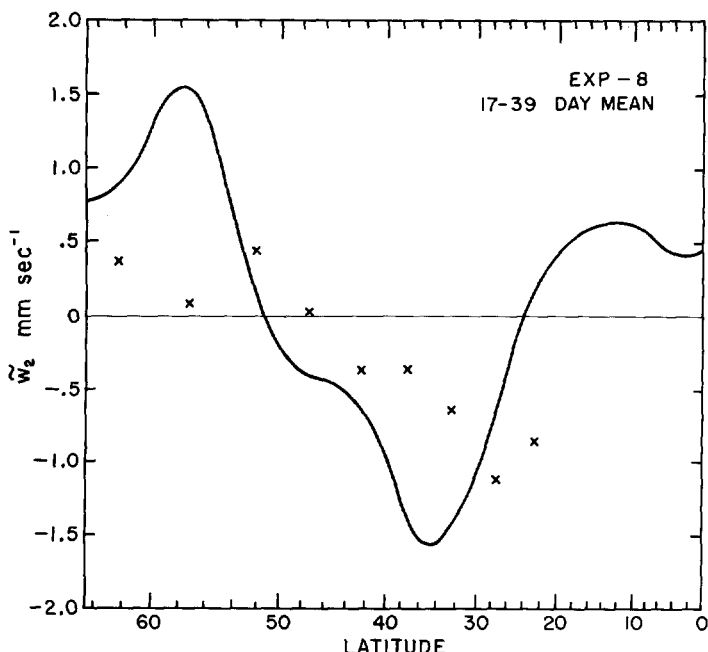


FIGURE 11.2.—The vertical velocity at 500 mb, averaged over 17-39 days. The crosses are deduced from annual mean observations by Mintz and Lang [33].

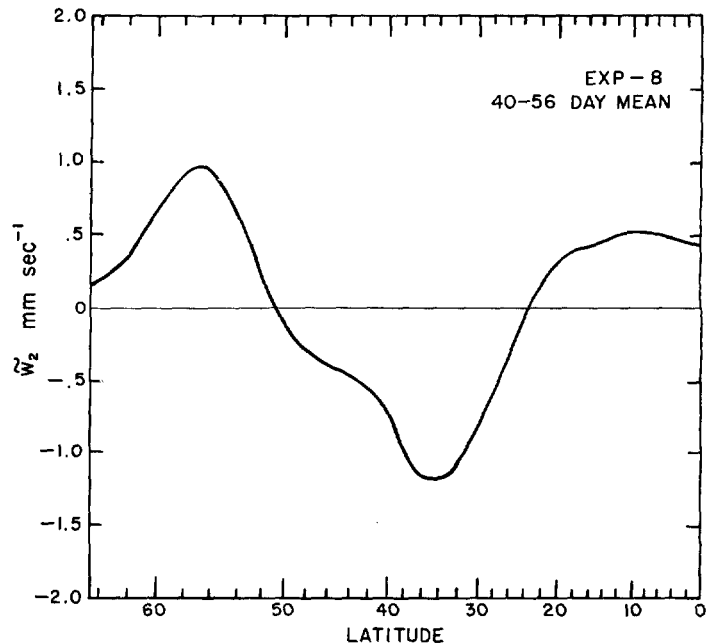


FIGURE 11.4.—The same as figure 11.2 but for 40-56 days.

and intensity of the meridional circulation show reasonable agreement with our results.

The mean zonal wind and vertical velocity distribution during the quasi-equilibrium period 40-56 days are shown in figures 11.3 and 11.4. Comparison with figures 11.1 and 11.2 shows little difference in $[u]/m$, but there is a 30 percent reduction in the intensity of \tilde{w}_2 .

12. THE MEAN MERIDIONAL MASS FLUX AND THE ZONAL GEOSTROPHIC BALANCE

By filtering external gravity waves, we have constrained the vertically integrated wind to be non-divergent and hence the mean flow is describable in terms of a stream function. On the other hand, the vertical shear component is not constrained, but we have seen evidence from the energy transformations involving the meridional circulation that there is a tendency for a domain mean geostrophic balance. To pursue this further, we consider the zonal mean of the meridional component of (2.2):

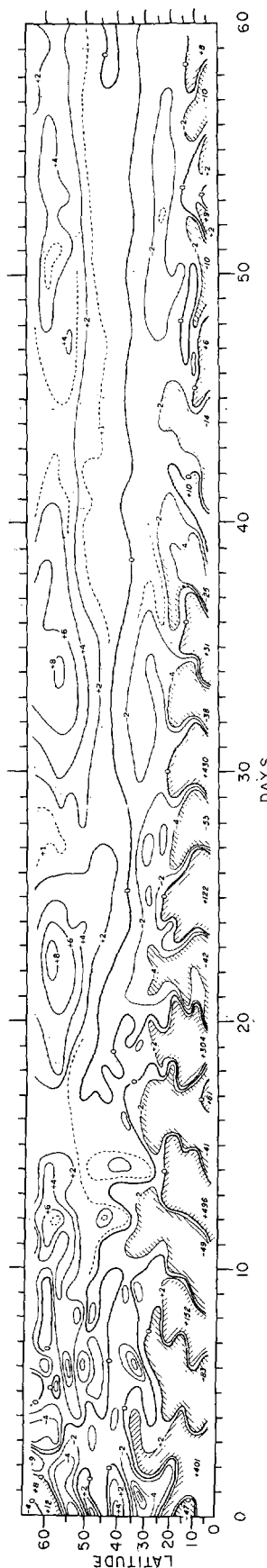


FIGURE 12.1.—The geostrophic departure of longitudinal mean of $[\bar{u}]/m$ in percent according to (12.2). The hatching indicates that contours have been omitted, however extrema are shown in italics.

$$\begin{aligned} \frac{\partial[\hat{v}]/m^2}{\partial t} = & -m \frac{\partial}{\partial y} \frac{[\hat{v}^2]}{m^3} + \frac{[\hat{D}\bar{v}]}{2m^2} - \frac{1}{m^2} \left(f[\hat{u}] + \frac{\alpha}{a} [\hat{u}^2] \right) \\ & - \frac{\partial[\hat{\Phi}]}{\partial y} + \frac{1}{m} [{}_H\hat{F}_v - v\bar{F}_v + 2vF_{v1}] \quad (12.1) \end{aligned}$$

Multiplication by m^{-2} has put it in terms of the poleward mass flux in the upper half of the model atmosphere which must just be balanced by the equatorward flux in the lower half.

A measure of the degree of geostrophic balance in the zonal component of the wind is obtained by considering just the non-viscous terms in (12.1) in which we set the transverse, i.e., the meridional component, $v \equiv 0$. The percentual geostrophic departure is then

$$\frac{\left[\frac{\hat{u}}{m} \left(f + \frac{\alpha}{a} \bar{u} \right) \right] + m \frac{\partial[\hat{\Phi}]}{\partial y}}{\left| m \frac{\partial[\hat{\Phi}]}{\partial y} \right|} \quad (12.2)$$

Figure 12.1 gives (12.2) as function of latitude and time. During the first 15 days the geostrophic departure is irregular at all latitudes. After this adjustment period we note that $[\hat{u}]/m$ is super-geostrophic north of 35° latitude and sub-geostrophic just to the south. Except near the equator, the geostrophic deviation is generally less than 10 percent. The super-geostrophic departures are at a maximum (7 to 8 percent) before and during low index, while at a minimum (1 to 2 percent) before and during high index. This supports our earlier observation (Section 8) that the ageostrophic components are excited in connection with the energy producing non-barotropic modes. It is of interest that the magnitude of the geostrophic departure at 5° latitude becomes progressively smaller with time, going from 500 percent at 12 days to less than 40 percent beyond 32 days to 10 percent or less after 45 days. This tendency toward geostrophic balance of $[\hat{u}]/m$ at equatorial latitudes is accompanied by a less dramatic but still perceptible increase in balance at higher latitudes. This coupling suggests again (cf. Section 7) that the ageostrophic components in low latitudes may respond to excitation from middle latitudes. The 17-39-day time mean, figure 12.2, shows the systematic effects with latitude more clearly, the departures being small even at 5° latitude.

The geostrophic departures are highly correlated with the gradient of the variance of the meridional wind component, as is suggested by the first term on the right side of (12.1). This may be seen more clearly and may be stated more precisely by noting that the non-viscous terms on the right side of (12.1) may be written as (see (2.8))

$$-\frac{[\hat{u}\eta]}{m^2} - \frac{\partial[\hat{\beta}]}{\partial y} \quad (12.3)$$

A calculation of

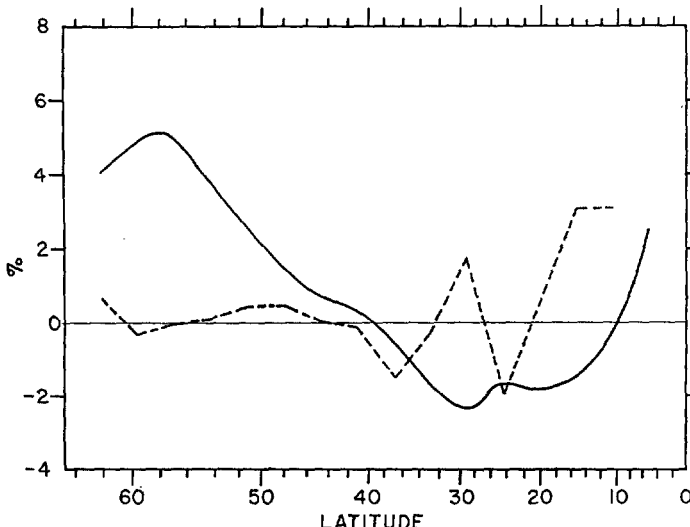


FIGURE 12.2.—The 17-39 day mean of figure 12.1 (solid line) and of equation (12.4) (dashed line).

$$\frac{\frac{\hat{u}\eta}{m} + m \frac{\partial[\hat{B}]}{\partial y}}{|m \frac{\partial[\hat{B}]}{\partial y}|} \quad (12.4)$$

as a function of latitude and time reveals a less systematic pattern than (12.2) in figure 12.1. The ratio (12.4) may be close to the round-off and truncation error since η and B are not primary forecast variables in the numerical integration, which therefore could account for its erratic character. However, its magnitude is probably meaningful. A plot of the 17-39-day mean of (12.4) is given also in figure 12.2. In the Ferrel circulation, from 35° latitude poleward, the departure is less than 1 percent. Equatorward the departure becomes quite large.

The significance of this result is that it may provide a useful balancing approximation for the baroclinic (or shear) component of the flow in mid-latitudes.

13. COMPUTATIONAL ASPECTS

A few words should be said about the programming and the computation time required. The forecast code, consisting of approximately 5000 instructions, ran at the rate of 0.4 model atmosphere days per computer hour on the 704 and 3 days per hour on the 7090. This includes duplication checking except in the elliptic part. The diagnostic integral codes (energy transformations, heat and angular momentum fluxes, etc.) required approximately 12,000 instructions. As is often the case, 95 percent of the computer time was occupied by the shortest program, i.e., the forecasting code.

14. SUMMARY AND CONCLUSIONS

Our object has been to account for the gross morphology of the atmosphere's general circulation, and to understand the processes by which it is maintained. To do this we have assumed that certain of the morphological characteristics are known a priori: that the vertical fine structure is virtually irrelevant so that it is adequate to use only two degrees of freedom, that the static stability varies relatively slightly in time and space and that we know its quasi-equilibrium value, that the atmosphere tends to be in radiative and thermal equilibrium in the large, that sound and external gravity waves contain relatively little energy and so may be ignored, that the details of the release of latent heat of condensation are not absolutely crucial so that some of the gross effects can be incorporated parametrically, and that kinematic and thermal effects of the land mass-ocean distribution are not essential to the question of the maintenance of the general circulation.

Despite these severe constraints, the problem which is left is far from trivial. We have succeeded in showing that the most efficient means for the poleward transfer of heat against the external heating gradient are the large-scale quasi-horizontal eddies in middle latitudes and the mean meridional circulation in low latitudes. The former agrees quite well with the observed eddy heat flux. As a consequence of the kinematics of these motions the upper half of the atmosphere carries zonal angular momentum poleward. If the lower boundary is rough, low-latitude easterlies and mid-latitude westerlies at the surface are created such that an angular momentum flux between the atmosphere and the earth just balances the high tropospheric poleward flux—as a result the total zonal angular momentum is virtually constant in time. Comparison with observation where possible yields surprisingly good agreement in the latitudinal distribution and in magnitude.

The efficiency of the quasi-horizontal eddies in the poleward heat flux lies with the small thermal Rossby number of middle latitude flows. The motions are thus quasi-geostrophic, and the equilibrium meridional temperature gradient is for the most part determined by the effective static stability. The meridional circulation, excited in connection with baroclinic processes, works against the quasi-geostrophic poleward heat transfer and potential to kinetic energy conversions. On the other hand the ageostrophic meridional circulation is unimportant in the poleward zonal angular momentum transfer but is predominantly responsible for the internal vertical momentum exchange, it carrying the earth's angular momentum.

The general circulation of the model is maintained by a cyclic evolution with a period of 11 to 17 days during the 60-day experiment. This cycle is the result of the non-linear interaction of essentially four processes:

(1) A quasi-time invariant meridional heating gradient.

(2) Quasi-geostrophic baroclinic instability which is activated when the meridional temperature gradient attains a critical value due to the external heating. The resulting highly efficient meridional heat transfer reduces the temperature gradient at a faster rate than the heating gradient can create it, to the point that it becomes subcritical.

(3) Non-linear transformation of eddy kinetic energy (resulting from the period of baroclinic instability) to kinetic energy of the barotropic components of the zonal wind.

(4) Viscous dissipation in all components of the energy partition, which over an index or energy cycle tends to balance the net energy input of the heating gradient.

The role of these processes has been known for 10 to 15 years, but that they should interact cyclically has not been completely obvious from atmospheric observations, although laboratory analogs have shown "vacillations". The reason probably lies with the fact that the kinematic and thermal asymmetries of the earth's surface disrupt any tendency for the entire atmosphere to act simultaneously in concert, and so obscure a clear cyclic behavior. Our assertion that vacillations are a necessary consequence is weakened by the fact that the end of the experiment is marked by an energy balance in which the fluctuations are virtually missing. This could very well be a result of too strong a poleward heat transfer by small-scale diffusion.

It is significant to note that the quasi-constant energy source results in a cyclic response. The longitudinal scale of eddies is essentially as predicted by geostrophic baroclinic theory. The meridional scale of the motions is also primarily determined by the internal dynamics, and not by an impressed scale such as in the heating or by orography.

The interaction of the above processes is perhaps most clearly viewed and understood in terms of the energy transformations among a seven-way partition of the total energy: the zonal mean and zonal eddy available potential energy, $[P]$ and P' , the kinetic energy of the zonal mean meridional circulation $[\hat{K}_v]$, the kinetic energy of the zonal mean and eddy components of the baroclinic modes $[\hat{K}_z]$ and \hat{K}' , and of the barotropic modes $[\bar{K}_z]$ and \bar{K}' . The reason for choosing such a partition is that, in addition to making it possible to diagnose the conventional exchanges between the zonal mean and perturbation components of the potential and kinetic energy, one may also observe the role of the ageostrophic components and the exchanges between the baroclinic and barotropic components of the motion.

The nature of the energy cycle may be determined from the form of the transformation functions and may be verified by the experimental results. Because of strong geostrophic coupling

$$\langle [P]*[\hat{K}_v] \rangle \approx \langle [\hat{K}_v]*[\hat{K}_z] \rangle$$

and over an index cycle they each have a mean value close to zero. At any one time, however, they are almost exactly out of phase with $\langle P'*K' \rangle$. If one isolates the effect of the Ferrel cell, then in mid-latitudes the non-geostrophic meridional circulation works against the quasi-geostrophic transformation by zonal circulations, considerably tempering purely geostrophic cyclogenesis. This leads us to conclude that the non-geostrophic modes are mainly excited in connection with the baroclinic branches of the energy cycle. However, we find that to maintain the mean meridional circulation $[\hat{K}_v]$ against frictional dissipation, a direct circulation must be associated with a mean zonal baroclinic current $[\hat{u}]$ which is sub-geostrophic and an indirect circulation with $[\hat{u}]$ which is super-geostrophic. In the presence of zonal waves, the zonal mean of the zonal shear kinetic energy $[\hat{K}_z]$ is maintained against dissipation by the perturbation kinetic energy $K' = \bar{K}' + \hat{K}'$ according to the first two terms of the inequality

$$\langle \hat{K}'*[K_z] \rangle_{NC} > \langle [\hat{K}_z]*\bar{K}' \rangle_{NC} >> \langle K'*[K_z] \rangle \approx \langle \bar{K}'*[K_z]*\hat{K}' \rangle > 0$$

in which $\langle [\hat{K}_z]*\bar{K}' \rangle_{NC}$ is also geostrophically coupled to $\langle [P]*P' \rangle$, their ratio being approximately 0.7. On the other hand, because the non-catalytic transfer, $\langle [\hat{K}_z]*\bar{K}' \rangle_{NC}$, greatly exceeds the catalytic transfer in the opposite sense, $\langle \bar{K}'*[K_z]*\hat{K}' \rangle$, \bar{K}' is thus maintained. The direct transfer $\langle \hat{K}'*\bar{K}' \rangle$ due to triple correlations is negligibly small. The ultimate link in the general circulation, the barotropic zonal energy $[\bar{K}_z]$, is maintained by \hat{K}' and \bar{K}' , the transformation from the latter being larger.

Since the energy dissipations are of the same order as the transformations it appears that the partitioning of energy dissipation in the atmosphere is quantitatively deducible from the observed transformations without any a priori assumption as to the dissipative mechanism. If we regard the zonal generation of potential energy as the energy source, our model requires that as much as almost half of the total energy dissipation must occur in the barotropic component, or that only 20 percent occurs in connection with surface stresses. This is in sharp contrast to estimates made from observation. It is not clear whether the model dissipation mechanism or the empirical estimates are at fault for the discrepancy.

It is significant to note that despite the good agreement with observation of the poleward large-scale lateral eddy transfer of heat and momentum, our model requires a significant transfer by sub-grid scale motions. No comparison with the corresponding transfer in the real atmosphere is available. In our model this transfer was introduced parametrically as a non-linear lateral diffusion and is subject to some adjustment through the coefficient k_H . Should k_H be made too small, then a systematic

accumulation of available potential and kinetic energy by the non-linear cascade would occur in the highest allowable spectral component, yielding what has been termed by Phillips [41] as a "non-linear computational instability."

The purpose for the introduction of the small-scale lateral diffusion was to simulate the *physically real* net cascade of energy from the larger than grid-size scale to the smaller scales which have been truncated by the discrete differencing. If we assert that there is no net accumulation of energy in the sub-grid scales, then the energy removed at grid scale must be taken as identical to the implied dissipation which must occur by molecular viscosity. The fact that such a formulation was used successfully for numerical integrations on the convective scale [22], where the grid scale was more than 1000 times smaller, suggests an element of validity in the approach. That is, if we can assume that the grid scale lies within an inertial sub-range, i.e., there is a net transfer of energy to higher wave numbers in the neighborhood of the grid scale, then we may express the exchange coefficient in the form $(k_H \Delta)^2 |D|$, where $k_H \sim 0.1-1.0$, Δ is the grid size and D is the deformation measured on grid scale.

The central differencing scheme employed in the present calculations has since been superseded by other schemes which in various respects have more desirable properties such as in computational efficiency ([13], [42], [23]), or in preserving certain integral properties (Arakawa—unpublished), or in altering the treatment of the non-linear terms ([50]), or by resorting to spectral techniques [43].

It is doubtful, however, that the results reported upon here, within the context of the assumed physical constraints, would materially be altered. It has already been argued that there is a physical necessity for removing energy from the highest admissible spectral components, but it is not clear that any of the newer differencing schemes, except the spectral method, gives fresh insight in properly treating the implied sub-grid scale transfers. For example, consider an "energy conserving" differencing technique such as that of Arakawa. Even if the integral of the energy spectrum is an invariant, the distribution of energy can be altered by non-linear interactions so that much of the energy may still be trapped in the highest wave numbers admissible by the finite grid. Although this cascade may be more correctly described by means of an "energy conserving" scheme, one still can not ignore the communication of that part of the energy spectrum where the cascade is explicitly described with that corresponding to the sub-grid scale.

It is, of course, important to be aware of the sensitivity of this model to the empirically prescribed parameters as well as to study its "general circulation" for physically realizable conditions differing from those of this basic experiment. These parameters include the viscous coefficients, the heating function, the static stability,

and the rotation rate. Experiments in which these parameters are varied will be described in subsequent reports.

The modest success of such a simple model encourages one to seek the explanation of some of the greater details of the atmosphere's general circulation which have been evaded here: the morphogenesis of the vertical thermal structure and its mutual adjustments with the dynamics, the role of the hydrologic cycle, the role of kinematic and thermal asymmetries of the lower boundary, the interactive transfer of heat, momentum, and water vapor at the lower boundary, interhemispheric interactions, the coupling of the stratosphere and the troposphere. Probing into these details would require a degree of model sophistication two to three orders of magnitude greater in computational complexity than we employed in the present study. Our lack of theoretical understanding of the model elements to simulate condensation, convection, radiative transfer, boundary layer exchanges, etc., is perhaps a more serious deterrent than a lack of adequate computational apparatus. To remove a dynamical constraint or to replace a semi-empirical parametric formulation by an internally non-linearly interactive theory requires that the newly acquired degree of freedom account for the systematic properties of the process (which were here constrained parametrically) as well as its exceptional behavior. Otherwise the generalization could do more harm than good. For example, only recently has the relaxation of the geostrophic or balance constraint resulted in stable integrations, while the introduction of baroclinic degrees of freedom has yet to yield a consistent improvement at 500 mb. over a barotropic model.

In pursuing the objective to generalize theoretical models we must ask ourselves whether greater detail in formulating the contributing processes is warranted by truncation errors, by sensitivity of the results to detail, by the resulting increase in computational complexity and time, and by ignorance of the way these processes really work. Very often this cannot be determined in advance, but must wait for computational experiments to be performed.

ACKNOWLEDGMENTS

In addition to those mentioned in the text, a number of my colleagues in the General Circulation Research Laboratory have materially contributed to making this study possible. The forecasting, integral-diagnostic, and input-output programs required over 17,000 computer instructions—a massive and difficult undertaking by any standards. The forecasting code was first laid out by G. O. Collins, no longer with the Laboratory. The working version of this code embodying the final physical ideas and mathematical techniques was due to R. D. Graham and J. L. Holloway. The latter, together with Mrs. W. M. Carlton and Miss E. A. Storlie, was responsible for the integral-diagnostic and input-output pro-

grams. S. Hellerman and G. D. Hembree assisted in the analysis of results, E. Rayfield drafted the figures, and Mrs. J. A. Snyder typed the manuscript. I would also like to express my thanks to D. K. Lilly, K. Bryan, and particularly S. Manabe for joining me in many fruitful discussions. On the whole this venture has demonstrated to me the value if not the necessity of a diverse, imaginative, and dedicated working group in large research undertakings.

REFERENCES

1. F. Albrecht, "Über die 'Glashauswirkung' der Erdatmosphäre und das Zustandekommender der Troposphäre," *Meteorologische Zeitschrift*, vol. 48, No. 2, Feb. 1931, pp. 57-68.
2. A. Arakawa, "Non-Geostrophic Effects in the Baroclinic Prognostic Equations," *Proceedings of the International Symposium on Numerical Weather Prediction in Tokyo, 1960*, Meteorological Society of Japan, Mar. 1962, pp. 161-175.
3. G. K. Batchelor, "The Theory of Axisymmetric Turbulence," *Proceedings of the Royal Society of London*, Series A, vol. 186, No. A1007, Sept. 1946, pp. 480-502.
4. F. A. Berson, "A Quantitative Analysis of the Evolution of Large-Scale Flow with Regard to the Effect of Eddy Motion," *Quarterly Journal of the Royal Meteorological Society*, vol. 79, No. 340, Apr. 1953, pp. 210-223.
5. B. Bolin, "On the Influence of the Earth's Orography on the General Character of the Westerlies," *Tellus*, vol. 2, No. 3, Aug. 1950, pp. 184-195.
6. D. Brunt, *Physical and Dynamic Meteorology*, Cambridge University Press, 1939, 428 pp.
7. H. S. Buch, "Hemispheric Wind Conditions During the Year 1950," Final Report on contract AF19(122)-153, Part 2, Massachusetts Institute of Technology, Dept. of Meteorology, May 1954, 126 pp.
8. M. I. Budyko, *Teplovoy Balans Zemnoj Poverkhnosti* [The Heat Balance of the Earth's Surface], Gidrometeorologicheskoe izdatel'stvo, Leningrad, 1956, 255 pp. (Translated by N. A. Stepanova, U.S. Weather Bureau, 1958, 259 pp.)
9. J. G. Charney, "On the Theory of the General Circulation of the Atmosphere," *The Atmosphere and the Sea in Motion*, Rockefeller Institute Press, New York, 1959, pp. 178-193.
10. J. G. Charney and A. Eliassen, "A Numerical Method for Predicting the Perturbations in the Middle-Latitude Westerlies," *Tellus*, vol. 1, No. 2, May 1949, pp. 38-54.
11. A. Defant, "Die Zirkulation der Atmosphäre in den Gemässigten Breiten der Erde," *Geografiska Annaler*, vol. 3, No. 3, 1921, pp. 209-266.
12. E. T. Eady, "Long Waves and Cyclone Waves," *Tellus*, vol. 1, No. 3, Aug. 1949, pp. 33-52.
13. A. Eliassen, "A Procedure for Numerical Integration of the Primitive Equations of the Two-Parameter Model of the Atmosphere," Scientific Report No. 4 on contract AF19(604)-1286, University of California at Los Angeles, Dept. of Meteorology, Mar. 1956, 53 pp.
14. R. Fjørtoft, "On the Changes in the Spectral Distribution of Kinetic Energy for Two-Dimensional, Non-Divergent Flow," *Tellus*, vol. 5, No. 3, Aug. 1953, pp. 225-230.
15. D. Fultz, "Studies in Experimental Hydrodynamic Analogues of the Atmosphere," Final Report on contract AF19(604)-1292, University of Chicago, Dept. of Meteorology, Dec. 1958, 25 pp.
16. D. Fultz et al., "Studies of Thermal Convection in a Rotating Cylinder with Some Implications for Large-Scale Atmospheric Motions," *Meteorological Monographs*, vol. 4, No. 21, American Meteorological Society, Boston, Dec. 1959, 104 pp.
17. D. Fultz and R. Kaylor, "The Propagation of Frequency in Experimental Baroclinic Waves in a Rotating Annular Ring," *The Atmosphere and the Sea in Motion*, Rockefeller Institute Press, New York, 1959, pp. 359-371.
18. B. Haurwitz, *Dynamic Meteorology*, McGraw-Hill Book Co., Inc. New York, 1941, 365 pp.
19. H. G. Houghton, "On the Annual Heat Balance of the Northern Hemisphere," *Journal of Meteorology*, vol. 11, No. 1, Feb. 1954, pp. 1-9.
20. H. Lettau, "A Study of Mass, Momentum, and Energy Budget of the Atmosphere," *Archiv für Meteorologie, Geophysik und Bioklimatologie*, Series A, vol. 7, 1955, pp. 133-157.
21. H. H. Lettau and B. Davidson (eds.), "Exploring the Atmosphere's First Mile," *Proceedings of the Great Plains Turbulence Field Program August 1-September 8, 1953*, vol. 1, Pergamon Press, London, 1957, 376 pp.
22. D. K. Lilly, "On the Numerical Simulation of Buoyant Convection," *Tellus*, vol. 14, No. 2, May 1962, pp. 148-172.
23. D. K. Lilly, "A Proposed Staggered-Grid System for Numerical Integration of Dynamic Equations," *Monthly Weather Review*, vol. 89, No. 3, Mar. 1961, pp. 59-65.
24. J. London, "A Study of the Atmospheric Heat Balance," Final Report on contract AF19(122)-165, (AFCRC-TR-57-287), New York University, Dept. of Meteorology and Oceanography, July 1957, 99 pp.
25. E. N. Lorenz, "Computations of the Balance of Angular Momentum and the Poleward Transport of Heat," *Studies of the Atmospheric General Circulation*, Final Report, Part 1, on contract AF19(122)-153, Massachusetts Institute of Technology, Dept. of Meteorology, May 1954, pp. 38-71.
26. E. N. Lorenz, "Available Potential Energy and the Maintenance of the General Circulation," *Tellus*, vol. 7, No. 2, May 1955, pp. 157-167.
27. E. N. Lorenz, "Simplified Dynamic Equations Applied to the Rotating-Basin Experiment," *Journal of the Atmospheric Sciences*, vol. 19, No. 1, Jan. 1962, pp. 39-51.
28. D. H. Lufkin, "Atmospheric Water Vapor Divergence and the Water Balance at the Earth's Surface," Scientific Report No. 4, on contract AF19(604)-2242, Massachusetts Institute of Technology, Dept. of Meteorology, June 1959, 44 pp.
29. S. Manabe and F. Möller, "On the Radiative Equilibrium and Heat Balance of the Atmosphere," *Monthly Weather Review*, vol. 89, No. 12, Dec. 1961, pp. 503-532.
30. Y. Mintz, "The Observed Zonal Circulation of the Atmosphere," *Bulletin of the American Meteorological Society*, vol. 35, No. 5, May 1954, pp. 208-214.
31. Y. Mintz, "Final Computation of the Mean Geostrophic Poleward Flux of Angular Momentum and of Sensible Heat in the Winter and Summer of 1949," Final Report on contract AF19(122)-48, University of California at Los Angeles, Dept. of Meteorology, Mar. 1955, pp. V-1 to V-9.
32. Y. Mintz, "Design of Some Numerical General Circulation Experiments," *Bulletin of the Research Council of Israel*, Section G, vol. 7, No. 2-3, Oct. 1958, pp. 67-114.
33. Y. Mintz and J. Lang, "A Model of the Mean Meridional Circulation," Final Report on contract AF19(122)-48, University of California at Los Angeles, Dept. of Meteorology, Mar. 1955, pp. VI-1 to VI-9.
34. J. Namias, "Thirty-Day Forecasting: A Review of a Ten-Year Experiment," *Meteorological Monographs*, vol. 2, No. 6, American Meteorological Society, Boston, July 1953, 83 pp.
35. L. Onsager, "Statistical Hydrodynamics," *Il Nuovo Cimento*, Supplement to vol. 6, Series 9, No. 2, 1949, pp. 279-287.
36. E. Palmén, "On the Mean Meridional Circulation in Low Latitudes of the Northern Hemisphere in Winter and the Associated Meridional and Vertical Flux of Angular Momentum," *Societas Scientiarum Fennica, Commentationes Physico-Mathematicae*, vol. 17, No. 8, 1955, pp. 1-33.

37. J. P. Peixoto, "Hemispheric Humidity Conditions During the Year 1950," Scientific Report No. 3 on contract AF19(604)-2242, Massachusetts Institute of Technology, Dept. of Meteorology, Oct. 1958, 142 pp.
38. J. P. Peixoto, "Hemispheric Temperature Conditions During the Year 1950," Scientific Report No. 4 on contract AF19(604)-2242, Massachusetts Institute of Technology, Dept. of Meteorology, Nov. 1960, 211 pp.
39. N. A. Phillips, "Energy Transformations and Meridional Circulations Associated with Simple Baroclinic Waves on a Two-Level Quasi-Geostrophic Model," *Tellus*, vol. 6, No. 3, Aug. 1954, pp. 273-286.
40. N. A. Phillips, "The General Circulation of the Atmosphere: A Numerical Experiment," *Quarterly Journal of the Royal Meteorological Society*, vol. 82, No. 352, Apr. 1956, pp. 123-164.
41. N. A. Phillips, "An Example of Non-Linear Computational Instability," *The Atmosphere and the Sea in Motion*, Rockefeller Institute Press, New York, 1959, pp. 501-504.
42. N. A. Phillips, "Numerical Integration of the Hydrostatic System of Equations with a Modified Version of the Eliassen Finite-Difference Grid," *Proceedings of the International Symposium on Numerical Weather Prediction in Tokyo, 1960*, Meteorological Society of Japan, Mar. 1962, pp. 109-120.
43. G. W. Platzman, "The Spectral Form of the Vorticity Equation," *Journal of Meteorology*, vol. 17, No. 6, Dec. 1960, pp. 635-644.
44. C. H. B. Priestley, "A Survey of the Stress Between the Ocean and Atmosphere," *Australian Journal of Scientific Research*, Series A, vol. 4, No. 3, Sept. 1951, pp. 315-328.
45. H. Riehl et al., "The North-East Trade of the Pacific Ocean," *Quarterly Journal of the Royal Meteorological Society*, vol. 77 No. 334, Oct. 1951, pp. 598-626.
46. C.-G. Rossby and R. B. Montgomery, "The Layer of Frictional Influence in Wind and Ocean Currents," *Papers in Physical Oceanography and Meteorology*, vol. 3, No. 3, Massachusetts Institute of Technology and Woods Hole Oceanographic Institution, Apr. 1935, 101 pp.
47. B. Saltzman, "The Zonal Harmonic Representation of the Atmospheric Energy Cycle—A Review of Measurements," The Travelers Research Center, Report TRC-9, Sept. 1961, 19 pp.
48. B. Saltzman and A. Fleisher, "The Modes of Release of Available Potential Energy in the Atmosphere," *Journal of Geophysical Research*, vol. 65, No. 4, Apr. 1960, pp. 1215-1222.
49. R. Shapiro and F. Ward, "The Time-Space Spectrum of the Geostrophic Meridional Kinetic Energy," *Journal of Meteorology*, vol. 17, No. 6, Dec. 1960, pp. 621-626.
50. F. G. Shuman, "Numerical Experiments with the Primitive Equations," *Proceedings of the International Symposium on Numerical Weather Prediction in Tokyo, 1960*, Meteorological Society of Japan, Mar. 1962, pp. 85-107.
51. J. Smagorinsky, "The Dynamical Influence of Large-Scale Heat Sources and Sinks on the Quasi-Stationary Mean Motions of the Atmosphere," *Quarterly Journal of the Royal Meteorological Society*, vol. 79, No. 341, July 1953, pp. 342-366.
52. J. Smagorinsky, "On the Inclusion of Moist Adiabatic Processes in Numerical Prediction Models," *Berichte des Deutschen Wetterdienstes*, Band 5, Nr. 38, 1957, pp. 82-90.
53. J. Smagorinsky, "On the Numerical Integration of the Primitive Equations of Motion for Baroclinic Flow in a Closed Region," *Monthly Weather Review*, vol. 86, No. 12, Dec. 1958, pp. 457-466.
54. J. Smagorinsky, "On the Dynamical Prediction of Large-Scale Condensation by Numerical Methods," *"Physics of Precipitation," Geophysical Monographs*, No. 5, American Geophysical Union, 1960, pp. 71-78.
55. J. Smagorinsky, "The Formulation of Eddy Transport Processes for the Quasi-Static Inertial Subrange of Atmospheric Motions" (in preparation).
56. V. Starr and R. M. White, "Balance Requirements of the General Circulation," *Studies of the Atmospheric General Circulation*, Final Report, Part 1, on contract AF19(122)-153, Massachusetts Institute of Technology, Dept. of Meteorology, May 1954, pp. 186-242.
57. P. D. Thompson, "Prognostic Equations for the Mean Motions of Simple Fluid Systems and Their Relation to the Theory of Large-Scale Atmospheric Turbulence," *Tellus*, vol. 6, No. 2, May 1954, pp. 150-164.
58. G. B. Tucker, "Mean Meridional Circulations in the Atmosphere," *Quarterly Journal of the Royal Meteorological Society*, vol. 85, No. 365, July 1959, pp. 209-224.
59. R. M. White and B. Saltzman, "On the Conversion Between Potential and Kinetic Energy in the Atmosphere," *Tellus*, vol. 8, No. 3, Aug. 1956, pp. 357-363.
60. W. K. Widger, Jr., "A Study of the Flow of Angular Momentum in the Atmosphere," *Journal of Meteorology*, vol. 6, No. 5, Oct. 1949, pp. 291-299.
61. A. Wiin-Nielsen, "A Study of Energy Conversion and Meridional Circulation for the Large-Scale Motion in the Atmosphere," *Monthly Weather Review*, vol. 87, No. 9, Sept. 1959, pp. 319-332.
62. A. Wiin-Nielsen, "On Transformation of Kinetic Energy Between the Vertical Shear Flow and the Vertical Mean Flow in the Atmosphere," *Monthly Weather Review*, vol. 90, No. 8, Aug. 1962, pp. 311-323.
63. A. Wiin-Nielsen and J. Brown, "On the Diagnostic Computations of Atmospheric Heat Sources and Sinks and Generation of Available Potential Energy," *Proceedings of the International Symposium on Numerical Weather Prediction in Tokyo, 1960*, Meteorological Society of Japan, Mar. 1962, pp. 593-613.
64. J. S. Winston and A. F. Krueger, "Some Aspects of a Cycle of Available Potential Energy," *Monthly Weather Review*, vol. 89, No. 9, Sept. 1961, pp. 307-318.

APPENDIX A

THE PARAMETERIZATION OF NON-ADIABATIC HEATING FOR THE VERTICALLY INTEGRATED ATMOSPHERE

It has been suggested by Charney [9] that Phillips' [40] simple heating function (which was only latitude dependent) could be somewhat generalized by assuming that: the atmosphere is transparent to solar radiation, the earth's surface absorbs as a blackbody, and the long-wave radiation from the ground is absorbed and reradiated by the atmosphere as a gray body. The radiative balance of a column may then be expressed in terms of a function of latitude and its mean temperature. It is possible to remove some of Charney's restrictive assumptions and to parameterize recent methods of calculation by Houghton [19], Budyko [8], and particularly London [24] in terms of the variables of our model. In particular these variables are the 500-mb. temperature, T_2 , and the divergence \hat{D} .

We implicitly assume that the heat absorbed by the atmosphere is distributed in the vertical by the large-scale dynamics, internal convective processes, and internal radiative exchanges such as to preserve the static stability, which is taken as constant in time and space.* The co-

efficients of the formulation of the net heating of the atmosphere will therefore parametrically embody the gross transmissive and absorptive properties of an atmospheric column. The discussion will be facilitated by referring to figure A1.

The solar radiation at the top of the atmosphere S_0 is in part reflected back to space by an amount $A_a S_0$ and in part absorbed by the atmosphere by an amount

$$x(1-A_a)S_0 \equiv S_a \quad (A1)$$

where A_a is the atmosphere's albedo and x its opacity to solar radiation. The remainder, $(1-x)(1-A_a)S_0$, reaches the earth's surface. Of this $A_*(1-x)(1-A_a)S_0$ is reflected space, while

$$(1-A_*)(1-x)(1-A_a)S_0 \equiv S_* \quad (A2)$$

is absorbed by the earth's surface. Here A_* is the albedo of the ground.

We assume the surface to emit long-wave radiation as a blackbody, i.e., at the rate σT_*^4 , where σ is the Stephan-Boltzmann constant and T_* the surface temperature. Only $\Gamma \sigma T_*^4$ is absorbed by the atmosphere because of its window with respect to long-wave radiation, where Γ is

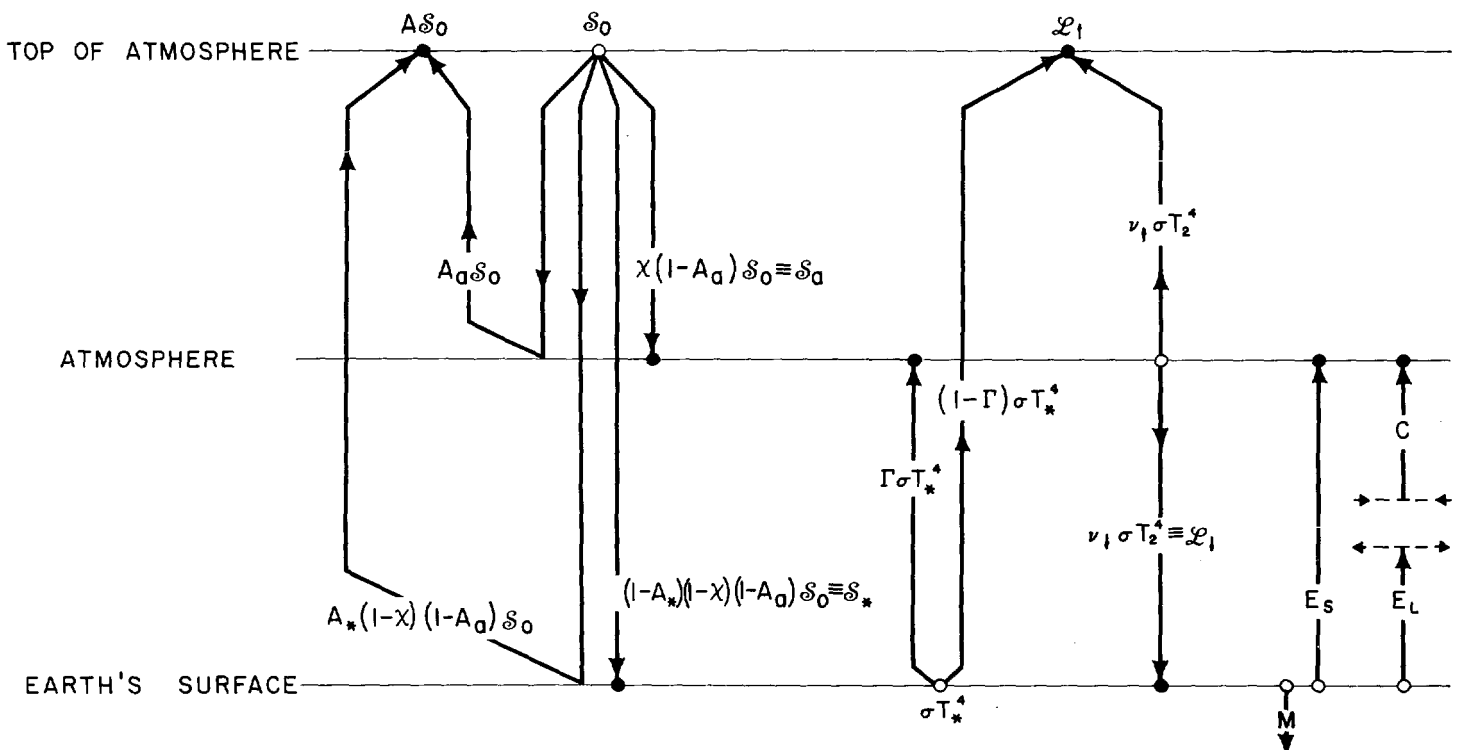


Figure A1.—Schematic diagram of the processes contributing to the heat balance. Symbols are defined in the text.

TABLE A1.—Annual mean data (ly. day^{-1} except T_2 which is in $^{\circ}\text{A.}$) from London [24]. Parentheses in row headings indicate London's terminology

	Latitude ($^{\circ}$)									Mean
	5	15	25	35	45	55	65	75	85	
1 S_0 (SR—insolation at top of atmosphere)	878.8	855.4	806.4	736.9	648.4	548.3	445.3	372.6	350.6	718.9
2 $S_a = \chi(1 - A_s)S_0$ (SR—total absorption in atmosphere)	157.0	149.0	140.0	122.8	110.2	95.4	86.0	81.0	79.2	126.3
3 $A_a S_0$ (SR—reflected back to space; atmosphere+cloud)	272.2	234.7	211.7	213.8	220.3	204.4	174.2	160.9	146.9	220.7
4 $A_s(1 - \chi)(1 - A_s)S_0$ (SR—reflected by earth's surface)	26.3	32.0	37.4	32.4	29.5	21.2	26.6	36.7	51.5	30.6
5 S_* (SR—total absorption at earth's surface)	422.6	438.1	417.2	367.9	289.1	226.8	158.4	94.7	73.1	341.0
6 σT_*^4 (LW—total radiation from earth's surface)	945.7	946.1	908.3	834.5	748.8	678.6	607.0	554.8	513.4	823.9
7 L_{\downarrow} (LW—back radiation from atmosphere)	811.1	797.4	753.5	692.3	632.9	576.7	522.0	468.7	420.8	694.7
8 $(1 - \Gamma)\sigma T_*^4$ (LW—from earth's surface to space; window radiation)	34.6	42.8	50.4	47.9	38.5	31.3	28.1	25.9	27.0	39.5
9 $\nu_{\uparrow} \sigma T_*^4$ (LW—from troposphere+stratosphere to space)	465.1	467.3	458.6	426.2	401.4	381.6	360.7	339.8	328.0	427.3
10 L_{\uparrow} (LW—total lost to space from troposphere+stratosphere+earth's surface)	499.7	510.1	509.0	471.2	440.3	413.3	389.2	364.0	353.2	466.4
11 T_2 (500-mb, annual mean temperature)	268.6	266.3	263.6	259.3	254.0	249.2	245.0	241.6	238.9	258.9
12 C (latent heat of condensation)	272.2	139.0	103.7	116.3	127.1	109.4	59.0	20.9	2.2	135.9

the long-wave absorptivity of the atmosphere. Hence $(1 - \Gamma)\sigma T_*^4$ goes to space. We assume that the atmosphere radiates as a blackbody at effective temperature $\nu_{\downarrow} T_2$ and $\nu_{\uparrow} T_2$ for downward and upward radiation, respectively. The parameters ν_{\downarrow} and ν_{\uparrow} are to be determined. Therefore the back radiation is

$$\nu_{\downarrow} \sigma T_*^4 \equiv L_{\downarrow} \quad (\text{A3})$$

and the long-wave radiation to space is $\nu_{\uparrow} \sigma T_*^4$. The total outgoing long-wave radiation is therefore

$$L_{\uparrow} \equiv (1 - \Gamma)\sigma T_*^4 + \nu_{\uparrow} \sigma T_*^4 \quad (\text{A4})$$

We denote by E_s and E_L the flux divergence of heat due to the eddy transport of sensible and latent heat from the earth's surface to the atmosphere and by M the flux divergence of heat in the oceans due to lateral ocean transports. Assuming no heat accumulation at the earth's surface, then T_* is an equilibrium temperature resulting from the local balance

$$M = S_* + L_{\downarrow} - \sigma T_*^4 - (E_s + E_L) \quad (\text{A5})$$

On the other hand, the atmosphere is not necessarily in local thermal equilibrium so that the net heating rate per unit area of a column must be

$$\frac{p_4 Q}{g} \equiv S_a + \Gamma \sigma T_*^4 - \nu_{\uparrow} \sigma T_*^4 - L_{\downarrow} + E_s + C \quad (\text{A6})$$

where Q is the heating rate per unit mass and C is the heat released by condensation.

Since the total absorption of solar radiation by the atmosphere and ground is

$$A \equiv S_a + S_* \quad (\text{A7})$$

then one may verify from (A4), (A5), and (A6) that

$$A = \frac{p_4 Q}{g} + L_{\uparrow} + M + E_L - C \quad (\text{A8})$$

Finally, upon eliminating T_* and L_{\downarrow} among (A3), (A5), and (A6), the net atmospheric heating may be written in the form

$$\frac{p_4 Q}{g} = (S_a + \Gamma S_*) + (1 - \Gamma)E_s + C - \Gamma(E_L + M) - \mu \sigma T_*^4 \quad (\text{A9})$$

where

$$\mu \equiv (1 - \Gamma)\nu_{\downarrow} + \nu_{\uparrow} \quad (\text{A10})$$

It is to be noted that the planetary albedo, which is usually defined as the fraction of the solar radiation at the top of the atmosphere that is not absorbed by the earth and atmosphere, is

$$A \equiv 1 - \frac{A}{S_0} \quad (\text{A11})$$

Hence at the top of the atmosphere, the "radiation excess" is

$$-AS_0 + S_0 - L_{\uparrow} = A - L_{\uparrow} = \frac{p_4 Q}{g} + M + E_L - C \quad (\text{A12})$$

The transmissive parameters χ , Γ , $\nu_{\downarrow}/\nu_{\uparrow}$ may be estimated from London's calculations. Since equilibrium is most valid for the annual mean, his seasonal calculations have been averaged arithmetically. They are tabulated in table A1 where London's terminology for each component is identified with the notation used here.

The derived quantities and parameters $M + E_s + E_L$, A_a , χ , A_s , $S_*/1 - A_s$, A , A , $\nu_{\downarrow}/\nu_{\uparrow}$, $A - L_{\uparrow}$, Γ , $S_a + \Gamma S_*$ are given in table A2. To calculate ν_{\uparrow} and ν_{\downarrow} individually we need the

TABLE A2.—*Derived quantities from table A1. Parentheses in row headings indicate equations and tables used from Appendix A.*

		ly. day ⁻¹	Latitude (°)									Mean
			5	15	25	35	45	55	65	75	85	
1	$M+E_s+E_L$ (5; 1.5, 1.6, 1.7)		+288.0	+289.4	+262.4	+225.7	+173.2	+124.9	+73.4	+8.6	-19.5	+211.8
2	A_a (-; 1.1, 1.3)		.310	.274	.263	.290	.340	.373	.391	.432	.419	.317
3	χ (1; 1.1, 1.2, 2.2)		.259	.240	.236	.235	.258	.278	.317	.382	.389	.262
4	A^* (2; 1.4, 1.5)		.0585	.0680	.0820	.0806	.0926	.0855	.1439	.2793	.4132	.0955
5	$S_*/1-A_*$ (-; 1.5, 2.4)	ly. day ⁻¹	449	470	454	401	318	248	184	131	124	371.4
6	A (-; 1.2, 1.5)	ly. day ⁻¹	579.6	587.1	557.2	490.7	399.3	322.2	244.4	175.7	152.3	467.3
7	A (10; 1.1, 2.6)		.340	.314	.309	.334	.384	.412	.451	.528	.566	.363
8	$\nu \uparrow \nu \downarrow$ (3; 1.7, 1.9)		1.744	1.706	1.643	1.624	1.577	1.511	1.447	1.379	1.283	1.615
9	$A-L\uparrow$ (-; 1.10, 2.6)	ly. day ⁻¹	+79.9	+77.0	+48.2	+19.5	-41.0	-91.1	-144.8	-188.3	-200.9	+0.86
10	Γ (4, 5, 7; 1.2, 1.7, 1.9, 2.1, 2.9)		.9634	.9548	.9445	.9461	.9481	.9533	.9530	.9564	.9509	.9523
11	S_*+TS_* (-; 1.2, 1.5, 2.10)	ly. day ⁻¹	564.1	567.3	534.0	470.9	384.3	311.6	237.0	171.6	148.7	451.1
12	$\nu \uparrow$ (-; 1.9, 1.11)		.760	.791	.813	.807	.826	.846	.851	.854	.859	.810
13	$\nu \downarrow$ (-; 2.8, 2.12)		1.32	1.35	1.34	1.31	1.30	1.28	1.23	1.18	1.10	1.30
14	μ (9a; 2.10, 2.12, 2.13)		.808	.852	.887	.878	.893	.906	.909	.905	.913	.872
15	E_s+E_L-C+M (-; 1.12, 2.1)	ly. day ⁻¹	+15.8	+150.4	+158.7	+109.4	+46.1	+15.5	+14.4	-12.3	-21.7	+75.9
16	$p_4Q/g-E_s$ (8; 2.9, 2.15)	ly. day ⁻¹	64.1	-73.4	-110.5	-89.9	-87.1	-106.6	-150.2	-176.0	-179.2	-75.0
17	$p_4Q/g+E_L+M$ (-; 2.1, 2.16)	ly. day ⁻¹	352.1	216.0	151.9	135.8	86.1	18.3	-85.8	-167.4	-198.7	136.8

observed annual mean 500-mb. temperature. This was determined as the arithmetic mean of London's seasonal temperatures by interpolation for standard elevations. T_2 is given in table A1. The quantities: $\nu \uparrow$, $\nu \downarrow$, μ , E_s+E_L-C+M , $(p_4Q/g)-E_s$, $(p_4Q/g)+E_L+M$ are given in table A2. The formulae and tabular data used in determining the above derived quantities also are given in table A2. The parameters Γ , $\nu \uparrow$, $\nu \downarrow$ are plotted in figure A2.

The intermediate results of Houghton's calculations are not given in as much detail, particularly in the long-wave radiation where he used an Elsasser chart, and hence not all of the parameters can be determined individually. For the purposes of comparison wherever possible, Houghton's data and calculations are given in rows 1-7 of table A3. In similar fashion we may determine χ , A_a , $A-L\uparrow$ and $S_*/1-A_*$ which are tabulated in rows 8-11. A comparison of χ for London's and Houghton's data is given in figure A3.

Budyko [8] calculated the heat balance at the earth's surface from 5° N. to 55° N. The first 5 rows in table A4 (taken from his table 14, p. 214) give S_* , E_s+E_L+M , E_L , E_s , M . The numbers in parenthesis give extrapolated values to the pole. Row 6 gives $C-E_L$ (taken from his fig. 73).

From table A2.16 we have for thermal equilibrium that the hemispheric mean $\{[E_s]\}=75$ ly. day⁻¹. This is twice as large as that calculated by Budyko for the Northern Hemisphere (table A4.4), both however giving a net transfer from earth to atmosphere. $\{[E_s+E_L+M]\}$ from London's data is 212. Assuming no interhemispheric heat exchange by the oceans, $\{[M]\}=0$ (Budyko

finds this to be 9.4), then $\{[E_L]\}=137$ from London's data which agrees with Budyko's 138. To find $E_s(\theta)$ consistent with London's $\{[E_s]\}$ we will use Budyko's $E_L(\theta)$ and normalize his $M(\theta)$ to give $\{[M]\}=0$. This latter step is done by subtracting 9.4 from Budyko's $M(\theta)$. Table A5 gives $M+E_L$ from Budyko's adjusted data, and with London's data: E_s , $C-E_L$, $(p_4Q/g)-\mu\sigma T_2^4$, p_4Q/g . For the purposes of comparison figure A4 shows $C-E_L$ as adjusted here, with Budyko's data only, and as calculated by Lufkin [28, table III].

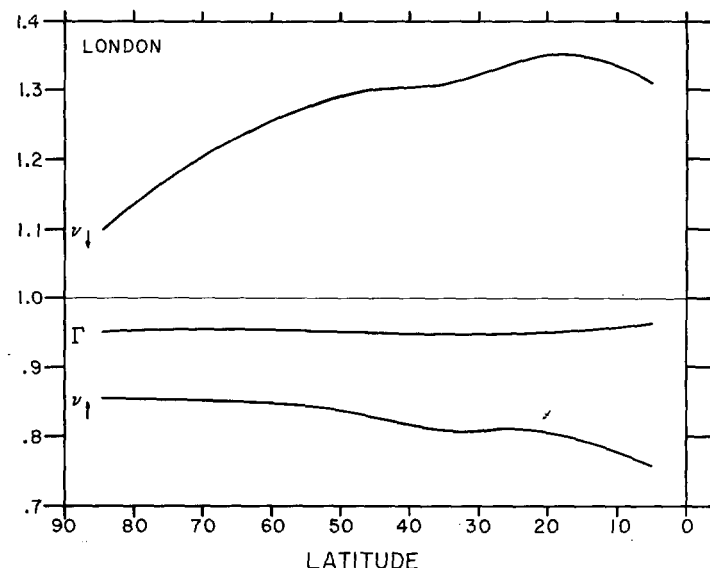


Figure A2.—The long wave radiation parameters deduced from London's [24] data.

TABLE A3.—Annual mean data from Houghton [19], rows 1–7 (parentheses in row headings indicate Houghton's terminology); rows 8–11 are derived quantities (parentheses in row headings indicate equations and tables used from Appendix A)

		Latitude ($^{\circ}$)										Mean
		0	10	20	30	40	50	60	70	80	90	
1 S_* (SR—absorbed at surface)	ly. day $^{-1}$	381	395	408	390	322	252	185	134	95	66	326.3
2 S_a (SR—absorbed in atmosphere)	ly. day $^{-1}$	192	183	166	142	122	100	76	58	52	51	136.5
3 A_s (surface albedo)		.071	.080	.098	.110	.102	.092	.091	.168	.36	.56	.106
4 A_p (planetary albedo)		.326	.310	.283	.284	.335	.389	.443	.527	.602	.669	.349
5 L^{\uparrow} (annual mean outgoing radiation $\times 461/472$)	ly. day $^{-1}$	476.6	490.3	491.3	480.5	458.1	431.7	409.2	390.7	376.0	371.1	460.4
6 S_0 (SR—outside atmosphere)	ly. day $^{-1}$	850	838	801	743	668	576	469	406	369	353	694.1
7 $A = S_a + S_p$ (SR—total absorbed)	ly. day $^{-1}$	573	578	574	532	444	352	261	192	147	117	462.8
8 χ (1; 2; 3.1, 3.2, 3.3)		.319	.299	.268	.245	.254	.265	.272	.265	.259	.254	.272
9 A_o (1; 3.2, 3.6, 3.8)		.292	.271	.228	.220	.280	.343	.404	.460	.456	.433	.296
10 $A - L^{\uparrow}$ (-; 3.5, 3.7)	ly. day $^{-1}$	+96	+88	+83	+51	-14	-80	-148	-199	-229	-254	+2.4
11 $S_a/1 - A_o$ (-; 3.1, 3.3)	ly. day $^{-1}$	410	429	452	438	359	277	203	161	148	150	361.8

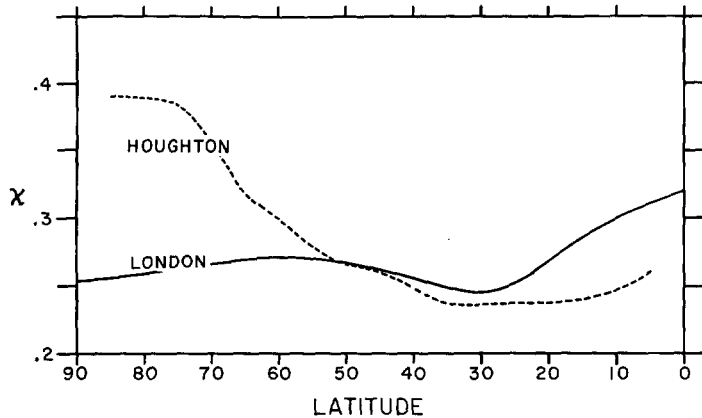


Figure A3.—A comparison of opacity of the atmosphere to solar radiation deduced from Houghton's [19] and London's [24] data.

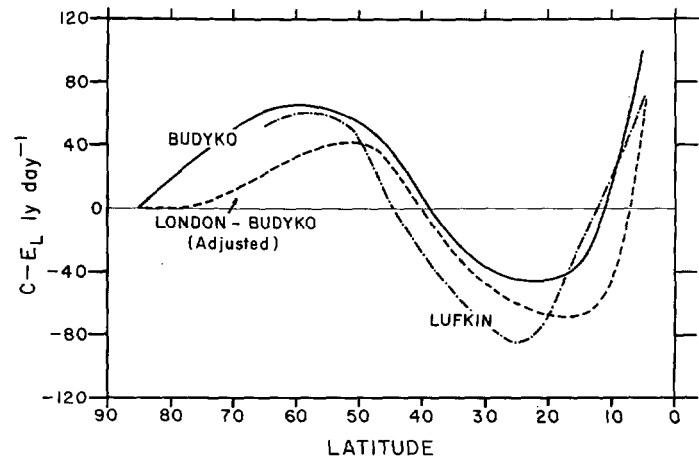


Figure A4.—A comparison of the condensation-evaporation heating rate difference given by Budyko [8] and Lufkin [28], and the adjustment of London's [24] and Budyko's data.

TABLE A4.—Annual mean data (ly. day $^{-1}$) for Northern Hemisphere from Budyko [8]. Parentheses in row headings show Budyko's terminology

		Latitude ($^{\circ}$)									Mean
		5	15	25	35	45	55	65	75	85	
1 S_* ($Q+g$)		408	447	447	400	312	249				
2 $S_a + L^{\uparrow} - \sigma T_*^4 = E_s + E_L + M$ (R)		277	277	236	189	126	77				
3 E_L (E)		197	206	164	145	99	69	(35)	(17)	(1)	138.0
4 E_s (P)		25	38	55	55	41	27	(16)	(7)	(0)	37
5 M (A)		+55	+33	+16	-11	-14	-19	(-22)	(-24)	(-25)	+9.4
6 $C - E_L$		+101	-33	-44	-20	+36	+65	+62	+37	+3	+19.4

TABLE A5.—Adjustment of London's and Houghton's data (units ly. day^{-1}). Parentheses in row headings indicate equations and tables used from Appendix A

	Latitude ($^{\circ}$)								Mean
	5	15	25	35	45	55	65	75	
1 $M+E_L$ ($-; 4.3, 4.5$)									
2 E_S ($-; 2.1, 5.1$)	+242.6	+229.6	+170.6	+124.6	+75.6	+40.6	+3.6	-16.4	-33.4
3 $C-E_L-M$ ($-; 2.15, 4.3, 5.1, 5.2$)	45.4	59.8	91.8	101.1	97.6	84.3	69.8	25.0	13.9
4 $p_4Q/g - \mu\sigma T_s^4$ ($9, 1.12, 5.2, 2.1, 2.10$)	+75.2	-67.0	-60.3	-28.7	+28.1	+40.4	+24.0	+3.9	+1.2
5 p_4Q/g ($-; 5.4, 1.11, 2.14$)	604.2	489.8	481.7	474.8	444.8	386.2	295.8	209.3	183.0
	+109.5	-13.6	-18.7	+11.2	+10.5	-22.3	-89.4	-151.0	-165.3
									-1.5

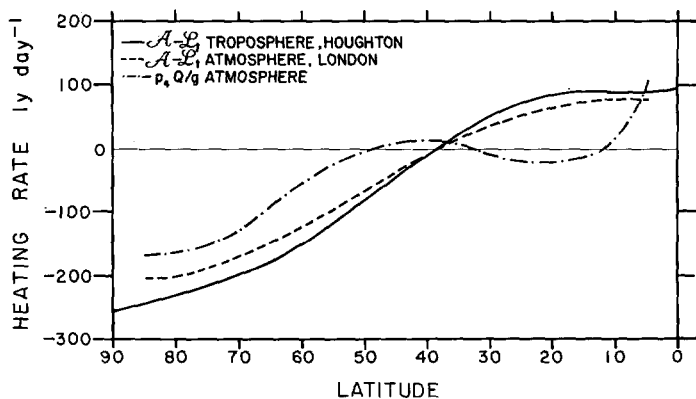


Figure A5.—A comparison of the radiative heating rate by Houghton [19] and London [24], with the net heating rate of the atmosphere deduced here.

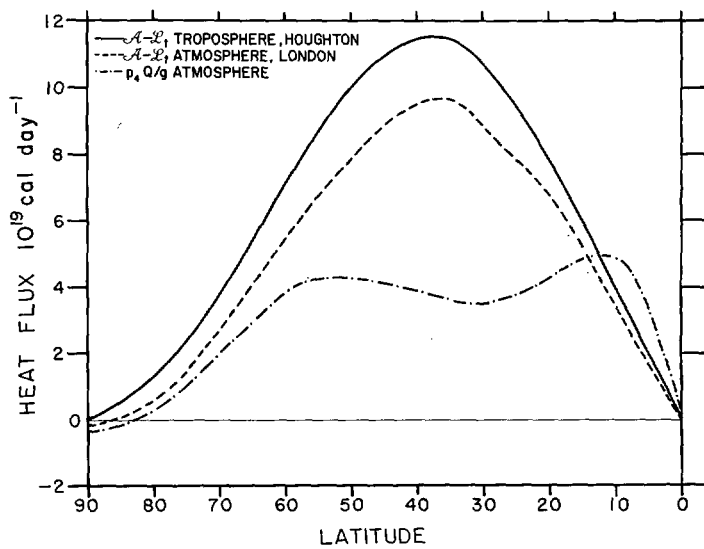


Figure A6.—The poleward heat fluxes required by the heating rates given in figure A5.

Figure A5 shows p_4Q/g thus computed in contrast to a pure radiative balance $A-L_{\uparrow}$ from London's and Houghton's calculations. The effect of $C-E_L-M$ is quite marked. Condensation near the equator gives an extremely large heating gradient with a minimum at 20° N, and a secondary maximum at 40° N. At middle and high latitudes the heating gradient is approximately the same as Houghton's.

The required atmospheric heat flux to balance London's (troposphere and stratosphere) and Houghton's (troposphere only) radiative gradients and that to balance the net heating calculated here are given in figure A6. Our curve for the flux required to balance the net non-adiabatic heating p_4Q/g is less than half of Houghton's and London's, having a double maximum which is due to latent heat of condensation. The poleward maximum is at 50° latitude and the tropical maximum is at 12° latitude. The fact that the latter is larger than the former is not to be taken too literally in light of the uncertainties of the data, but the fact that there are two maxima seems to be quite real. This curve then represents the required sensible heat transport by atmospheric adiabatic dynamics.

We may subtract from the net sensible heat flux required by the atmosphere p_4Q/g (fig. A6) Mintz's [31]

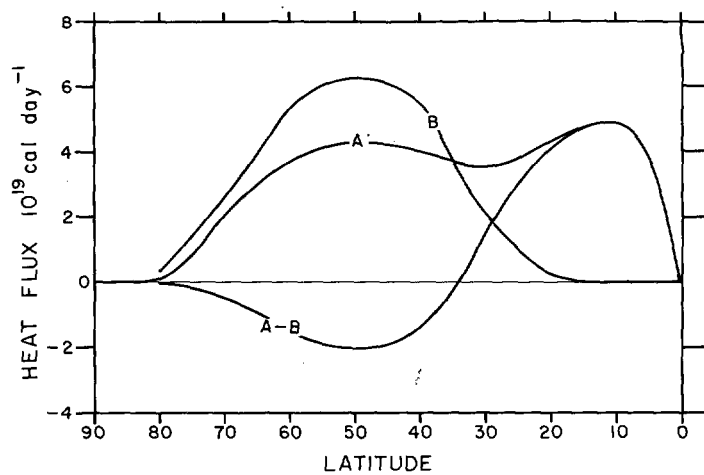


Figure A7.—The poleward heat flux required by the atmosphere, curve A (from fig. A6); the observed large-scale flux according to Mintz [31], curve B; the flux required by all other dynamical processes, curve A-B.

quasi-geostrophic large-scale eddy heat transfer (fig. 9.7). The residual, which is shown in figure A7, is what is required by other atmospheric transport processes—the ageostrophic large-scale eddy transfer, the meridional circulation, and small-scale heat diffusion. The small-scale poleward eddy heat transfer would probably be small and positive at all latitudes, so that the residual curve, if displaced slightly to more negative values, essentially represents the transport by the meridional circulation if we ignore the ageostrophic eddy transfer. It predicts a direct Hadley circulation at low latitudes and an indirect Ferrel circulation in middle latitudes. If the flux due to $p_4 Q/g$ were larger in magnitude, as the radiation balance alone requires (see fig. A6), then the heat transfer by the meridional circulation would be large and positive at all latitudes, implying a very strong single direct Hadley circulation. Since this would be at variance with other evidence of the nature of the mean meridional circulation, we take this to mean that the $p_4 Q/g$ curve in figures A5 and A6 is essentially correct.

Equation A9 permits the simple heating model to be expressed in terms of the parameters determined empirically and still be dependent on T_2 as a dependent variable.

We have already imposed local radiative equilibrium at the earth's surface. If we require the atmosphere to be in thermal equilibrium in the large then

$$\int_0^{2\pi} \int_{-\pi/2}^{\pi/2} \frac{p_4 Q}{g} \cos \theta d\theta d\lambda = 0$$

which by (A9) yields

$$\{[\mu \sigma T_2^4]\} = \{[S_a + \Gamma S_* + C - \Gamma(M + E_s + E_L) + E_s]\} \quad (\text{A13})$$

Since T_2 enters as a model dependent variable, (A13) imposes a constraint on the planetary mean temperature. This may best be seen by linearizing μ and T_2 such that

$$\mu = \{[\mu]\} + \mu'' \quad (\text{A14})$$

$$T_2 = \{[T_2]\} + T_2' \quad (\text{A15})$$

and the planetary mean values of μ'' and T_2'' vanish. By the binomial theorem

$$\mu T_2^4 \approx \{[\mu]\} \{[T_2]\}^4 + \{[T_2]\}^4 \mu'' + 4\{[\mu]\} \{[T_2]\}^3 T_2'' \quad (\text{A16})$$

to first order approximation.

Since μ and $(S_a + \Gamma S_*) + C - \Gamma(M + E_s + E_L) + E_s$ have only been determined as functions of latitude from London's and Budyko's data, for radiative equilibrium of the Northern Hemisphere, we may write (A13) as

$$\{[T_2]\}^4 = \frac{\{[S_a + \Gamma S_* + C - \Gamma(M + E_s + E_L) + E_s]\}}{\sigma \{[\mu]\}} \quad (\text{A17})$$

From London's data $\{[S_a + \Gamma S_* + C - \Gamma(M + E_s + E_L) + E_s]\} = 459.1 \text{ ly. day}^{-1}$, $\{[\mu]\} = 0.8716$ and with $\sigma = 1.177 \times 10^{-7} \text{ ly. day}^{-1} \text{ deg.}^{-4}$, we have that $\{[T_2]\} = 258.6^\circ \text{ A.}$ This

coincides with London's actual mean temperature 258.9° A. despite the linearization. Hence we may write

$$\frac{p_4 Q}{g} = c - b T_2' \quad (\text{A18})$$

where

$$\left. \begin{aligned} c &= S_a + \Gamma S_* + C - \Gamma(M + E_s + E_L) + E_s \\ &\quad - \sigma \{[\mu]\} \{[T_2]\}^4 - \sigma \{[T_2]\}^4 \mu'' \end{aligned} \right\} \quad (\text{A19})$$

and

$$b = 4\sigma \{[\mu]\} \{[T_2]\}^3 = 7.097 \text{ ly. day}^{-1} \text{ deg.}^{-1}$$

The heating rate resulting from released latent heat, C , is largely determined by the dynamics and an attempt will be made to formulate this process parametrically. The development will be based on a condensation model constructed by the writer [52], [54]. The individual change of potential temperature due to dynamical condensation or evaporation is given by:

$$\frac{d \ln \Theta}{dt} = \delta \omega \left(\frac{d \ln \Theta}{dp} \right)_{\Theta_E = \text{const.}} \quad (\text{A20})$$

(δ as used here is not to be confused with the notation in Section 4.) If the cloud stage is ignored and the air is assumed always saturated with respect to upward vertical motion then

$$\delta = \begin{cases} 0, & \omega \geq 0 \\ 1, & \omega < 0 \end{cases} \quad (\text{A21})$$

$(d \ln \Theta / dp)_{\Theta_E = \text{const.}}$ is a function of temperature and pressure only. We assume that the condensation takes place at a mean level of 700 mb., but that the heat released is redistributed through the entire vertical column so as to maintain the static stability. Hence the heating rate per unit area for the entire column is

$$C = \frac{p_4}{g} \left(\delta \omega c_p T \left(\frac{d \ln \Theta}{dp} \right)_{\Theta_E = \text{const.}} \right)_{700 \text{ mb.}} \quad (\text{A22})$$

Consistent with our model, ω varies linearly between 1000 and 500 mb. so that

$$\omega_{700 \text{ mb.}} = 0.6 \omega_2 = 0.3 \hat{p} \hat{D} \quad (\text{A23})$$

Hence we may write $(\delta \omega)_{700 \text{ mb.}}$ according to (A21) as

$$(\delta \omega)_{700 \text{ mb.}} = 0.3 \hat{p} \frac{\hat{D} + |\hat{D}|}{2} \quad (\text{A24})$$

Using the standard temperature for 700 mb., 269° A. , then at 700 mb. $(d \ln \Theta / dp)_{\Theta_E = \text{const.}} = -0.100/700 \text{ mb.}$ We shall now express the coefficient of $\delta \omega$ in (A22) in terms of quantities at 500 mb. For the standard atmosphere at 500 mb., $d \ln \Theta / dp = -0.106/500 \text{ mb.}$ With

$$2\gamma_s^2 = \hat{p} g h \left(\frac{d \ln \Theta}{dp} \right)_{2, \text{std.}} \quad (\text{A25})$$

where $h=7.9$ km. for the standard atmosphere, we have

$$\left(\frac{d \ln \Theta}{dp}\right)_{\Theta_E=\text{const., } 700 \text{ mb.}} = 1.35 \frac{\gamma_s^2}{\hat{p}gh} \quad (\text{A26})$$

Inserting (A24) and (A26) into (A22) we have

$$C = \frac{p_4}{kg} 0.40 \gamma_s^2 \frac{\hat{D} + |\hat{D}|}{2} \quad (\text{A27})$$

Evaluating the modelling coefficients we have

$$\frac{C}{(\hat{D} + |\hat{D}|)/2} = 1.4 \times 10^3 \text{ ly.} = \frac{\{[C]\}}{\{[|\hat{D}|]\}/2} \quad (\text{A28})$$

since $\{[\hat{D}]\} = 0$. To assess the magnitudes, we revert

to the more familiar vertical velocity which we approximate by $w_2 \approx -h\hat{D}/2$, whence

$$\frac{\{[C]\}}{\{[w_2]\}/2} \approx 300 \frac{\text{ly. day}^{-1}}{\text{cm. sec.}^{-1}} \quad (\text{A29})$$

Upon taking London's estimate of $\{[C]\} = 136$ ly. day⁻¹ (from table A1.12) we have that $\{[w_2]\} \approx 0.9$ cm. sec.⁻¹, which seems reasonable.

Returning to (A27), we may now write (A9) as

$$\frac{p_4 Q}{g} = (S_a + \Gamma S_*) - \mu \sigma T_*^4 + (1 - \Gamma) E_s - \Gamma (E_L + M) + \frac{p_4}{kg} 0.4 \gamma_s^2 \frac{\hat{D} + |\hat{D}|}{2} \quad (\text{A30})$$

APPENDIX B

A NON-DIMENSIONAL FORM OF THE BAROCLINIC INSTABILITY CRITERION

Phillips [39] has derived the geostrophic baroclinic instability criterion for a linearized two-level model corresponding to the one being discussed in this paper. In our notation the criterion is

$$\mathcal{R}^2(2 - \mathcal{R}^2) \gtrless \left(\frac{2\beta\gamma_s^2}{f^2 \hat{U}}\right)^2 \begin{array}{l} \text{unstable} \\ \text{neutral} \\ \text{stable} \end{array} \quad (\text{B1})$$

where $\mathcal{R} = \sqrt{2}(n\gamma_s/af)^2 = \sqrt{2}(c_g/c_i)^2$, $\beta = mdf/dy = 2\Omega/ma$ and n/a is the magnitude of the two-dimensional wave number so that n is non-dimensional, while c_g and c_i are the speed of long internal gravity and inertial waves, respectively. Furthermore $2\gamma_s^2 = h^2 g \partial \ln \Theta / \partial z$, where $h = 7.9$ km, is a scale height defined as the depth of the half-mass of the atmosphere and geostrophically $\hat{U} = hdU/dz = -ghf^{-1} \partial \ln \Theta / \partial y$.

We define the Richardson number as

$$R_I \equiv g \frac{\partial \ln \Theta / \partial z}{(\partial U / \partial z)^2} = \frac{f^2}{g} \frac{\partial \ln \Theta / \partial z}{(\partial \ln \Theta / \partial y)^2} \quad (\text{B2})$$

If we then define the thermal Rossby number as

$$R_{OT} \equiv \frac{\hat{U}}{af} = -\frac{gh}{af^2} \frac{\partial \ln \Theta}{\partial y} \quad (\text{B3})$$

then the non-dimensional product

$$R_I R_{OT} = -\frac{h}{a} \frac{\partial \ln \Theta / \partial z}{\partial \ln \Theta / \partial y} = m\alpha I \quad (\text{B4})$$

is an inverse normalized measure of slope of the isentropes.

From the above definitions we also have that

$$\mathcal{R} = \frac{n^2}{\sqrt{2}} R_I R_{OT}^2 \quad (\text{B5})$$

Hence the stability criterion may be written as

$$\mathcal{R}^2(2 - \mathcal{R}^2) \gtrless I^2 \begin{array}{l} \text{unstable} \\ \text{neutral} \\ \text{stable} \end{array} \quad (\text{B6})$$

The condition for the maximum value of I^2 above which instability is not possible is that the left side of (B6) be a maximum, i.e., that $\mathcal{R} = \pm 1$. Concerning ourselves with statically stable motions, we must take the positive root,

$$\mathcal{R} = 1 \quad (\text{B7})$$

Let us examine the consequences of assuming that the linear critical condition (the equality in (B6)) is presumably the equilibrium about which a non-linear system would oscillate under the influence of energy generation and dissipation. The generation and dissipation, however, must balance in the long run for such an equilibrium to exist. For equilibrium at the most unstable level, we get upon inserting $\mathcal{R} = 1$ in the equality of (B6) that $I^2 = 1$. This corresponds to the greatest lower bound of I^2 with respect to $\mathcal{R} \geq 0$ for stability. From (B4) we have that the roots $I = \pm 1$ correspond to $\partial \ln \Theta / \partial y \leq 0$. In the troposphere $\partial \ln \Theta / \partial y < 0$ or

$$I = 1 \quad (\text{B8})$$

With this root taken in (B4) and (B5) we have that

$$n^2 R_{OT} = \frac{\sqrt{2}}{m\alpha} \quad (\text{B9})$$

$$\frac{R_I}{n^2} = \frac{(m\alpha)^2}{\sqrt{2}} \quad (\text{B10})$$

$$R_I R_{OT} = \tan \theta = -\frac{h}{a} \frac{\partial \ln \Theta / \partial z}{\partial \ln \Theta / \partial y} \quad (\text{B11})$$

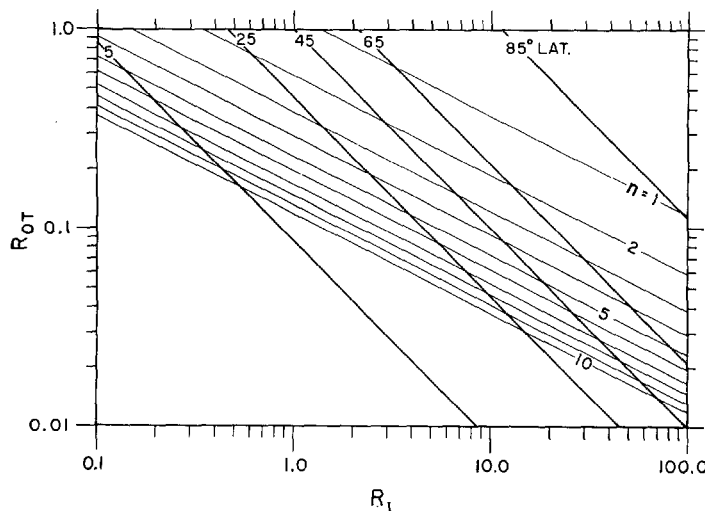


Figure B1.—The equilibrium baroclinic stability criterion: The wave number, n , as a function of the Richardson number, R_I , the thermal Rossby number, R_{OT} , and latitude.

From (B9) and (B10) we have that at a given latitude the most unstable wave number n is a function only of R_I or of R_{OT} (fig. B1).

From the thermodynamic equation for adiabatic changes in a quasi-steady state we have that the heat flux divergence in the vertical balances that in the horizontal, or for the zonal mean that

$$\frac{w}{v} \sim -\frac{\partial \ln \Theta / \partial y}{\partial \ln \Theta / \partial z} \quad (\text{B12})$$

i.e., the slope of the stream-surface equals that of the isentropes. Taken with the equilibrium condition (B11) we have

$$\frac{w}{v} \sim \frac{h}{a} \operatorname{ctn} \theta \quad (\text{B13})$$

Hence in middle latitudes $w/v \sim 1.2 \times 10^3$, which predicts the quasi-horizontal nature of the disturbances to good agreement with observation.

We note from figure B1 that since n increases with decreasing R_{OT} for a given R_I , the scale of the perturbations is reduced to the point where they would presumably become significantly ageostrophic. Hence we could expect that the geostrophic baroclinic instability theory is valid in a closed range spanning approximately an order of magnitude of variation in R_{OT} .

From (B11) we have that the equilibrium slope of the isentropes depends only on cotangent of the latitude. In fact since $|I|=1$ is the greatest lower bound of $|I|$ then it means that the magnitude of the equilibrium slope of the isentropes is at a minimum. Since the magnitude of the slope of the isentropes is a measure of the zonal available potential energy, this seems to constitute a minimum energy principle akin to those occurring in

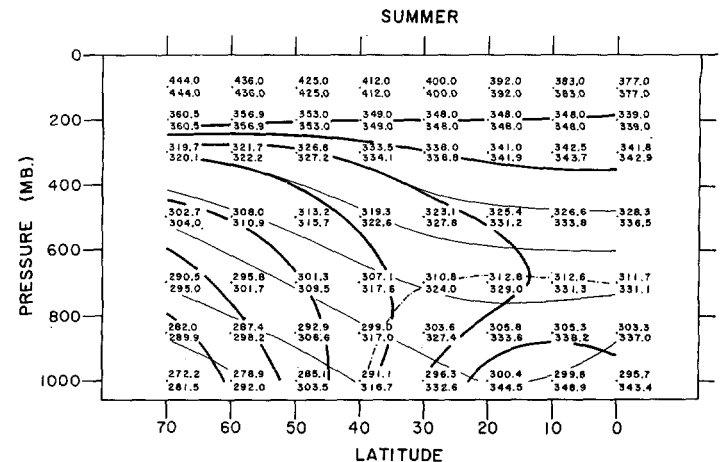


Figure B2.—The summer distribution of potential temperature, Θ (upper numbers, thin lines), by Peixoto [38]; and of partial equivalent potential temperature, Θ_{PE} (lower numbers, heavy lines), deduced from the data of Peixoto [37], [38].

classical thermodynamics, a result which in essence was derived by Eady [12]. Interpreted for the atmosphere, more correctly the condition (B11) must take into account the effects of partial condensation on the effective static stability [54]. We will do this somewhat more precisely than was done in parameterizing condensation in Appendix A.

The conventional equivalent potential temperature for saturated air is

$$\Theta_E = \Theta \exp(L_h r_s / c_p T) \approx \Theta \left(1 + \frac{L_h r_s}{c_p T}\right) \quad (\text{B14})$$

where L_h is the latent heat of condensation and r_s is the saturation mixing ratio. We define the partial equivalent potential temperature for moist air as

$$\Theta_{PE} \equiv \Theta \exp(L_h r / c_p T) \approx \Theta \left(1 + \frac{L_h r}{c_p T}\right) \quad (\text{B15})$$

where r/r_s is the relative humidity. Therefore

$$\Theta_{PE} \approx \Theta + (\Theta_E - \Theta)r/r_s \quad (\text{B16})$$

To verify (B11) for the atmosphere, we employ the data of Peixoto [37], [38]. Figures B2, B3, and B4 show Θ_{PE} and Θ in meridional cross-sections for summer, winter, and the annual mean, where we have assumed the relative humidity to be equal at 500 and 300 mb., and negligible at and above the 200-mb. level. $\partial \ln \Theta_{PE} / \partial z$ was evaluated between 1000 mb. and 250 mb. (interpolated), while $\partial \ln \Theta_{PE} / \partial y$ was evaluated over a 20° latitude span at 500 mb. and we have taken $h=7.9$ km. The inverse of the ratio on the right side of (B11) computed from the observed Θ_{PE} is plotted in figure B5. Also shown is the theoretically deduced dependence, $\operatorname{ctn} \theta$. The latitudinal variability agrees quite well between 30° and 60° latitude. Absolute coincidence

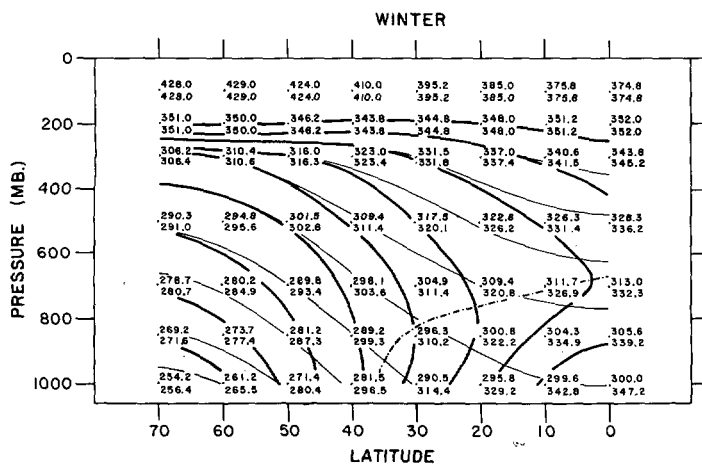


Figure B3.—The same as figure B2, but for winter.

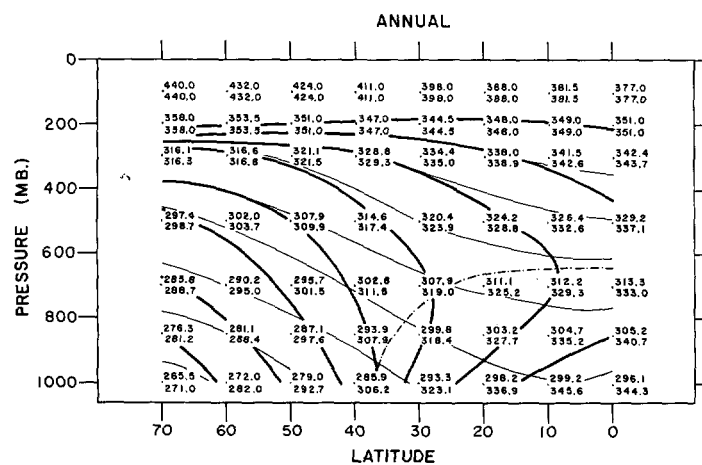
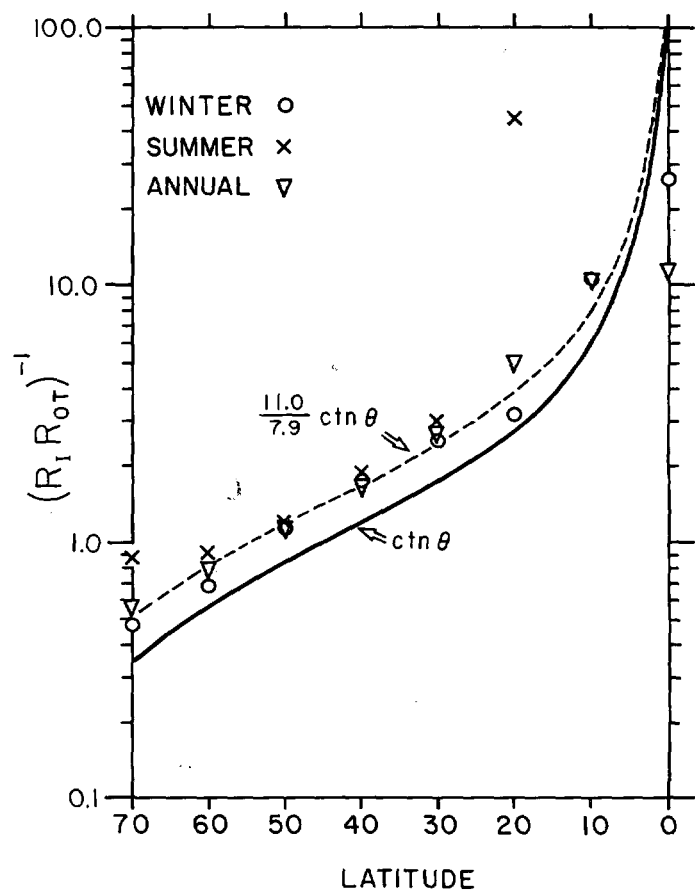


Figure B4.—The same as figure B2, but for annual mean.

would have been improved if h were taken to be 11 km. The deviations at high and low latitudes are in part due to the β -plane kinematics used in deriving the criterion. But more important at low latitudes is the fact that the assumption $R_{\text{ot}} \ll 1$ is becoming invalid, so that the predominant processes responsible for energy transformations and heat transport are meridional circulation and small-scale convection. The latter is suggested by the fact that in summer $R_i < 0$ at 0° and 10° latitude, and therefore the data have not even been plotted.

These results suggest that it might be consistent within the context of the model being discussed in this paper to parameterize the static stability as a given function of latitude, rather than as a spatial constant. This has not been done in the work reported upon here.

The requirement for the invariance of the slope of the isentropes seems to be verified by laboratory experiment [16]. In their notation, $R_i^* R_{\text{ot}}^* \propto S_z^*/R_{\text{ot}}^* \propto \Delta_z T/\Delta_T T$ ap-

Figure B5.—A comparison of the theoretical equilibrium $(R_1 R_{\text{ot}})^{-1}$ and the observed (with θ_{PE} used instead of Θ).

pears to be invariant along the transition curve from symmetric to wave regimes for the range $6 \times 10^{-3} < R_{\text{ot}}^* < 3 \times 10^{-1}$. The further implication then is that for $R_{\text{ot}}^* < 9 \times 10^{-2}$, where $\Delta_z \theta$ and R_{ot}^*/G^* are constant, S_z^*/G^* and therefore $\Delta_z T$ are constant. On the other hand, for $R_{\text{ot}}^* > 9 \times 10^{-2}$, where $R_{\text{ot}}^* \sqrt{G^*}$ is approximately constant, S_z^*/G^* and $\Delta_z T$ vary as $(R_{\text{ot}}^*)^3$.

(B11) permits an estimate of the equilibrium zonal available potential energy. Approximating the temperature deviation by $T'' = \delta y \partial T / \partial y = \hat{\Phi}/R$, where $\delta y = 0$ is the latitude θ_0 at which T attains its mean value, then using (B11), we have that

$$[\hat{\Phi}] = -2\gamma_s^2 \frac{R[T]}{gh} \frac{\delta y}{a} \operatorname{ctn} \theta \quad (\text{B17})$$

Inserting in (8.11) yields:

$$[\mathcal{P}_d] = \left\{ \left(\frac{\gamma_s R[T]}{gh} \frac{\delta y}{a} \operatorname{ctn} \theta \right)^2 \right\} \approx \gamma_s^2 \left(\frac{R\{[T]\}}{gh} \right)^2 \frac{\theta_0^2}{3} \operatorname{ctn}^2 \theta_0 \quad (\text{B18})$$

Hence $\{\mathcal{P}_d\}$ is proportional to the static stability. We have seen from (3.4) that $\{[T]\}$ is largely deducible from $\{[A]\}$ and that in fact $R\{[T]\}/gh \approx 1$. Therefore for $\theta_0 = \pi/4$ and with the standard static stability, we find that $\{\mathcal{P}_d\} \sim 1$ joule gm.⁻¹. This agrees in magnitude with Lorenz's [26] estimate from an assumed value for T'' .

If within the limits of small-perturbation quasi-geostrophic constraints the zonal available potential energy is a function of the static stability only, then what effect should the variation of the meridional heating gradient have? Let us assume that the total energy is conserved over a long period, i.e., the total dissipation balances the potential energy generated by the heating gradient. Hence for a given static stability, to maintain

the equilibrium temperature gradient requires that baroclinic instability, which is actuated discontinuously and is responsible for fluctuations of the available potential energy about its equilibrium, occur more frequently and more vigorously the greater the heating gradient. This would only affect the period and amplitude of the index cycle, meeting the requirement for greater poleward heat transport to maintain the equilibrium temperature gradient.

Thus one would conclude that the observed seasonal temperature gradient variations are a secondary effect, associated with mutual adjustments with the variations of effective static stability $d\ln\Theta_{PE}/dz$ (cf. fig. B5).

APPENDIX C NOTATION CONVENTIONS

a	radius of earth, 6371 km.	u	eastward Mercator map wind component
b	heating coefficient for linearized form, defined by (A19)	v	northward Mercator map wind component
c	heating coefficient for linearized form, defined by (A19)	\mathbf{V}	Mercator map wind vector, $i u + j v$
$c_d/2$	drag coefficient	w	vertical velocity, dz/dt
c_g	speed of long internal gravity waves	x	eastward Mercator map coordinate
c_i	speed of long inertial waves	y	northward Mercator map coordinate
c_p	specific heat of air at constant pressure, 0.239 cal. gm. ⁻¹ deg. ⁻¹	z	height
c_R	radiative heating coefficient for linearized form, defined by (3.6)	z_4	height of p_4 surface
c_v	specific heat of air at constant volume, 0.170 cal. gm. ⁻¹ deg. ⁻¹	z_4'	height of boundary between Prandtl and Ekman layers
f	Coriolis parameter, $2\Omega\alpha$	z_*	roughness length
g	acceleration of gravity, 981 cm. sec. ⁻²	A	planetary albedo
h	scale height: the depth of half mass of the standard atmosphere, $\hat{z}=7.9$ km.	A_a	atmosphere's albedo
i	x -finite difference index	A_*	earth's albedo
i	unit vector positive eastward	C	heat released by condensation
j	y -finite difference index	$ D $	magnitude of the horizontal deformation tensor, defined by (4.24)
j	unit vector positive northward	D_s	shearing stress, defined by (4.23)
k	p -finite difference index	D_T	tension stress, defined by (4.23)
k_0	von Kármán's constant, 0.4	E_L	flux divergence of heat due to eddy transport of latent heat
k_H	lateral diffusion constant	E_S	flux divergence of heat due to eddy transport of sensible heat
l	ratio of the magnitude of the surface wind to the extrapolated surface wind	\mathbf{F}	horizontal frictional force vector
m	$\sec \theta$, Mercator map factor	${}^H\mathbf{F}$	horizontal frictional force vector due to stresses in horizontal planes, defined by (4.22)
n	magnitude of the horizontal two-dimensional wave number times a	${}^H\mathbf{F}$	horizontal frictional force vector due to stresses in vertical planes, preliminarily defined by (4.2)
p	pressure	${}^H\mathbf{F}$	horizontal frictional force vector due to vertical surface stresses, preliminarily defined by (4.4)
r	mixing ratio	\mathbf{F}_I	horizontal frictional force vector due to vertical internal stresses, preliminarily defined by (4.4)
r_s	saturation mixing ratio	G	difference between horizontal frictional and inertial force vectors, defined by (2.4)
t	time		

I	horizontal inertial force vector, defined by (2.5)	Γ	long wave absorptivity of the atmosphere
J	number of grid-points in N-S direction, including boundaries	Δ	horizontal map grid increment
K	eddy viscosity due to stresses in vertical planes	Δt	time differencing increment
K_E	mean eddy viscosity in Ekman layer	Θ	potential temperature
L	$\oint dx = 72\Delta$	Θ_E	equivalent potential temperature
L_h	latent heat of condensation	Θ_{PE}	partial equivalent potential temperature defined by (B15)
M	flux divergence of heat in oceans due to lateral ocean transports	Λ	lapse rate
Q	non-adiabatic heating rate per unit mass due to all processes except lateral diffusion	Λ_d	adiabatic lapse rate
Q_R	non-adiabatic heating rate per unit mass due to radiative transfer	Ξ	arbitrary "circulating" energy transformation deviation from domain mean geopotential, $\phi'' = \phi - \{\phi\}$
R	gas constant for air, 2.87×10^6 erg gm. ⁻¹ deg. ⁻¹	Ω	angular velocity of earth's rotation
R_I	Richardson number, defined by (B2)	A	total absorption of solar radiation by atmosphere and earth
R_{OT}	thermal Rossby number, defined by (B3)	B	"Bernoullian" energy, defined by (2.10)
T	temperature	D	horizontal divergence
T_2	500-mb. or vertical mean temperature	E	energy
T_*	temperature of earth's surface	F	energy sinks
U	zonal mean eastward earth wind speed	H	κ times the heating rate per unit mass due to lateral flux divergence by small-scale eddies.
Y	y at the poleward boundary	I	$R_I R_{OT} / m \alpha$
α	$\sin \theta$	K	kinetic energy per unit mass
β	mdf/dy	L_{\uparrow}	total outgoing radiation
γ	measure of the effective static stability due to condensation processes, taken as a fraction of γ_s	L_{\downarrow}	back radiation
γ_s	measure of the static stability at 500 mb., $h(g\partial \ln \Theta / \partial z)^{1/2}/2$	P	available potential and latent energy per unit mass
δ	acute angle between surface wind and geopotential lines	P_a	available potential energy per unit mass
ϵ	roughness parameter, defined by (4.7)	R	$\sqrt{2}(c_g/c_i)^2$
ξ	vertical component of relative vorticity	S	energy sources
η	vertical component of absolute vorticity	S_a	solar radiation absorbed by atmosphere
θ	latitude	S_b	solar radiation at top of atmosphere
κ	$R/c_p = 0.287$	S_{\ast}	solar radiation absorbed by earth's surface
λ	longitude		
μ	$(1 - \Gamma)\nu_{\downarrow} + \nu_{\uparrow}$		
ν_{\uparrow}	normalization parameter for upward long-wave atmospheric radiation		
ν_{\downarrow}	normalization parameter for downward long-wave atmospheric radiation		
ξ	dummy variable		
ρ	density		
σ	Stephan-Boltzmann constant, 1.177×10^{-7} ly. day ⁻¹ deg. ⁻⁴		
τ	time finite difference index		
τ	stress vector in vertical plane		
v	dummy variable		
ϕ	geopotential		
x	opacity to solar radiation		
ψ	stream function corresponding to vertically integrated flow		
ψ^*	stream function tendency, $d\psi/dt$		
ω	dp/dt		

We will use a short hand notation for various types of integrals. The mapping is by Mercator projection [53]. The zonal mean is

$$[\xi] \equiv \frac{1}{L} \oint \xi dx, \quad L \equiv \oint dx \quad (C1)$$

or

$$[\xi]_j = \frac{1}{72} \sum_{i=0}^{71} \xi_{ij} \quad (C2)$$

and

$$\xi \equiv [\xi] + \xi' \quad (C3)$$

A time mean between $t_0 = \tau_0 \Delta t$ and $t_q = \tau_q \Delta t$ of a zonal mean is

$$\tilde{\xi}_j = \frac{1}{t_q - t_0} \int_{t_0}^{t_q} [\xi]_j dt = \frac{1}{t_q - t_0} \left(\frac{[\xi]_{j_0}^{\tau_0}}{2} + \sum_{\tau=\tau_0+1}^{\tau_q-1} [\xi]_j^{\tau} + \frac{[\xi]_{j_q}^{\tau_q}}{2} \right) \quad (C4)$$

We define

$$\tilde{\xi}_v - \tilde{\xi} \tilde{v} \equiv \widetilde{\xi^* v} \quad (C5)$$

Meridional integrals from the equator to an arbitrary latitude y will be evaluated according to:

$$\int_0^y \xi \frac{dy}{m^2} = \left(\frac{1}{2} \frac{\xi_0}{m_0^2} + \sum_{j=1}^{j-1} \xi_j / m_j^2 + \frac{1}{2} \frac{\xi_j}{m_j^2} \right) \Delta \quad (C6)$$

The meridional mean is

$$\{\xi\} \equiv \frac{1}{\int_0^y \frac{dy}{m^2}} \int_0^y \xi \frac{dy}{m^2} \quad (C7)$$

$$= \frac{\frac{1}{2} \frac{\xi_0}{m_0^2} + \sum_{j=1}^{16} \xi_j / m_j^2 + \frac{1}{2} \frac{\xi_{17}}{m_{17}^2}}{\frac{1}{2} \frac{1}{m_0^2} + \sum_{j=1}^{16} \frac{1}{m_j^2} + \frac{1}{2} \frac{1}{m_{17}^2}} \quad (C8)$$

$$= \frac{\sum_{j=0}^{16} (\xi / m^2)_{j+1/2}}{\sum_{j=0}^{16} m_{j+1/2}^{-2}} \quad (C9)$$

where either (C8) or (C9) is used if ξ is known at the j or at the $j + \frac{1}{2}$ grid points, respectively. The area mean of ξ is therefore $\{\xi\}$.

It will be useful to deal with deviations from the area mean which is defined through

$$\xi \equiv \{\{\xi\}\} + \xi'' \quad (C10)$$

The vertical structure will be described by the following notation. The posterior subscripts 0, 1, 2, 3, and 4 will denote a quantity at 0, 250, 500, 750, and 1000 mb., respectively, the lower boundary being set at p_4 . If we denote by

$$\bar{\xi} \equiv \xi_1 + \xi_3, \hat{\xi} \equiv \xi_1 - \xi_3 \quad (C11)$$

then it follows that

$$2\bar{\xi}_v = \bar{\xi}_v + \hat{\xi}_v \quad (C12)$$

$$2\hat{\xi}_v = \hat{\xi}_v + \hat{\xi}_v \quad (C13)$$

$$2\bar{\xi}^2 = \bar{\xi}^2 + \hat{\xi}^2 \quad (C14)$$

$$\hat{\xi}^2 = \hat{\xi} \hat{\xi} \quad (C15)$$

We summarize the energy transformation conventions introduced in Section 8. If \mathcal{E}_i is a particular energy partition then

$$\frac{d\mathcal{E}_i}{dt} = \langle (\mathcal{E} + S + F) * \mathcal{E}_i \rangle \quad (8.16)$$

where \mathcal{E} , S , F are the sums of the energy partitions, sources, and sinks, respectively.

The transformation from partition A to B is

$$\langle A * B \rangle$$

and the following identities hold:

$$\langle A * B \rangle \equiv -\langle B * A \rangle \quad (8.13)$$

$$\langle A * A \rangle \equiv 0 \quad (8.14)$$

$$\langle A * (B + C) \rangle \equiv \langle A * B \rangle + \langle A * C \rangle \quad (8.15)$$

If two transformations $\langle A * C \rangle$ and $\langle C * B \rangle$ are catalytic with respect to their common energy component C then:

$$\left. \begin{aligned} \langle A * C \rangle &= \langle A * C \rangle_c + \langle A * C \rangle_{NC} \\ \langle C * B \rangle &= \langle C * B \rangle_c + \langle C * B \rangle_{NC} \end{aligned} \right\} \quad (8.77)$$

$$\langle A * C \rangle_c \equiv \langle C * B \rangle_c \quad (8.78)$$

$$\langle A * C * B \rangle \equiv -\langle B * C * A \rangle \equiv \frac{\langle A * C \rangle_c + \langle C * B \rangle_c}{2} \quad (8.79)$$

$$\langle A * C \rangle - \langle C * B \rangle \equiv \langle A * C \rangle_{NC} - \langle C * B \rangle_{NC} \quad (8.80)$$

PARAMETERS OF THE NUMERICAL MODEL

Differencing

$p_k = k \times 250$ mb., $k = 0, 1, 2, 3, 4$; so that $p_2 = p_4/2 = -\hat{p} = 500$ mb.

$\Delta = 555$ km.

$J = 18$

$\Delta t = 20$ min.

Thermal

$\{[T_2]\} = 251^\circ$ A.

$2\gamma_2^2 = 8250$ m.² sec.⁻² (equivalent to $\Lambda_2 = 6.5$ deg. km.⁻¹)

$2\gamma^2 = 6600$ m.² sec.⁻²

Radiative

$b = 4.7$ ly. day⁻¹ deg.⁻¹

$c(\theta)$, figure 3.1

Small-scale eddy diffusion

Boundary layer

$\epsilon_b^2 / K_E = 10^4$ sec.

$l = 0.6$

$(c_d/2)_4 = 0.012$

Internal vertical

$(\rho K)_2 = 50$ gm. cm.⁻¹ sec.⁻¹

Lateral

$k_H = 0.28$